

Federal University of Rio Grande do Sul  
School of Engineering  
Graduate Program in Civil Engineering

**NUMERICAL ANALYSIS OF  
CROSS-LAMINATED TIMBER BUILDING  
UNDER SEISMIC LOADING: ASSESSMENT  
UNDER EN 1998 AND NBR 15421  
REGULATIONS**

**Lucas Costa Victoria**

Porto Alegre  
2023

LUCAS COSTA VICTORIA

**NUMERICAL ANALYSIS OF CROSS-LAMINATED TIMBER  
BUILDING UNDER SEISMIC LOADING: ASSESSMENT  
UNDER EN 1998 AND NBR 15421 REGULATIONS**

Master's Dissertation presented to the Graduate Program in Civil  
Engineering of the Federal University of Rio Grande do Sul as  
part of the requirements of the Master in Engineering.

Porto Alegre  
2023

**LUCAS COSTA VICTORIA**

**NUMERICAL ANALYSIS OF CROSS-LAMINATED  
TIMBER BUILDING UNDER SEISMIC LOADING:  
ASSESSMENT UNDER EN 1998 AND NBR 15421  
REGULATIONS**

This master's dissertation was considered suitable for obtaining the title of MASTER IN ENGINEERING, in the field of Structures. Its final version was approved by the supervising professor and the Graduate Program in Civil Engineering of the Federal University of Rio Grande do Sul.

Porto Alegre, November 7<sup>th</sup>, 2023

Prof<sup>a</sup>. Letícia Fleck Fadel Miguel  
Ph.D. from Federal University of Rio Grande do  
Sul, Brazil  
Advisor

Prof. Jorge Manuel Branco  
Ph.D. from University of Minho, Portugal  
Co-advisor

Prof. Nilo Consoli  
Ph.D. from Concordia University, Canada  
Coordinator of the PPGECC/UFRGS

**BOARD OF EXAMINERS**

**Prof. Inácio Benvegno Morsch (UFRGS)**  
Ph.D. from Federal University of Rio Grande do Sul, Brazil

**Prof. Liércio André Isoldi (FURG)**  
Ph.D. from Federal University of Rio Grande do Sul, Brazil

**Prof. Helder Manuel da Silva e Sousa (UMinho)**  
Ph.D. from University of Minho, Portugal

## ACKNOWLEDGEMENTS

Prima facie, I shall express my gratitude to my advisor, Prof. Ph.D. Letícia Fleck Fadel Miguel, who walked me through this journey without any hesitation. Since the beginning, there has been no bad weather that it would not be possible to overcome. To this irresolution and all knowledge shared during the past few months, I would like to demonstrate my thankfulness.

I shall also express my appreciation and indebtedness to Prof. Ph.D. Jorge Manuel Branco, who also conducted me through this dissertation as my co-advisor. This recognition is a way of thanking for the hours dedicated to sharing the passion for sustainability in construction. This work would certainly not be possible if it was not for the effortless dedication it was offered.

This work would not be possible if it were not for the incessant help of my fellow M.Sc. Caroline Dapieve Aquino, who presented me with this topic and awakened in me the possibility to contribute with more sustainable Civil Construction. To that, I express my gratitude and would like to thank for all meetings, messages, e-mails and contributions throughout this journey. I also extend this acknowledgement to M.Sc. Zabih Mehdipour, who had great contribution in understanding and helping the use of modelling tools.

I would also like to express my sincere gratefulness to the experts who made part of the board of examination, Prof. Ph.D. Inácio Benvegnu Morsch, Prof. Ph.D. Liércio André Isoldi and Prof. Ph.D. Helder Manuel da Silva e Sousa. Without your contribution, this project would not be possible.

Getting through this dissertation required not only academic background and supervision but also the correct tools to achieve the proposed objectives. That's why it is important to express gratitude to Dlubal Software GmbH, which conceded licenses with no restriction to this research of the RFEM software.

In addition, I would like to acknowledge all professors of the Graduate Program in Civil Engineering of the Federal University of Rio Grande do Sul and the Program itself. This journey would not be possible if it wasn't for the example of great researchers and Doctors who dedicate their lives to producing Science. I shall also extend this acknowledge to all professors of the Federal University of Rio Grande, my *alma mater*, who had great importance in my academic and professional life.

Lastly, I would like to express my gratitude to my family, especially my parents Ivo and Sylvia, and to my lifemate, Luiza, who played an important role in giving me the incentive to persist in reaching the final objective of this process that is materialised in the present study.

"If we work marble, it will perish;  
if we work upon brass, time will efface it;  
if we rear temples, they will crumble into dust;  
but if we work on men's immortal minds;  
if we impress them with high principles;  
the just fear of God and love for their fellow men,  
we engrave on those tablets something  
which no time can efface,  
and which will brighten and brighten to all eternity."

(Daniel Webster)

## ABSTRACT

VICTORIA, L. C. **Numerical analysis of Cross-laminated Timber Building under seismic loading: assessment under EN 1998 and NBR 15421 regulations** 2023. 115p. Dissertation (Master of Engineering) – Graduate Program in Civil Engineering, Federal University of Rio Grande do Sul, Porto Alegre.

Civil Construction is getting increasingly concerned with decreasing the environmental impact of its activities. Because of that, new materials and techniques are being developed with the main objective of fulfilling housing necessities as well as sustainability. In this way, it is established that the research objective is the assessment of seismic activity in Cross-Laminated Timber structures. This material is considered an engineered timber and is an alternative to accomplish sustainable goals. Its construction is done by means of glued lamellae with different grain directions, orthogonally disposed, making it possible to resist in and out of plane loadings. Alongside that, it brings agility and productivity to the construction process, an important factor in decreasing the costs of the whole project. However, there is still little development of the material in the literature, being recently incorporated into norms and codes, making its implementation easier for designers and will be able to enlarge its application. This research focused on the ability of the structure to dissipate energy through ductility calculations. The goal was to improve the design process and reduce the use of connectors by considering the plastic level to dissipate energy. The analysis was conducted using RFEM software and the numerical model was validated with experimental values found in the literature. It was possible to reach reductions in displacements up to almost 55% when comparing DC1 and DC2 results. Pushover analysis indicated that the proposed building is considered with high ductility behaviour, despite the overdesign it was carried out to the place it was originally proposed. The present study concluded that NBR 15421 has still much to improve its method since it encompasses regions with medium to low seismicity and resulted in the highest displacement values in average due to its lack of energy dissipation consideration. Alongside that, it was performed an alteration in the material of slabs, considering hybrid CLT-concrete to assess performance and it was concluded that the whole design may be benefited from the usage of heavier structure aiming to achieve better levels of comfort.

**Keywords:** *Seismic design. Cross-Laminated Timber. Eurocode 8. NBR 15421.*

## RESUMO

VICTORIA, L. C. **Análise numérica de edifício em Madeira Lamelada Colada Cruzada submetido à atividade sísmica: avaliação sob as normas EN 1998 e NBR 15421 2023.** 115p. (Mestre em Engenharia) – Programa de Pós-Graduação em Engenharia Civil, Universidade Federal do Rio Grande do Sul, Porto Alegre.

A Construção Civil está cada vez mais preocupada em diminuir o impacto ambiental de suas atividades. Por causa disso, novos materiais e técnicas estão sendo desenvolvidos com o principal objetivo de atender às necessidades habitacionais e à sustentabilidade. Dessa forma, estabeleceu-se que o objetivo da pesquisa é a avaliação da atividade sísmica em estruturas de Madeira Lamelada Colada Cruzada (MLCC). Esse material é considerado uma madeira engenheirada e é uma alternativa para alcançar metas sustentáveis. Sua construção é feita por meio da colagem de lâminas de madeira com diferentes direções de fibras, dispostas ortogonalmente, o que torna possível resistir a carregamentos dentro e fora do plano. Além disso, ele traz agilidade e produtividade ao processo de construção, fator importante na redução dos custos de todo o projeto. No entanto, ainda há pouco desenvolvimento desse material na literatura, sendo recentemente incorporado em normas e códigos, o que facilita sua implementação por parte dos projetistas e amplia sua aplicação. Esta pesquisa concentrou-se na capacidade da estrutura de dissipar energia por meio da determinação das deformações em patamar plástico. O objetivo é melhorar o processo de projeto e reduzir o uso de conectores, considerando o nível plástico para dissipar energia. A análise foi conduzida usando o software RFEM e o modelo numérico foi validado com valores experimentais encontrados na literatura. Foi possível alcançar reduções nos deslocamentos de até quase 55% ao comparar os resultados de DC1 e DC2. A análise pushover indicou que o edifício proposto possui um comportamento de alta ductilidade, apesar do superdimensionamento originalmente proposto. O presente estudo concluiu que a NBR 15421 ainda tem muito a melhorar em seu método, uma vez que abrange regiões com sismicidade média a baixa e resultou nos maiores valores de deslocamento em média devido à falta de consideração da dissipação de energia. Além disso, foi realizada uma alteração no material das lajes, considerando CLT-concreto híbrido para avaliar o desempenho, e concluiu-se que todo o projeto pode se beneficiar do uso de uma estrutura mais pesada visando alcançar melhores níveis de conforto.

**Palavras-chave:** *Análise sísmica. Madeira Lamelada Colada Cruzada. Eurocódigo 8. NBR 15421.*

## LIST OF FIGURES

Figure 1.1 – Stadthaus Building in Murray Groove Street, London. (Wood Skyscrapers, <i>s.d.</i> ). . . . .	21
Figure 2.1 – CLT panels conception (De MATOS, 2020). . . . .	23
Figure 2.2 – Typical connectors used with CLT panels. (a) coupled wall with lap joint; (b) 90° corner joint; (c) coupled wall with external spline joint; (d) wall intersection/T-shaped joint; (e) coupled wall with internal spline joint; (f) single wall joined with steel plates; (g) decoupling strip; (h) fasteners - hold-downs and angle brackets. (DI BELLA; MITROVIC, 2020) . . . . .	26
Figure 2.3 – Real scale CLT building, tested Experimental CLT cle at the University of Minho lab facilities. (De MATOS, 2020). . . . .	27
Figure 2.4 – First CLT building in Brazil (Fran Parente ( <i>s.d.</i> )). . . . .	29
Figure 2.5 – Scheme of CLT manufacturing. . . . .	30
Figure 3.1 – Single-degree-of-freedom system subjected to arbitrary load (DAGDELEN; RUHANI, 2018) . . . . .	34
Figure 3.2 – Schematic definition of hypocentre and epicentre. In red, it is presented seismic waves (Swiss Seismological Service ( <i>s.d.</i> )). . . . .	36
Figure 3.3 – Seismic Waves: primary, secondary, Rayleigh and Love (Adapted from Martínez-Moreno (2015)). . . . .	37
Figure 3.4 – Fourier Transform graphic representation (MED, 2018) . . . . .	39
Figure 3.5 – Eurocode 8 designing scheme. . . . .	45
Figure 3.6 – EC8 elastic response spectrum pattern (EN 1998, 2021). . . . .	47
Figure 3.7 – Portuguese seismic zoning (NP EN 1998-1, 2010). . . . .	48
Figure 3.8 – Isopleth map to Brazilian seismic zones (NBR 15421, 2023). . . . .	53
Figure 3.9 – Design response spectrum variation according to the period (T) (Adapted from NBR 15421 (2023)). . . . .	55
Figure 3.10 – Determination of the target displacement for the equivalent SDOF system (EN 1998, 2021). . . . .	58
Figure 4.1 – Geometry of the analysed building - ground and second pavements (dimensions in mm) (De MATOS, 2020). . . . .	61
Figure 4.2 – Building façades (dimensions in mm). (a) AA' façade; (b) CC' façade; (c) BB' façade; and (d) DD' façade. . . . .	62
Figure 4.3 – Numerical model used in the present study. . . . .	62
Figure 4.4 – Force versus displacement curves. (a) 1 <sup>st</sup> LEC; (b) Equivalent Energy Elastic-plastic; and (c) bilinear curve (De MATOS, 2020); . . . . .	63
Figure 4.5 – Metallic connectors: (a) Hold-down; and (b) Angle Bracket. Adapted from Tie (2020); . . . . .	64



Figure 4.6 – Load-slip curve under shear for 16X-400 configuration. . . . .	65
Figure 4.7 – Detailing of 16X-400 STS connection. Elevation and plan view, respectively. (BROWN et al., 2021) . . . . .	65
Figure 4.8 – Representation of a beam element. (DIANA, s.d.). . . . .	66
Figure 4.9 – Representation of the MITC4 element. (DVORKIN; PANTUSO; REPETTO, 1995) . . . . .	67
Figure 4.10 – Representation of the MITC3 element. (LEE; LEE; BATHE, 2014) . . . .	67
Figure 4.11 – Hydraulic jack action over time during the tests: (a) monotonic test in the longitudinal direction; (b) monotonic test in the transverse direction; and (c) cyclic test in the transverse direction. (De MATOS, 2020). . . . .	68
Figure 4.12 – Maximum displacements in mm: (a) monotonic test in the longitudinal direction; (b) monotonic test in the transverse direction; and (c) cyclic test in the transverse direction. (De MATOS, 2020). . . . .	69
Figure 4.13 – Story Drift comparison: experimental and numerical model results. . . . .	70
Figure 4.14 – Deformed configuration after hydraulic jack load application. . . . .	71
Figure 4.15 – Experimental and numerical model comparison of base shear forces versus displacement at the top. . . . .	71
Figure 4.16 – Accelerogram of an event in Villacollemandina, Italy - 22nd September 2022 (Adapted from Luzi et al. (2016)). . . . .	73
Figure 4.17 – Accelerogram of an event in Manteigas, Portugal - 15th January 2018 (Adapted from Luzi et al. (2016)). . . . .	74
Figure 4.18 – Computation routine to generate accelerogram. . . . .	75
Figure 4.19 – Power Spectrum generated with Kanai-Tajimi filter to $\omega_s = 37.3$ rad/s and $\xi_s = 0.3$ . . . . .	76
Figure 4.20 – Ground accelerations over time generated using Kanai-Tajimi spectrum - $\omega_s = 37.3$ rad/s and $\xi_s = 0.3$ . . . . .	77
Figure 4.21 – Ground accelerations over time generated using Kanai-Tajimi spectrum - $\omega_s = 30.33$ rad/s, $\xi_s = 0.3$ and PGA = 0.15g. . . . .	77
Figure 4.22 – Ground accelerations over time generated using Kanai-Tajimi spectrum - Rock - $\omega_s = 8\pi$ rad/s, $\xi_s = 0.6$ and PGA = 0.15g. . . . .	78
Figure 4.23 – Ground accelerations over time generated using Kanai-Tajimi spectrum - Stiff Soil - $\omega_s = 5\pi$ rad/s, $\xi_s = 0.6$ and PGA = 0.15g. . . . .	78
Figure 4.24 – Ground accelerations over time generated using Kanai-Tajimi spectrum - Soft soil - $\omega_s = 2.4\pi$ rad/s, $\xi_s = 0.85$ and PGA = 0.15g. . . . .	78
Figure 5.1 – NBR 15421 (2023) elastic response spectrum. . . . .	80
Figure 5.2 – Portuguese elastic response spectrum. . . . .	80
Figure 5.3 – Italian elastic response spectrum. . . . .	81
Figure 5.4 – Stiffness changes through models. . . . .	85

Figure 5.5 – Load-displacement under tension curve comparison (Adapted from Rothoblaas (s.d.)). . . . .	87
Figure 5.6 – Load-displacement under shear curve comparison (Adapted from Rothoblaas (s.d.)). . . . .	87
Figure 5.7 – Stiffness changes through Rothoblaas’ models. . . . .	90
Figure 5.8 – Displacement profile in determined location due to different Kanai-Tajimi loading. . . . .	91
Figure 5.9 – Displacement profile due to real seismic loading. . . . .	93
Figure 5.10 – Displacement profile comparison of normalised loadings - PGA = 0.15g. . . . .	93
Figure 5.11 – Load pattern similar to first vibration mode - 1 kN/m and 0.5 kN/m at the top and middle, respectively. . . . .	97
Figure 5.12 – Equivalent SDOF transformation. . . . .	97
Figure 5.13 – Equivalent SDOF capacity curve. . . . .	98
Figure 5.14 – Equivalent SDOF capacity and bilinear curves. . . . .	99
Figure 5.15 – Comparison between RSC and Bilinear Capacity curves. . . . .	100
Figure 5.16 – CLT-concrete composite panel representation (SETRAGIAN; KUSUMA, 2018). . . . .	101
Figure 5.17 – Models capacity curve comparison. . . . .	102

## LIST OF TABLES

Table 2.1 – Finger joints configurations (Adapted from Brandner (2013)). . . . .	24
Table 3.1 – Ductility Classes proposed in the literature (REBOUÇAS et al., 2022). . . .	42
Table 3.2 – Consequence Classes (Adapted from EN 1998 (2021)). . . . .	43
Table 3.3 – Standard site categorisation (EN 1998, 2021). . . . .	44
Table 3.4 – Site amplification factors (Adapted from EN 1998 (2021)). . . . .	47
Table 3.5 – Default values of behaviour factors for regular elevation Cross-Laminated Timber buildings (EN 1998, 2021). . . . .	51
Table 3.6 – Capacity rules for DC2 and DC3 (EN 1998, 2021). . . . .	51
Table 3.7 – Standard site categorisation (Adapted from NBR 15421 (2023)). . . . .	52
Table 3.8 – Storey drift limitation (Adapted from NBR 15421 (2006)). . . . .	56
Table 4.1 – Experimental and numerical displacement in transverse direction results in comparison. . . . .	70
Table 4.2 – Properties used in Kanai-Tajimi’s method (SEYA; TALBOTT; HWANG, 1993). . . . .	76
Table 5.1 – Average displacements, maximum base shear and average stiffness by load case. . . . .	81
Table 5.2 – Modified models with AE116. Percentage of metallic connectors kept in the model. . . . .	83
Table 5.3 – Average displacements, maximum base shear and average stiffness by load case for model 1. . . . .	83
Table 5.4 – Average displacements, maximum base shear and average stiffness by load case for model 2. . . . .	83
Table 5.5 – Average displacements, maximum base shear and average stiffness by load case for model 3. . . . .	83
Table 5.6 – Average displacements, maximum base shear and average stiffness by load case for model 4. . . . .	83
Table 5.7 – Average displacements, maximum base shear and average stiffness by load case for model 5. . . . .	84
Table 5.8 – Average displacements, maximum base shear and average stiffness by load case for model 6. . . . .	84
Table 5.9 – Average displacements, maximum base shear and average stiffness by load case for model 7. . . . .	84
Table 5.10 – Average displacements, maximum base shear and average stiffness by load case for model 8. . . . .	84
Table 5.11 – Average displacements, maximum base shear and average stiffness by load case for model 9. . . . .	84

Table 5.12 – Average displacements, maximum base shear and average stiffness by load case for Rothoblaas changed model 0. . . . .	88
Table 5.13 – Average displacements, maximum base shear and average stiffness by load case for Rothoblaas changed model 1. . . . .	88
Table 5.14 – Average displacements, maximum base shear and average stiffness by load case for Rothoblaas changed model 2. . . . .	88
Table 5.15 – Average displacements, maximum base shear and average stiffness by load case for Rothoblaas changed model 3. . . . .	88
Table 5.16 – Average displacements, maximum base shear and average stiffness by load case for Rothoblaas changed model 4. . . . .	88
Table 5.17 – Average displacements, maximum base shear and average stiffness by load case for Rothoblaas changed model 5. . . . .	89
Table 5.18 – Average displacements, maximum base shear and average stiffness by load case for Rothoblaas changed model 6. . . . .	89
Table 5.19 – Average displacements, maximum base shear and average stiffness by load case for Rothoblaas changed model 7. . . . .	89
Table 5.20 – Average displacements, maximum base shear and average stiffness by load case for Rothoblaas changed model 8. . . . .	89
Table 5.21 – Average displacements, maximum base shear and average stiffness by load case for Rothoblaas changed model 9. . . . .	89
Table 5.22 – Average displacements, maximum base shear and average stiffness by load case for model 3 - DC2. . . . .	94
Table 5.23 – Average displacements, maximum base shear and average stiffness by load case for model 6 - DC2. . . . .	94
Table 5.24 – Average displacements, maximum base shear and average stiffness by load case for Rothoblaas changed model 3 - DC2. . . . .	94
Table 5.25 – Average displacements, maximum base shear and average stiffness by load case for Rothoblaas changed model 6 - DC2. . . . .	94
Table 5.26 – Model 3 results comparison between DC1 and DC2. . . . .	95
Table 5.27 – Model 6 results comparison between DC1 and DC2. . . . .	95
Table 5.28 – Rothoblaas changed model 3 results comparison between DC1 and DC2. . . . .	95
Table 5.29 – Rothoblaas changed model 6 results comparison between DC1 and DC2. . . . .	96
Table 5.30 – Significant Damage Limit State Displacements. . . . .	100
Table 5.31 – Average displacements (mm), maximum base shear (kN) and average stiffness (kN/m) by load case for hybrid CLT-concrete model. . . . .	102

## LIST OF ABBREVIATIONS AND ACRONYMS

ABNT	<i>Associação Brasileira de Normas Técnicas</i> (in English: Brazilian Association of Technical Standards)
CLT	Cross-laminated Timber
GLULAM	Glued-laminated Timber
NBR	<i>Norma Brasileira Regulamentadora</i> (in English: Brazilian Regulatory Standard)
SDOF	Single-degree-of-freedom
MDOF	Multi-degree-of-freedom
CEN	<i>Comité Européen de Normalisation</i> (in English: European Normalisation Committee)
EN	European Standard
EC8	Eurocode 8 - EN 1998
CC	Consequence Class
NDP	National Defined Parameter
DC	Ductility Class
SPT	Standard Penetration Test
LEC	Load Envelope Curve
EEEP	Equivalent Energy Elastic-Plastic
PGA	Peak Ground Acceleration
FT	Fully-Threaded
STS	Self-Tapping Screw
RSC	Response Spectrum Curve

## LIST OF SYMBOLS

$S_a$	Spectral acceleration
$T$	Period
$\mathbf{M}$	Mass matrix
$\mathbf{C}$	Damping matrix
$\mathbf{K}$	Stiffness matrix
$\vec{u}$	Acceleration vector
$\vec{u}$	Velocity vector
$\vec{u}$	Displacement vector
$l_{FJ}$	Finger joint length
$p$	Pitch
$b_t$	Tip width
$b_n$	Base width
$l_t$	Tip gap
$\alpha$	Flank angle
$v(b_n)$	Loss in cross section
$M$	Seismic magnitude
$A$	Seismic waves amplitude
$\Delta t$	Time interval
$M_o$	Seismic moment
$\mu$	Rock shear module
$S$	Rupture Area
$D$	Average displacement
$M_w$	Seismic moment magnitude
$\mathcal{F}$	Fourier transform

$\omega$	Frequency in rad/s
$f$	Frequency in Hz
$g$	Time domain generic function
$\mu_L$	Local ductility
$\mu_S$	Storey ductility
$\mu_G$	Global ductility
$\phi_{max}$	Maximum rotation in elastic region
$\phi_y$	Yield rotation
$v_{s,H}$	Equivalent value of the shear wave velocity of the superficial soil deposit
$H$	Depth
$h$	Thickness of the soil layer
$H_{800}$	Seismic bedrock depth
$d_r$	Interstorey drift
$\lambda_s$	Drift limitation coefficient
$h_s$	Interstorey height
$S_e(T)$	Elastic response spectrum
$T$	Vibration period of a linear SDOF
$S_\alpha$	Maximum response spectral acceleration
$S_\beta$	5% damped response spectrum
$T_A$	Short-period cut-off associated to the zero-period spectral acceleration
$F_A$	Ratio between $S_\alpha$ and zero-period spectral acceleration
$T_C$	Upper corner period period of the constant spectral acceleration range
$T_B$	Lower corner period of the constant spectral acceleration range
$T_D$	Corner period at the beginning of the constant displacement response range of the spectrum
$\eta$	Damping correction factor

$r_\alpha$	Empirical factor related to $F_\alpha$
$r_\beta$	Empirical factor related to $F_\beta$
$S_{\alpha,RP}$	Spectral parameter for $T_{ref}$ considering performance factor
$S_{\beta,RP}$	Spectral parameter for $T_\beta = 1s$ considering performance factor
$g$	Gravity acceleration
$F_{Rk,d}$	Strength characteristic value in dissipative zones
$F_{Rd,d}$	Strength design value in dissipative zones
$k_{deg}$	Degradation under cyclic loading factor
$k_{mod}$	Load duration and moisture content factor
$\gamma_M$	Material partial factor
$\gamma_{Rd}$	Overstrength factor
$F_{Ed,E}$	Design seismic effect in the non-dissipative joint or member
$F_{Ed,G}$	Non-seismic design actions during seismic situation
$\Omega_d$	Minimum value of all overstrength ratios
$V_{Rd,a}$	Design lateral strength of shear-wall and storey
$V_{Ed,E}$	Design global shear in shear-wall and storey
$M_{Ed,E}$	Design rocking moment
$F_{Rd,b}$	Non-dissipative design strength
$\bar{v}_s$	Propagation average shear waves velocity
$\bar{N}$	SPT blows average number
$C_s$	Seismic response coefficient
$W$	Structure weight
$H_b$	Horizontal force at structure's base
$a_{gs0}$	Amplified spectral acceleration for 0 s period
$a_{gs1}$	Amplified spectral acceleration for 1 s period
$C_a$	Soil amplification coefficient for 0 s period



$C_v$	Soil amplification coefficient for 1 s period
$F_i$	Characteristic force applied in determined storey
$C_{v,i}$	Vertical distribution coefficient
$\mu_p(t_s)$	Mean value of sample function in instant $t_s$
$p(t)$	Sample function
$e$	Euler-Mascheroni constant
$S(\omega)$	Artificial seismic spectrum
$S_0$	Spectral density constant
$\omega_g$	Ground natural frequency in rad/s
$\xi_g$	Soil damping

# SUMMARY

<b>1</b>	<b>INTRODUCTION</b>	<b>19</b>
1.1	OBJECTIVES	21
1.2	DISSERTATION OVERVIEW	22
<b>2</b>	<b>LITERATURE REVIEW</b>	<b>23</b>
2.1	CROSS-LAMINATED TIMBER: BACKGROUND	23
2.1.1	CLT in Europe and Portugal	27
2.1.2	CLT in Latin America and Brazil	28
2.2	STATE-OF-THE-ART	30
<b>3</b>	<b>THEORETICAL FOUNDATION</b>	<b>33</b>
3.1	SINGLE-DEGREE-OF-FREEDOM (SDOF) SYSTEM	33
3.2	MULTI-DEGREE-OF-FREEDOM (MDOF) SYSTEM	34
3.3	SEISMIC ENGINEERING	35
3.3.1	Seismic Activity	35
3.3.2	Seismic Waves	36
3.3.3	Intensity and Magnitude	37
3.4	RESPONSE SPECTRUM CURVES	38
3.5	DUCTILITY	40
3.6	EN 1998:2021	42
3.6.1	Ductile Design for Timber Structures	48
3.7	ABNT NBR 15421:2023	52
3.8	PUSHOVER ANALYSIS AND N2 METHOD	56
<b>4</b>	<b>METHODOLOGY</b>	<b>59</b>

4.1	CALCULATION PARAMETERS . . . . .	59
4.2	NUMERICAL MODEL . . . . .	60
4.3	MODEL VALIDATION . . . . .	68
4.4	LOAD CASES . . . . .	72
4.4.1	Seismic Data . . . . .	72
4.4.2	Kanai-Tajimi Spectrum . . . . .	75
<b>5</b>	<b>RESULTS AND DISCUSSION . . . . .</b>	<b>79</b>
5.1	RESPONSE SPECTRUM CURVES . . . . .	79
5.1.1	Parametric Study on Angle Bracket Sizing . . . . .	82
5.1.2	Parametric Study on Angle Bracket Mechanical Behaviour	86
5.2	ARTIFICIAL KANAI-TAJIMI AND REAL EVENT ACCELE- ROGRAMS . . . . .	90
5.3	ANALYSIS UNDER DUCTILE CLASS 2 . . . . .	94
5.4	PUSHOVER ANALYSIS - N2 METHOD . . . . .	96
5.4.1	Pushover Load Pattern . . . . .	96
5.4.2	Equivalent SDOF of the MDOF structure . . . . .	96
5.4.3	Target Displacement . . . . .	97
5.4.4	MDOF Displacement Results . . . . .	99
5.5	HYBRID CLT-CONCRETE COMPOSITE BUILDING . . . . .	100
5.6	RESULTS COMPARISON . . . . .	103
<b>6</b>	<b>FINAL CONSIDERATIONS . . . . .</b>	<b>105</b>
	<b>REFERENCES . . . . .</b>	<b>107</b>
	<b>APPENDIX A MATLAB KANAI-TAJIMI GENERATION CODE .</b>	<b>114</b>

## 1 INTRODUCTION

Construction is not only a temporary project, comprehending the time needed to completely deliver a finished building but also a whole economic sector with fundamental importance. If it is observed solely the physical work developed *in situ*, a great part of the production chain is ignored. Engineering is now paying more attention to the whole process, such as the impact of each material and method employed. As a consequence of that, it is possible to notice new materials aiming to improve construction sustainability and productivity. Even though it is a crucial demand, construction can be very harmful to the environment, since it is responsible for a good share of greenhouse gases, solid waste and natural resources consumption. In Brazil, for example, concrete and masonry constructions are marked to represent a high production cost, low planning, low worker qualification and high wastage (OLIVEIRA, 2018).

Cross-laminated timber (CLT) is an option largely used worldwide when these aspects are taken into consideration. It is considered an engineered material manufactured offsite and it has strength in both directions due to its lamination method. When compared to reinforced concrete or steel constructions, CLT has the advantage of being able to reduce the weight of the whole building when finished. Lighter structures demand less material in foundations and fewer fossil fuel-driven vehicles are necessary in transportation. Allied with sustainability, productivity is also a point of discussion in favour of CLT, once it can provide time reduction in construction, crucial to investors, and fewer workers onsite.

Regarding CLT production, logs are laminated in cross-grain panels and assembled normally in 3 up to 7 layers with orthogonal directions. This method guarantees strength to CLT elements to demands in or out of the plane, once it has fibre alongside its length and width. One can note that the CLT production method is very similar to Glued Laminated Timber (GLULAM), only differed by the lamellae glued without grain direction changes and aimed to create linear elements. CLT, on its hand, aims to create structural panels for walls and floors. This comparison between GLULAM and CLT can be easily simplified with older materials already in use in Civil Construction, such as reinforced concrete, when objectifies shaping load-bearing linear elements, and structural masonry, to build load-bearing walls, observed material differences. When two directions are taken into consideration, in a slab case, for example, reinforced concrete and CLT will have similar properties. However, timber designing buildings, GLULAM or CLT-based, will have metallic connectors playing an important role in building stiffness and, in the end, the whole behaviour under static and dynamic loads. In Branco et al. (2019) it is possible to observe that, under lateral loads, CLT building failure will occur mainly at these elements and

this will represent the weakest point in the structure. Therefore, this is an important step taken into consideration during the designing stage.

Timber structures, in most types, need special attention to surface preparation aiming for shrinkage and swelling prevention, due to water absorption, fire degradation and acoustics. As a consequence of that, CLT has offsite steps to establish weathering resistance under use. To be specific, it is provided with an oven-dried preparation to ensure that the wood reaches 12% moisture, aiming for microorganism attack prevention and shrinkage due to water loss. Fire and water absorption can be easily repelled with onsite surface preparation, in the finishing stage, with the aid of appropriate varnish usage, assuring flame retardant and waterproofing behaviours. As a natural material, timber has different physical and mechanical properties when compared to concrete and steel. Both the latter can be described as isotropic, where properties are valid in all directions, while the former has anisotropic characteristics when fibre direction will matter to define final element properties. Wood, more specifically, can be described as orthotropic, where properties vary along two orthogonal axes. In summary, loads must be placed in parallel to the grains' direction to obtain the best strength out of the material, especially in tension and compression. Concerning acoustic behaviour, traditional timber framed buildings, due to their lower density, have poor classifications in terms of performance when compared to other constructive methods. Still, CLT panels offer better acoustic performance than other timber structures due to their significantly higher density, offering better isolation (PANG; ROSOWSKY, 2010).

Despite its usage in buildings worldwide, with examples with up to 9 storeys in the United Kingdom (Stadhaus Building, located in London, presented in Figure 1.1), it is not a construction system with extensive content available in the literature. State of art in CLT buildings is presented in Chapter 2. In observation of that, studies are conducted to evaluate CLT buildings under dynamic loads, such as wind and seismic, and concerning designing methods. Therefore, it is needed to better understand these structures submitted to dynamic loads and connectors behaviour aiming to establish better designing techniques and optimised structures.

Recently, the *Comité Européen de Normalisation* (CEN), the recognised association by the European Union to develop European Standards (EN), started a process to review the EN 1998 (Eurocode 8). This code relates to the designing criteria of earthquake-resistant structures and brings specific recommendations to each construction system and was first launched in 2004. The most recent draft, made by CEN/TC250/SC8 and dated May 2021, to be simply referred to as Eurocode 8 (EC8) from now on, pays attention to site categorisation and amplification factors modifications. This revision was proposed in order to better describe the soil influence in the analysis. Alongside that, modifications in site amplification factors were performed to achieve a better formulation, with a smoother transition between classes (PAOLUCCI et al., 2021). Moreover, aiming to fulfil the European Commission's objective to embrace new materials

(M/515, 2019) the recent review also included CLT aspects into timber construction materials. This is an important step towards technology acceptance since it brings safety to Engineers in the designing phase.



Figure 1.1 – Stadthaus Building in Murray Grove Street, London.  
(Wood Skyscrapers, *s.d.*).

## 1.1 OBJECTIVES

This work aims to address parallels between experimental data available in the literature and models created following the Eurocode 8 new proposition and NBR 15421 prescriptions. With this in mind, practical objectives can be described as:

- a) **Modelling:** Perform a numerical analysis of the real scale CLT building tested in De Matos (2020). The model shall be validated with results available in the literature.
- b) **Building Ductility:** this goal is to verify the building response as it was designed to compass with ductility criteria. Different methods will be employed to assess the adequacy of the design for the seismic region proposed, *i.e.*, Guimarães, Portugal. Consequently, a discussion of the implications of adopting specific ductility criteria for different seismic risks will be conducted.

- c) Seismic Excitation: use real events to evaluate the seismic performance of the CLT building in the proposed scenarios. Introduce an artificial accelerogram by means of the Kanai-Tajimi filtering in order to induce resonance and to evaluate the results on different occasions. Employment of Response Spectrum Curves to analyse the prescriptions of both normatives, comparing each other under a normalised scenario.
- d) Design Improvements: suggest a less conservative design to the experimental building according to Eurocode 8 and NBR 15421. Compare the results obtained and make recommendations on structural enhancement.

## 1.2 DISSERTATION OVERVIEW

This study is separated into four different approaches: model validation, according to experimental data; building improvement following both European and Brazilian standards by means of a parametric evaluation; assessment of the building's behaviour when submitted to real events loading and to Kanai-Tajimi filtering accelerogram; and, finally, a non-linear static analysis to evaluate the seismic capacity of the structure. In the end, all results are compared and conclusions are taken and explored.

In terms of the document construction, chapters are separated as follows:

- Chapter 1: CLT introduction and presentation of concerns that motivate the study of a sustainable construction system.
- Chapter 2: a literature review of relevant topics concerning CLT state-of-art revision.
- Chapter 3: theoretical foundation regarding pertinent subjects to the study, such as building designing, structural behaviour and seismic engineering. Presentation of Eurocode 8 and NBR 15421 methodologies.
- Chapter 4: Methodology of analysis. This chapter will present all details concerning the numerical models and validations of the simulations. Being the main tool used in this study, the formulation of the numerical model shall be very clear and concise to the reader, in order to enable the reproduction and improvement of the methods used.
- Chapter 5: presentation of the obtained results due to the application of the previous methodology.
- Chapter 6: Final considerations and recommendations to design.

## 2 LITERATURE REVIEW

Here, a brief state-of-the-art concerning the relevant topics addresses this study is presented. A review of Cross-laminated Timber will be provided and explained its usage and applications, as well as the generic approach to its implementation in the construction market.

### 2.1 CROSS-LAMINATED TIMBER: BACKGROUND

Cross-laminated Timber is one product of the Construction Industry aimed to improve productivity allied with green buildings and sustainable ballast in all systems and materials. Many studies have been carried out in the past few years concerning CLT construction due to its use in new buildings in Central Europe. More recently, North American and Australian markets have been also adopting CLT as building material (LAGUARDA-MALLO; ESPINOZA, 2016).

CLT has been developed since the '90s, being the first study carried out in Switzerland and Austria (CREPELL; GAGNON, 2010). It is a strong alternative to traditional heavy structural systems, such as concrete and steel. CLT panels are produced out of spruce (*picea abies*) sideboards with approximately 400 kg/m<sup>3</sup> (UNTERWIESER; SCHICKHOFER, 2013) and these lamellae are glued following the same grain orientation, with finger joint connections, to form CLT layers. Then, after the layer production, each one of them is glued with a perpendicular grain direction. A schematic representation is made in Figure 2.1. Regarding panel solidarization, it is usually employed quasi-rigid adhesive bounding, including 3 different types: phenoplast- and aminoplast-adhesives, one-component polyurethane adhesives (1K-PUR) and emulsion-polymer-isocyanate adhesives (EPI) (SIKORA; HARTE; MCPOLIN, 2014).

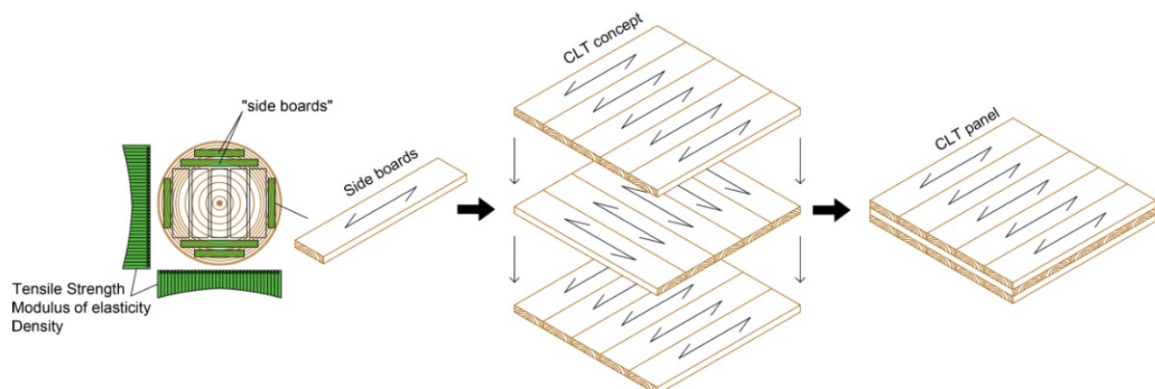
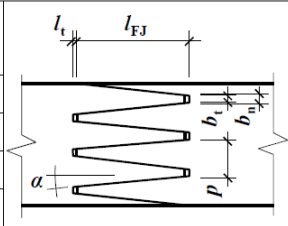


Figure 2.1 – CLT panels conception (De MATOS, 2020).



It is important to bring under consideration wood treatment before lamellae glueing. As presented in Figure 2.1, sideboards are used to form layers, which present higher stiffness and strength than other zones of the log. However, one can note that nothing was mentioned concerning wood growth characteristics which represent weak spots, not matching strength requirements, such as knots or even inadequate wood processing. With that in mind, the material preparation is done by cutting out these points and reconnecting lamellae and, to guarantee proper load transfer, finger joints are specified. This type of connection is intended to maximise bonding surface without longitudinal material losses and enables simple and fast joints between elements (BRANDNER, 2013). An overview of recommended finger joint profiles is presented in Table 2.1. The same table also presents a schematic edgewise finger joint, where the connection is visible in the side face, in contrast to the flatwise, where the finger configuration is only visible on the narrow lamella face. Also, finger joints must be placed in different cross sections, aiming to distribute them along the CLT layer.

Table 2.1 – Finger joints configurations (Adapted from Brandner (2013)).

$l_{FJ}$ [mm]	$p$ [mm]	$b_t$ [mm]	$b_n$ [mm]	$l_t$ [mm]	$\alpha$ [°]	$v(b_n)$ [%]	
15	3.8	0.42	0.52	0.5	5.6	13.6%	
20	5.0	0.50	0.60	0.5	5.7	12.0%	
20	6.2	1.00	1.11	0.5	6.0	17.8%	
50	12.0	2.00	2.48	3.0	4.6	20.7%	

$l_{FJ}$  ... finger length;  $p$  ... pitch;  $b_t$  ... tip width;  $b_n$  ... base width;  $l_t$  ... tip gap;  $\alpha$  ... flank angle;  $v(b_n)$  ... loss in cross section

The design of CLT structures is still not completely reflected by codes. Different studies show that, despite the growing use of this technology, there is a lack of a method to properly specify and detail CLT-based shear walls and floor diaphragms (LUKACS; BJÖRNFOT; TOMASI, 2019). However, it is very well accepted, as presented by Branco et al. (2019) and Scotta et al. (2016), that metallic connectors play an important role in the design of CLT structures and are considered key points to structural safety. Typically, two types of connectors are employed: angle brackets, to provide shear resistance, and hold-downs, to ensure uplift resistance - see Figure 2.2(h). To design these connectors, accordingly to Lukacs, Björnfot and Tomasi (2019), the methods used can be summarised as:

If not explicitly stated, all of the methods resist overturning by hold-downs (HD), and translation by angle brackets (AB) exclusively as was first proposed by Ceccotti et al. [6]<sup>1</sup>. This means that an interaction of vertical and horizontal forces in the connections is not typically considered as there is limi-

<sup>1</sup> Citation in the original text: CECCOTTI, A.; FOLLESA, M.; LAURIOLA, M.P.; SANDHAAS, C.; MINOWA, C.; KAWAI, N.; et al. Which seismic behaviour factor for multi-storey buildings made of Cross-Laminated wooden panels? In: **39th CIB W18 Meeting - CIB-W18/39-15-4**. Florence, Italy: [s.n], 2006

ted experimental data and no current design guidance (Reynolds et al. [17]<sup>2</sup>). Thus, the load-carrying capacity ( $F$ ) of the CLT shear wall can be simplified as  $F = \min(F_R; F_T)$  where  $F_R$  and  $F_T$  denotes the load-carrying capacity by rotation and translation respectively.

As stated in Aquino (2020), for dowel-type joints it is necessary to follow two design criteria: one analysis concerning local stress and the other regarding the structure studied globally. Firstly, it is necessary to study the connector's plasticity locally as well as the timber cross-section strength at the joint. This is done to guarantee that it will be able to dissipate energy throughout its deformation without brittle failure. This property will be better discussed in Section 3.5. Then, when globally observed, it is necessary to specify connector spacing between each other to ensure that their sole strength, when summed, will be equal to designing rotation and translation load-carrying demands. Despite the study being conducted for a specific type of wood joint, it is the method employed for other types as well, such as those presented in Figure 2.2.

Recently, De Matos (2020) carried out a series of studies aiming to establish a numerical approach concerning a pushover analysis to a 2-storey CLT building. Initially, it was proposed an experimental campaign of typical connectors made out of steel, was used to connect CLT panels among each other and to the foundations. In this project, two connectors models were used: HTT22, hold-downs, and the AE116, angle brackets, both from the American manufacturer Simpson Strong-tie. These connectors were experimentally tested in accordance to the CEN EN 12512 (2006) to obtain load-displacement curves. Then, a real-scale CLT building was submitted to quasi-static tests in order to assess the 3D performance under lateral loadings.

<sup>2</sup> Citation in the original text: REYNOLDS, T.; FOSTER, R.; BREGULLA, J.; CHANG, W.; HARRIS, R.; RAMAGE, M. Lateral-Load Resistance of Cross-Laminated Timber Shear Walls. **Journal of Structural Engineering**, vol. 143, n. 12, 2017.

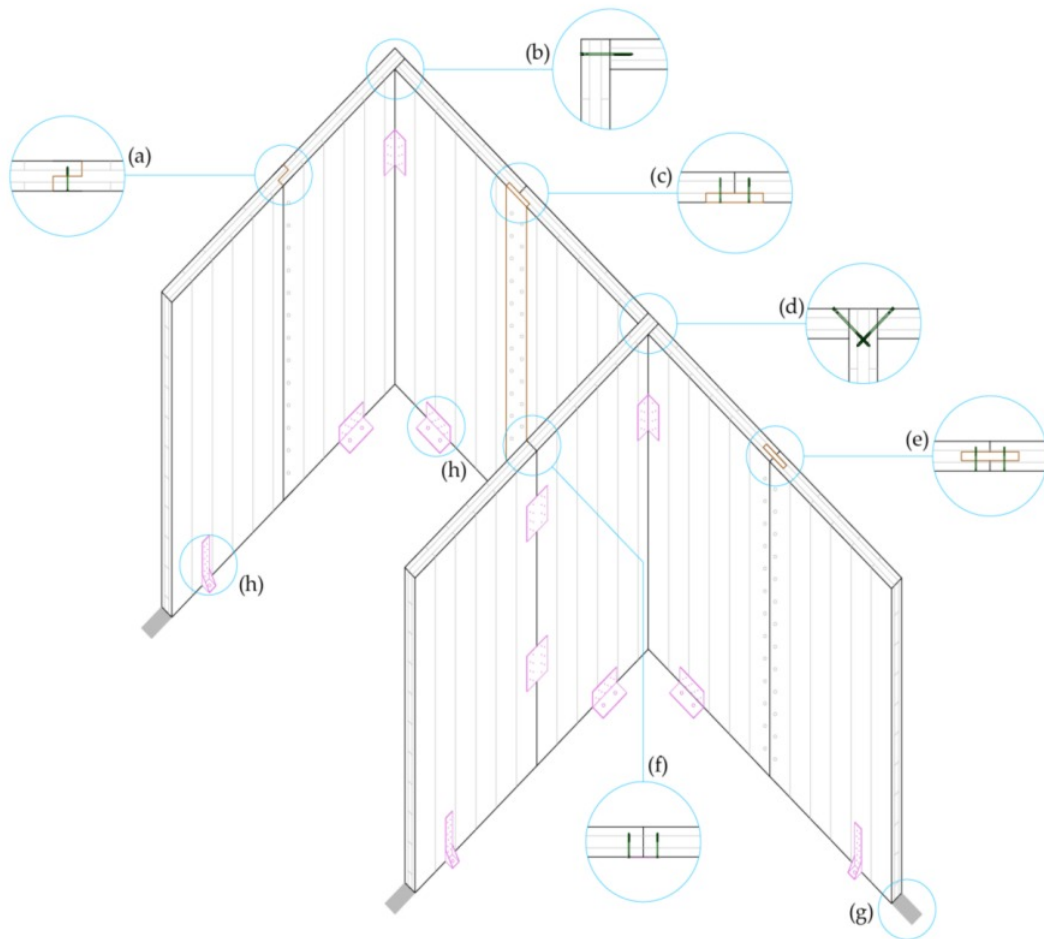


Figure 2.2 – Typical connectors used with CLT panels. (a) coupled wall with lap joint; (b) 90° corner joint; (c) coupled wall with external spline joint; (d) wall intersection/T-shaped joint; (e) coupled wall with internal spline joint; (f) single wall joined with steel plates; (g) decoupling strip; (h) fasteners - hold-downs and angle brackets. (DI BELLA; MITROVIC, 2020)

The tested building, see Figure 2.3, layout had a 4.5 m width, 9.1 m length and a total height of 5.04 m. It was architecturally designed to be a truthful edification, *id est*, with wall and floor openings characteristic of a realistic building. An asymmetric geometry was assumed in the design to evaluate torsion under seismic loads. Walls CLT panels used in the construction were made out of spruce (*Picea abies*) with 5 layers of 20 mm each, reaching 100 mm thickness, while floor panels were 3-layered with 40 mm thickness, reaching 120 mm total. Considering wood orthotropic properties, fasteners were only applied to the shear walls in each direction tested (De MATOS, 2020).



Figure 2.3 – Real scale CLT building, tested Experimental CLT cle at the University of Minho lab facilities. (De MATOS, 2020).

The building was submitted to two types of loads: lateral concentrated load and distributed load, perpendicular to floors. The first one was done to represent seismic action and was simulated with hydraulic jacks. The last was added to recreate a real scenario with a live load, simulated with water vats in the experiment.

### 2.1.1 CLT in Europe and Portugal

CLT is mainly used as a construction material in Europe. Since its development, carried out in Europe in the 1990s, it has been used as a competitive alternative to steel, masonry and concrete constructions. Global production is mainly concentrated in central Europe and has grown considerably. In its first 15 years, from 1995 to 2010, CLT production doubled from 100,000 to 200,000 m<sup>3</sup> annually (ESPINOZA et al., 2016). German-speaking countries hold 80% of all installed production capacity, being Austria, Germany and Switzerland the main manufacturers. Allied with new constructions, CLT is considered a good alternative to building rehabilitation, considering the need to provide corrective maintenance, presenting advantages, such as material compatibility; reduced self-weight; reduction in elements dimensions; and rapid assembling (COSTA, 2013).

In Portugal, however, traditionally wood is most considered to be used decoratively. Structural and sealing usage became more popular after the 1755 Lisbon earthquake when it needed rapid

reconstruction. Albeit public perception over timber construction made it not interesting to explore when compared to other materials, wood became an option again in the occasion of the industrialisation of the sector, at the end of the XX century. Nowadays, timber construction still represents the minority of the construction market, representing 5% of new buildings, however with greater technology and using prefabricated elements. As in Brazil, the Portuguese people still associate timber construction with fragility and fire susceptibility (MEZEIRO, 2018).

Europe has seen lots of CLT buildings being raised in the last few years. It was a result of a joint effort made by the industry and construction market with academia and researchers (CRESPELL; GAGNON, 2010). Examples are the already mentioned 9-storey Stadthouse, in London, the 14-storey Treet, in Bergen, and the 18-storey Mjøstårnet, in Brumunddal. All of these multi-storey buildings with medium to high heights are examples of successful implementation of the CLT technology, allied or not with other structural elements - GLULAM beams, for example.

### 2.1.2 CLT in Latin America and Brazil

As previously mentioned, Civil Construction in Brazil is marked to have high rates of waste, low manpower qualification and low index of industrialisation. These aspects certainly contribute to and have a great impact on the low productivity of the sector. Traditionally, building in Brazil means the employment of heavy and high-embodied energy construction materials, such as concrete – reinforced or precast – and masonry – sealing only or structural.

New construction methods in Brazil bump into these socioeconomic factors in manpower and still in buyers' and investors' acceptability of lighter constructive methods. It is common sense, despite the lack of scientific foundation, that masonry necessarily represents durability and safety, disregarding technology embedded in lighter materials (GOMES; LACERDA, 2014). However, considering wood structures are not cultural in the region, companies are developing CLT assembly industries with promises of competitive values when compared to traditional systems. The first multi-storey building was concluded firstly in 2020, located in São Paulo – see Figure 2.4. This represents that, despite imposed barriers, sustainable construction is getting space in the construction market and must be the object of studies to improve techniques.

Another factor to be taken into consideration for the expansion of CLT use in Brazil is the climate it is inserted. One of the main concerns in mass timber construction is ensuring its durability throughout its lifespan. The lamination method contributes to the stability of the dimensional properties of the panels. However, there is still vulnerability of the CLT structure to moisture, which is an important point to be addressed in order to prevent failure of the structural system (ARAUJO et al., 2023). The autoclave treatment of the wood to prevent organic attacks allied with controlled moisture are the main techniques used to reduce the vulnerability of wood structures (BRANDNER, 2013; BELIZÁRIO et al., 2023). Also, the cladding used in the finishing phase is

an important factor to contribute to the conservation matter of the structural system, as in other materials also. These techniques can be incorporated in the chain of production as presented in Fig. 2.5.



Figure 2.4 – First CLT building in Brazil (Fran Parente (*s.d.*)).

Recently, the Brazilian code for timber structures design was reviewed and mass timber materials were included with some calculation remarks. It is the case of glued laminated and cross-laminated timber. It is an important step for timber engineering in Brazil since standardisation is up-to-date concerning new technologies, incentivising new projects with safety measures already in the designing phase. With this new code, 25 years after the last revision, Brazil's code got similar assessments of timber construction as CEN EN 1995 (2004), which specifically addresses the designing of timber structures in Europe.

Regarding the usage of light construction in timber over Latin America, it is possible to notice the implementation of these new techniques in Chile. However, the initiative to introduce the technology in the Chilean construction market is subsidised with the financial support of *Corporación de Fomento - CORFO* and *Cámara Chilena de la Construcción*. The project aims to study the technical and economic viability of this method of construction as well as study local timber aspects and performance to analyse usage for social housing in Chile (PINA et al., 2015).

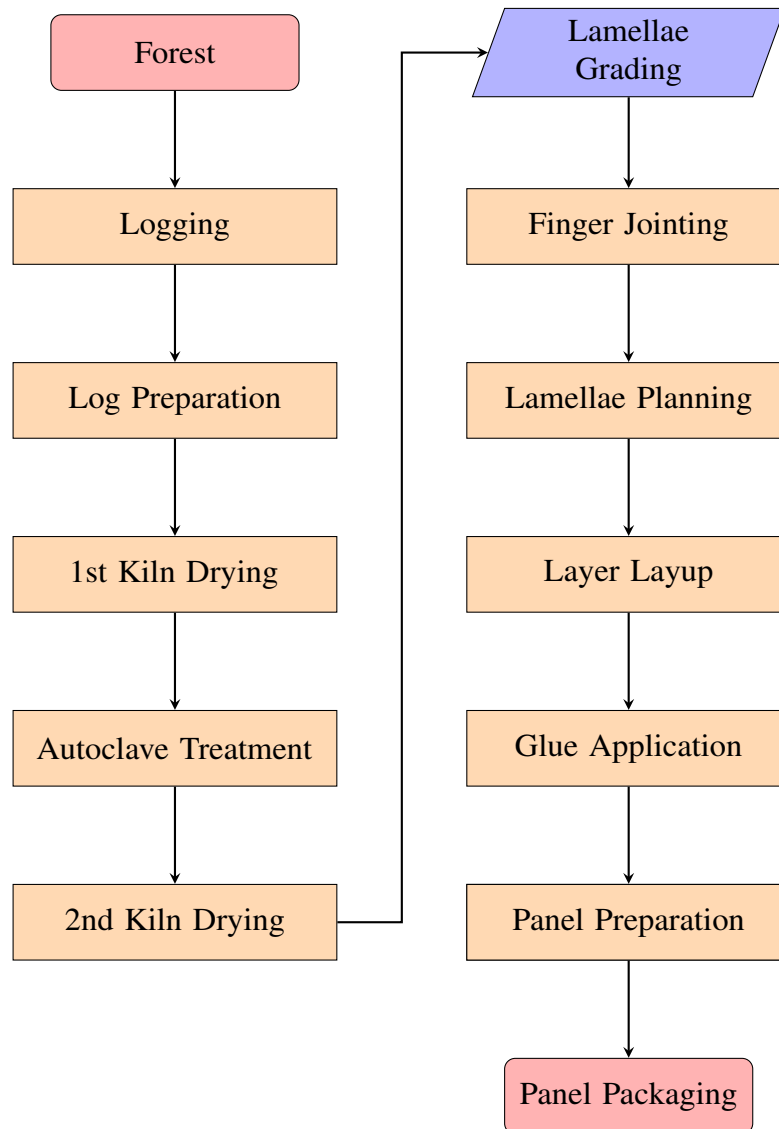


Figure 2.5 – Scheme of CLT manufacturing.

## 2.2 STATE-OF-THE-ART

As previously stated, the increasing interest in mass timber construction, especially the CLT, resulted in various research carried out in different places. The literature concerning this material is mainly produced by Canada, China, Italy and United States (TEIXEIRA et al., 2023).

Concerning CLT structural response, it is important to evaluate the wood species' mechanical properties to better assess its usage in a structural system. Many studies can be found in the literature regarding the bending and shear performance of CLT panels considering different species, such as:

- the Spruce-pine-fir and Douglas fir-Larch in ANSI/APA PRG 320 (2018);
- Canadian hemlock in He, Sun and Li (2018);

- Irish Sitka spruce in Sikora, McPolin and Harte (2016);
- Australian Radiata pine in Navaratnam et al. (2020); and
- Southern pine in Hindman and Bouldin (2014).

Alongside that, it is also possible to find local wood species in Brazil with mechanical properties characterisation, as seen in:

- *Pinus taeda* in Vilela and Mascia (2021);
- *Eucalyptus grandis* in Garcia et al. (2021); and
- *Hevea brasiliensis* in Garcia et al. (2021).

The material characterisation is a major step in structural calculation. With this information available in the literature, it is possible to apply to the model the mechanical properties considering the timber availability in the region. The modelling of CLT structures is usually carried out using Finite Element Analysis. Thus, there are two main practical approaches to consider the CLT panel within a FEM model: some authors adopt the composite theory allied with the shear analogy method (BLASS; FELLMOSE, 2004; MARTÍNEZ-MARTÍNEZ; ALONSO-MARTÍNEZ; DÍAZ, 2018) and others follow the plate theory (STURZENBECHER; HOFSTETTER; EBERHARDSTEINER, 2010). It is also possible to use 3D modelling with solid elements, with a cost of high computational effort. Recently, Mendes (2020) conducted an experimental and numerical analysis concerning the CLT panel modelling, comparing different theories. During this study, the author modelled the panels experimentally built using Classical Plate Theory (CPT), First Order Shear Deformation Theory (FSDT), Murakami's Zig-Zag Plate Theory (MZZT), Ren's Plate Theory (RPT) and Pagano's Layer-wise Theory (REDDY, 2004). It showed the importance of taking into consideration the shear influence when modelling these types of structures, especially when using shell elements in the mesh construction. Theories that neglect the influence of shear, such as FSDT, need the usage of shear-correction factors in displacement and tension calculation.

Studies have also been conducted on the seismic resilience of Cross-Laminated Timber structures with the aim of assessing their safety. To achieve this requirement, it is essential to establish in the design the elements responsible for giving the model a ductile behaviour since timber is prone to brittle failure (JORISSEN; FRAGIACOMO, 2011). This is presented as the main challenge of new studies since this structural system has limited ductile parts to provide general inelastic behaviour (LI; TSAVDARIDIS, 2023). In Tran and Jeong (2021), the authors presented analytical procedures to evaluate the nonlinear and elasto-plastic behaviour under lateral forces of shear



walls. The achieved differences between the lateral resistance of predicted and experimental curves were near 10.7%. In Li and Tsavdaridis (2023) it is presented an analysis of newly proposed reinforcements to shear wall systems. The study shows that these new designs can improve dynamic performance as dowel-type fasteners are used in higher diameters. Alongside the technical applicability, the authors also approach the constructability and manufacturability of these connectors, to analyse if their usage is viable. Besides the difficulties intrinsic to the structural system, CLT has shown promising seismic-resistant properties in several studies. However, there are still much to improve concerning simplified numerical methods to predict response under dynamic excitations (IZZI et al., 2018).

### 3 THEORETICAL FOUNDATION

Dynamic analysis of buildings under seismic loads is normally designed according to local codes. In this study, EN 1998, broadly known as the Eurocode 8 (EC8), and NBR 15421 procedures were adopted. The aim is to study CLT implementation considering both codes since it has been recently introduced to Brazilian norms while EC8 is under revision to introduce important advances towards timber construction. Both codes are in use of the Response Spectral Curves Method, which is further explained in Section 3.4. The former is used to design structures in Europe, complemented by some National Annexes in some countries, and the latter is yet shyly used in Brazil to verify the building behaviour under seismic loads, a country with no seismicity issues so far.

The focus of this study is on Single-degree-of-freedom and Multi-degree-of-freedom systems, with the goal of providing the reader with a comprehensive grasp of the study process. To achieve this, the study elucidates the simplifying assumptions made by both codes to facilitate practical design. Moreover, it offers an in-depth exploration of seismic concepts utilized in the analysis.

#### 3.1 SINGLE-DEGREE-OF-FREEDOM (SDOF) SYSTEM

The simplest system subject to a dynamic analysis is a single-degree-of-freedom (SDOF) one. The degree of freedom can be described as the number of variables needed to fully characterise the position of all masses studied in the problem. That is, if a system of 2 masses can be determined with only one variable, being the second function of the other, it can be studied as an SDOF system. Many times, the number of masses in the structure may be the same as the number of degrees of freedom, but it is not correct to establish its definition this way since it has its particularities. Concerning dynamic loads, the essence of analysis is introducing an excitation to the system, aiming to reach the displacement values, and consequently, velocity and acceleration, that will be able to achieve the equilibrium when an external force is introduced to Equation 3.1. SDOF system with arbitrary load can be described in Figure 3.1.

The solution of the equilibrium equation is done with numerical techniques. Two methods are widely used as the most important to solve Equation 3.1 with arbitrary transient loads, the central finite differences scheme, used in nonlinear systems, and the Duhamel integral, used in linear systems. Basically, finite differences need restrictions concerning time steps used, increasing computational processing time and effort, making Duhamel the best option for linear analysis.

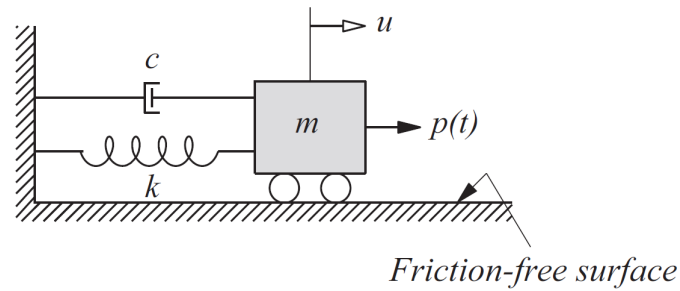


Figure 3.1 – Single-degree-of-freedom system subjected to arbitrary load (DAGDELEN; RUHANI, 2018)

Unfortunately, the Duhamel technique is based on the superimposition of vibration modes, making its usage not a good fit for nonlinear systems, without further linearisation methods (NEELA, 2011).

### 3.2 MULTI-DEGREE-OF-FREEDOM (MDOF) SYSTEM

As an evolution of an SDOF system, MDOF structures need, by definition, more than one coordinate to describe the whole position of the deformed shape when subjected to vibration. Multi-storey buildings are examples of MDOF systems that have as many modal shapes as the number of degrees of freedom. The response of the edification to an external force comprehends the response of each mode when analysed separately, into one superimposed deformed shape. Hence, each modal shape has a portion of contribution and a so-called modal participation factor. Studies show that the higher the natural frequency is, the lower its participation factor when observing the seismic excitation. This happens because the phenomenon of resonance becomes more and more absent since the frequency gets far from the frequency of the excitation it is submitted. Therefore, to reduce computational effort, it is possible to infer structural response with good levels of accuracy with only the first modes of vibration. The equilibrium equation of damped systems without external forces can be determined as:

$$\mathbf{M}\ddot{\vec{u}} + \mathbf{C}\dot{\vec{u}} + \mathbf{K}\vec{u} = 0 \quad (3.1)$$

where  $\mathbf{M}$ ,  $\mathbf{C}$  and  $\mathbf{K}$  are the mass, damping and stiffness values, respectively and  $\vec{u}$  is the displacement vector and its first and second-time derivative (velocity and acceleration, respectively). Its solution in the time domain can be done with the aid of the Laplace transform, reaching results with initial conditions of displacement or velocity.

As a consequence of superimposition, one can note that modal analysis provides the opportunity to interpret the whole multi-degree-of-freedom structure, with  $N$  modal shapes, into  $N$  SDOF

systems. That simplification brings velocity to the solution since it can be applied to the methods previously presented in Section 3.1.

### 3.3 SEISMIC ENGINEERING

Seismic Engineering is the field of Civil Engineering science which dedicates itself to comprehending seisms, commonly referred to as earthquakes. For its complete understanding, geology aspects are necessary to fully describe the phenomenon and, consequently, its action in structures. In this section, basic topics are presented to conceptualise seism definition and types of occurrence, as well as its methods of measurement.

#### 3.3.1 Seismic Activity

Seism can be described as the Earth's surface vibration and it can be described as a natural or an artificial seism. Natural seisms are generated as the tectonic plates move in the Earth's mantle and shock themselves into each other, resulting in strong vibration throughout the terrestrial crust. Also, seisms can be a product of volcanic activity and gas displacement inside Earth's crust and mantle. In brief, seismic activity is permanent and will occur whenever one of these movements is detected and, considering the energy involved in the process, one can axiomatically infer that its consequences can be disastrous. On the other hand, artificial seisms are those vibrations generated due to human activity, such as big soil impacts, soil drilling and explosions. Both phenomena can be described as seisms considering their propagation waves, volumetric and superficial ones, which will be further discussed. In summary, these movements are a consequence of rapid energy liberation and dissipation as seismic waves (PENÃ, 2012).

Earthquakes can be transcribed into an acceleration in the soil where it is being measured its influence. To better understand earthquakes, it is important to highlight that as closer to the surface, the more severe their consequences to human society. This distance to the surface is called focal depth (ASSUMPÇÃO; DIAS NETO, 2000). The origin of a seism is called hypocentre, which can be synonymously called focus. However, its measurement is, typically, made at Earth's surface, where the point directly above, inscribed in the crust surface, is called epicentre (see Figure 3.2).

These nomenclatures are made to differ and better describe an earthquake and be able to measure its impact. This seismic activity is detected in a determined region with the aid of seismographs, where accelerations in 3 orthogonal directions are measured and registered. This obtained data is called an accelerogram and, when extracted the information of interest, *id est*, the observed direction, it can be introduced to structures to analyse response to the excitation.

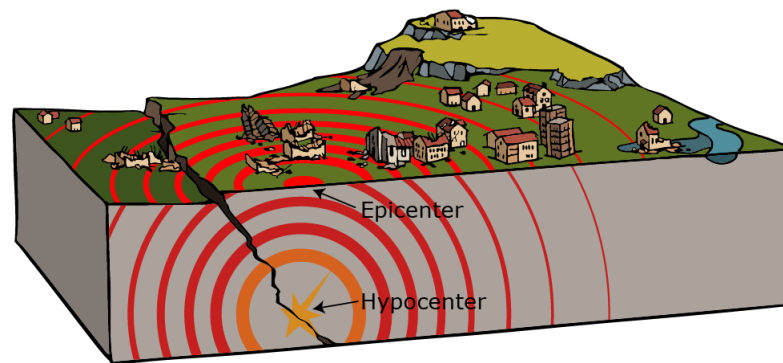


Figure 3.2 – Schematic definition of hypocentre and epicentre. In red, it is presented seismic waves (Swiss Seismological Service (s.d.)).

### 3.3.2 Seismic Waves

The energy dissipation of an earthquake provokes the generation of seismic waves that travel through Earth's mantle and crust. There are different types of waves, such as P and S waves, referring to deep waves, and R and L waves, referring to surface vibration. P is an abbreviation for primary, considering it is the first one to arrive at the measured point. They are responsible for generating compression and expansion in Earth's interior and can be described as longitudinal waves. Regarding the other type of deep waves, S stands for secondary as they are the second to be detected in a seismograph. They are transverse waves and have as a consequence shear stress in solids to achieve equilibrium with its action. The other type of waves are the surface ones, which are slower than deep ones and considering their lower frequencies, can be more harmful to structures. Their propagation starts at the epicentre and they have two types: Rayleigh and Love waves. In summary, primary waves are responsible for compressing behaviour in ground volume while secondary are generate shear loading with lower velocity and higher amplitude when compared to the first ones. Rayleigh waves are slower than primary and secondary and are the result of P and S waves interference. Finally, Love waves are the interference of different S waves and particle motion occurs in the horizontal plane (CHAPMAN, 2004).

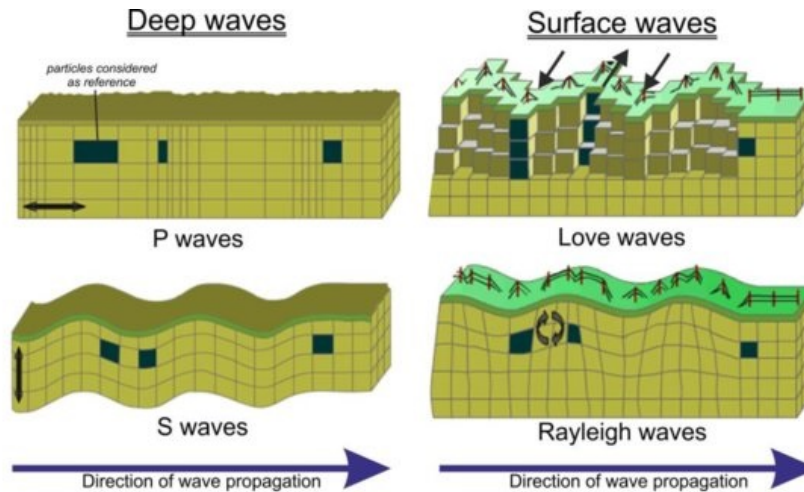


Figure 3.3 – Seismic Waves: primary, secondary, Rayleigh and Love (Adapted from Martínez-Moreno (2015)).

### 3.3.3 Intensity and Magnitude

Seism measurement is made with the aid of equipment capable of registering acceleration over time of a specific point. This type of equipment is called a seismograph, the instrument is constituted of a pendulum or a mass in a spring and often mounted on a piece of paper to register the accelerogram as the earthquake occurs. Nowadays, it is also possible to use digital seismographs as a more accurate alternative when compared to analogical options. The acceleration is a function of the differential motion resulting as a consequence of mass inertia, which tends to remain at rest. This measure is used to define seismic magnitude, which remains unchanged despite the distance to the earthquake and represents the amount of energy liberated by the seism at its hypocentre.

Magnitude is a quantitative property, that is determined using different scales. The most known and used is the Richter Scale (RICHTER, 1935). It consists in a classification of the seism from 1 to 9, or greater, varying from microearthquakes, *id est* rarely noticeable to people, in the first degree and great events with near or total destruction of buildings and permanent changes in ground topography for the last one. Despite its vast use, it is not the most recommended scale to be used when higher degrees are taken into consideration, being less representative of the energy measured (ROSSATO; MIGUEL; MIGUEL, 2016). The magnitude  $M$  is obtained by the equation:

$$M = \log_{10}A + 3\log_{10}(8\Delta t) - 2.92, \quad (3.2)$$

where  $A$  is the seismic wave amplitude, in millimetres, measured in the seismogram; and  $\Delta t$  is the time interval between the beginning of the primary and the secondary waves, measured in

seconds. Richter scale can also be referred to as local magnitude.

Nowadays, studies are conducted using the moment magnitude scale, created in 1979 (HANKS; KANAMORI, 1979). It was motivated because of the saturation at large magnitudes of other scales at the time, as previously mentioned. That being said, the formulation is based on the seismic moment  $M_o$ , which can be defined by:

$$M_o = \mu SD, \quad (3.3)$$

where  $\mu$  is the shear module of the rocks in the earthquake, usually taken as 30 GPa;  $S$  is the area of the rupture; and  $D$  is the average displacement. After the determination of the seismic moment, it is possible to reach out the seismic moment magnitude, taken as  $M_w$  and calculated with Equation 3.4.

$$M_w = \frac{2}{3} \log_{10} M_o - 10.7 \quad (3.4)$$

The seismic intensity is characterised as being a qualitative property of earthquakes, related to the effects on people and structures. As a consequence of that, intensity can vary from region to region, normally losing significance as the distance from the epicentre increases. To measure intensity, it is possible to use the Modified Mercalli scale, broadly used as a spin-off of the Mercalli scale, created in 1884 by Giuseppe Mercalli. As it measures the damage caused to inhabited areas, it empirically labels the phenomena into 12 categories and is useful for studying historical events.

In summary, intensity and magnitude are not the same property of an earthquake, being the latter the appropriate for energy release measure, as an intrinsic characteristic of a seism, and the former to evaluate mainly social consequences in a determined location. Both scales are commonly published associated, aiming to translate the impact of an earthquake into a feasible understanding.

### 3.4 RESPONSE SPECTRUM CURVES

Seismic activity is measured in a time series and its recorded amplitude represents ground acceleration. The obtained signal can be rewritten as a superimposition using the Fourier Transform, which approximates the original signal using the summation of multiple sinusoidal functions. Attached is a space transformation via numerical integration, changing the domain of analysis

to the frequency. The operation in a frequency domain data set also represents the same operation under the time domain, being this property the justification for its usage, since it can demand lower effort to perform it when compared to the time domain (MIGUEL; MIGUEL; LOPEZ, 2017). In summary, the Fourier Transform is done by applying Equation 3.5, where  $\omega$  is the frequency,  $g$  is the time domain function and  $\mathcal{F}$  is the Fourier Transform of  $g$ . A graphic representation of the transformation is presented in Figure 3.4.

$$F(\omega) = \int_{-\infty}^{\infty} e^{-i\omega t} g(t) dt = \mathcal{F}\{g(t)\} \quad (3.5)$$

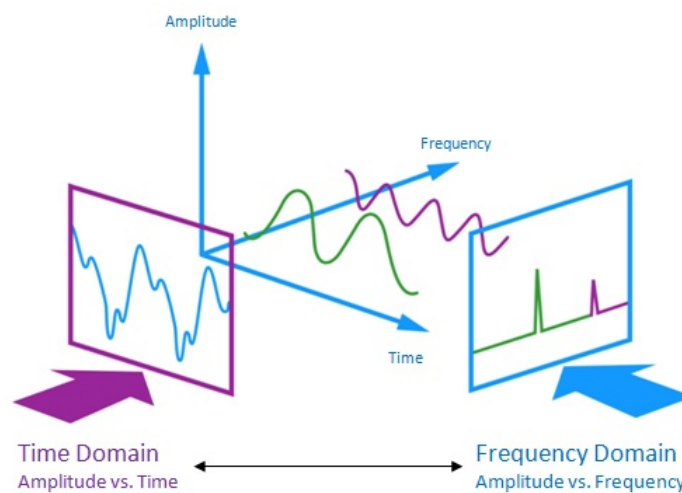


Figure 3.4 – Fourier Transform graphic representation (MED, 2018)

When this transformation is performed, the obtained function is called a spectrum. Spectra are broadly used curves in Engineering problems and they represent the existing amount of energy in the signal by frequency. In other words, the frequencies with higher amplitudes, and consequently higher power, in a spectrum are easily detectable and present in the signal, being this information of extreme importance since structural response will be determined by the proximity of the building's natural frequencies and excitation's frequencies. When there is a similarity in those values, the phenomenon of resonance will increase amplitude and, consequently, will demand more of the whole structural system.

That being said, one can infer that the main information needed to evaluate structural safety under seismic activity depends on those factors presented: natural and excitation frequencies. The former is a structure property, being determined in the designing phase. The latter, otherwise, is information obtained for each specific event of an earthquake and will be as different as the characteristics of the geographic failure or other seism. Considering it is not possible to oversee all events that will occur during the lifetime of construction, codes worldwide are typically introduced in designing response spectrum curves that must be followed by Engineers to guarantee safety. These types of spectra are commonly expressed in a curve showing spectral acceleration ( $S_a$ , in  $m/s^2$ ) over the period ( $T$ , in s).



### 3.5 DUCTILITY

Natural phenomena intensity varies according to a recurrence time within a Gaussian distribution, i.e., as the time-lapse becomes higher, it has a lower probability, however greater structural demand. So, establishing a low recurrence time to reduce demanding loads implies an unsafely designed solution, since it would despise events with considerable occurrence probability and high chances of exceeding ultimate limit states. Typically, in Civil Engineering projects, hydrology, wind or seismic related, it is adopted 50 years of recurrence time, meaning structures shall be able to resist events with only a 2% probability of being exceeded in magnitude.

In observation, one can note that despite the need to guarantee structural reliability under extreme conditions, when submitted to average excitations structures will work with high safety factors if all elements are designed to behave in elastic regions. This consideration leads to more stiff elements to prevent it from reaching the yield point. In Fragiacom, Dujic and Sustersic (2011) and Elghazouli (2017) it is possible to observe that ductile design is an alternative to guarantee safety within the economic limits. This approach enables energy dissipation during events by subjecting the material to plastic deformation. On the other hand, designing considering ductile behaviour must consider other failure mechanisms that may lead to a brittle failure and special attention to plastic deformations. Main concerns that lead to ductile structures can be described as (JORISSEN; FRAGIACOMO, 2011):

- **Large deformations:** elastic designing is based on infinitesimal strain theory, in which displacements are much smaller than the element's dimensions. This consideration is not valid when observing ductile design, since there is the assumption, under the finite strain theory, that deformations are considerable and original configuration can not be treated as equivalent to the deformed one. This is the desired failure to any structure since this prevents the building from going under or collapsing without being able to warn occupants - brittle failure - when it is demanded with an exceptional load (such as wind, seismic, snow or any other human excitation not foreseen);
- **Force and stress redistribution:** within cross-sections, it is possible to reach higher values of structural load-bearing capacity, when compared to elastic analysis. It is only possible to achieve a plastic analysis if some sort of ductility is available;
- **Energy dissipation:** higher structural ductility propitiates a higher energy dissipation, resulting in less important seismic, or any other dynamic load, acting on the structure. This phenomenon will be further described in the modal analysis theoretical foundation. For instance, it can be understood as a way to dissipate energy due to structural properties; and
- **Structural Robustness:** as one can note in Kirkegaard et al. (2011), ductility provides good

gains in robustness. That is, with a small increase in ductility it can achieve considerable extra reliability since it is designed to achieve large deformations. Thus, it is possible to ensure that local structural problems, such as a single-member failure, will not be as harmful to the whole building as they would be under elastic design.

As previously highlighted the importance of ductile design to Engineering, it is essential to define ductility and understand its usage in structural projects. Elghazouli (2017) determines it as:

Ductility is defined as the ability of a structure or member to withstand large deformations beyond its yield point (often over many cycles) without fracture. In earthquake engineering, ductility is expressed in terms of demand and supply. The ductility demand is the maximum ductility that the structure experiences during an earthquake, which is a function of both the structure and the earthquake. The ductility supply is the maximum ductility the structure can sustain without fracture. This is a purely structural property.

So, in the face of the definition above, one can note that ductility is an intrinsic property of a building's structural system. Hence, it is axiomatic that ductility behaviour is strongly related to the structure constituent elements, considering they have distinct mechanical properties. Concerning CLT structures, ductility is highly correlated to its steel connections, since timber has quasi-brittle behaviour under tension and shear (SANDHAAS, 2012). Ductile behaviour in timber structures is, consequently, attached to the capacity of the connection to dissipate energy throughout its deformation process (REBOUÇAS et al., 2022).

However, the literature is not unanimous concerning the ductility definition, especially concerning its calculation. Park (1988) defined it as the ability of a structure to undergo cyclic deformations in the plastic range without substantial reduction in strength (MATEJČEKOVÁ-FARHAT; ÁROCH, 2013). In Llanes-Tizoc et al. (2019) it is carried out a study to define local, storey and global ductility as a way to establish ductility measurement. It defines local ductility as the rotational capacity of a determined member submitted to bending moment or the axial deformation capacity of a member under tension loads. Storey and global ductility are directly related to the displacement of the storey itself or the building's roof. All definitions presented in Llanes-Tizoc et al. (2019) are presented below.

**Definition 1** *Local ductility: a member submitted to bending load in a given connection can be described as the ratio between the maximum curvature out of the elastic region to the curvature of the connection when it steps into the plastic region. In analogy, it is used the same ratio to member under tension load. It is expressed mathematically in terms of Equation 3.6, where subindex  $L$  represents the local ductility,  $\phi$  is related to the rotation and can be replaced by  $\delta$  in case of axial loading and  $_{max}$  refers to the maximum value in the elastic region.*

$$\mu_L = \frac{\phi_{max}}{\phi_y} \quad (3.6)$$

This ratio in Equation 3.6 can be compared to values available in the literature to understand connection ductility and can be categorised as presented in Table 3.1.

Table 3.1 – Ductility Classes proposed in the literature (REBOUÇAS et al., 2022).

Classification	Average Ductility Ratio
Brittle	$\mu \leq 2$
Low Ductility	$2 < \mu < 4$
Moderate Ductility	$4 < \mu \leq 6$
High Ductility	$\mu > 6$

**Definition 2** *Storey ductility: the ratio between the maximum displacement during the excitation to the displacement at the start of the yield level of any member in the storey. It is expressed mathematically in terms of Equation 3.7, where subindex S is the designation of storey ductility.*

$$\mu_S = \frac{\Delta_{max}}{\Delta_Y} \quad (3.7)$$

**Definition 3** *Global ductility: when globally analysed, the building's ductility is measured using the summation of all storey ductilities, calculated with Equation 3.8, where n is the number of pavements.*

$$\mu_G = \frac{1}{n} \sum_{i=1}^n \mu_{S,i} \quad (3.8)$$

### 3.6 EN 1998:2021

The Eurocode 8 (EC8), a standard currently applied to European countries, concerns the design regulations for earthquake-resistant structures. It is divided into six parts, regarding each main topic: buildings, bridges, retrofitting, silos, tanks and pipelines, foundations and towers. The relevant part for the present study is also divided into another 10 sections, 5 of them the specific rules for each construction material, such as reinforced concrete, steel, composite steel-concrete, timber and masonry buildings. The other sections are general topics, common requirements

and design criteria. Considering it is applied in many different countries with, as well, different topographies and other aspects, Eurocodes are typically used with the National Appendix of the respective country in the project is taking place, to fulfil all local requirements alongside the European normatives.

Building design according to EC8 is done using limit states, consequence classes and displacements evaluation. European regulation takes into consideration 3 limit states to evaluate building seismic performance, such as Near Collapse (NC), Significant Damage (SD) and Deformation Limit (DL). NC and SD shall be treated as Ultimate Limit States, while DL should be considered as a Serviceability Limit State. Regarding the consequence classes, there are 3 of those which can be seen in Table 3.2. Considering the building in the present study, it is possible to classify it as CC2.

On top of that, EC8 advocates for two design premises: the first one is related to the building's structure, which shall be able to resist horizontal action in any direction; the second one considers that the building's performance under seismic activity must be considered in the early stages to be able to achieve EC8 requirements. The structure can be divided into two systems, being the primary members the ones responsible for providing complete lateral load due to seismic activity.

Table 3.2 – Consequence Classes (Adapted from EN 1998 (2021)).

Consequence Class	Description	Example
CC1	Low consequences for loss of human life and negligible social-economic losses.	Agricultural buildings
CC2	Medium consequences for loss of human life and considerable social-economic losses.	Residential buildings
CC3	High consequences for loss of human life and very great social-economic losses.	Hospital, stadiums, etc.

EC8 also recommends the separation of CC3 into two classes, CC3-a and CC3-b. CC3-a refers to buildings whose seismic resistance is important considering the consequences attached to their collapse, such as schools, assembly halls, cultural institutions, etc. CC3-b are buildings of installations of vital importance for civil protection, such as hospitals, fire stations, police departments, etc.

The displacement evaluation as a parameter of design is established in EC8 as a Nationally Determined Parameter (NDP). *Id est*, the values presented in the EC8 shall be used solely when there are no determinations in the National Appendix. It is also considered an NDP for the return periods of seismic actions, the performance factors and the local seismic hazard.

To fully characterise a seismic action, it is needed to take into consideration the seismicity of the region and the soil properties relevant to the analysis. Considering  $H_{800}$  is the depth of the seismic bedrock formation identified by the shear wave velocity,  $v_s$ , of at least equal to 800 m/s and  $v_{s,H}$  the equivalent value of the shear wave velocity of the superficial soil deposit defined by:

$$v_{s,H} = \frac{H}{\sum_{i=1}^N \frac{h_i}{v_i}} \quad (3.9)$$

where  $h_i$  is the thickness of the  $i$ -th soil layer;  $v_i$  is the shear wave velocity of the  $i$ -th soil layer;  $N$  is the total number of soil layers from the ground surface to the depth; and  $H$  is the depth, taken 30 m if  $H_{800}$  is higher or equal to 30 m and its value if it is not higher. Then, it is possible to classify soil using Table 3.3. To simplify soil categorisation, Annex A establishes more practical ways to determine soil properties, such as Standard Penetration Test, Cone Penetration Test, Field Vane Test, etc.

Table 3.3 – Standard site categorisation (EN 1998, 2021).

	Ground Class	Stiff	Medium Stiffness	Soft
Depth Class	$v_{s,H}$ range	$400 \text{ m/s} \leq v_{s,H} \leq 800 \text{ m/s}$	$250 \text{ m/s} \leq v_{s,H} \leq 400 \text{ m/s}$	$150 \text{ m/s} \leq v_{s,H} \leq 250 \text{ m/s}$
	$H_{800}$ range			
Very Shallow	$H_{800} \leq 5 \text{ m}$	A	A	E
Shallow	$5 \text{ m} < H_{800} \leq 30 \text{ m}$	B	E	E
Intermediate	$30 \text{ m} < H_{800} \leq 100 \text{ m}$	B	C	D
Deep	$H_{800} > 100 \text{ m}$	B	F	F

In summary, Figure 3.5 shows a flowchart containing all steps to a correct seismic-resistant building design. Despite its simplicity, it contains all the phases that must be followed by Engineers to fully observe the EC8 usage.

Regarding the deformation capacity of the whole structural system, EC8 provides three ductility classes: DC1, DC2 and DC3. They can be defined as follows (EN 1998, 2021):

- DC1: the overstrength capacity is taken into account, while the deformation and energy dissipation capacities are disregarded;
- DC2: the local overstrength capacity, deformation and energy dissipation are taken into account. Global plastic mechanisms are controlled;
- DC3: the ability of the structure to form a global plastic mechanism at SD limit state and its local overstrength, deformation and energy dissipation capacity are taken into account.

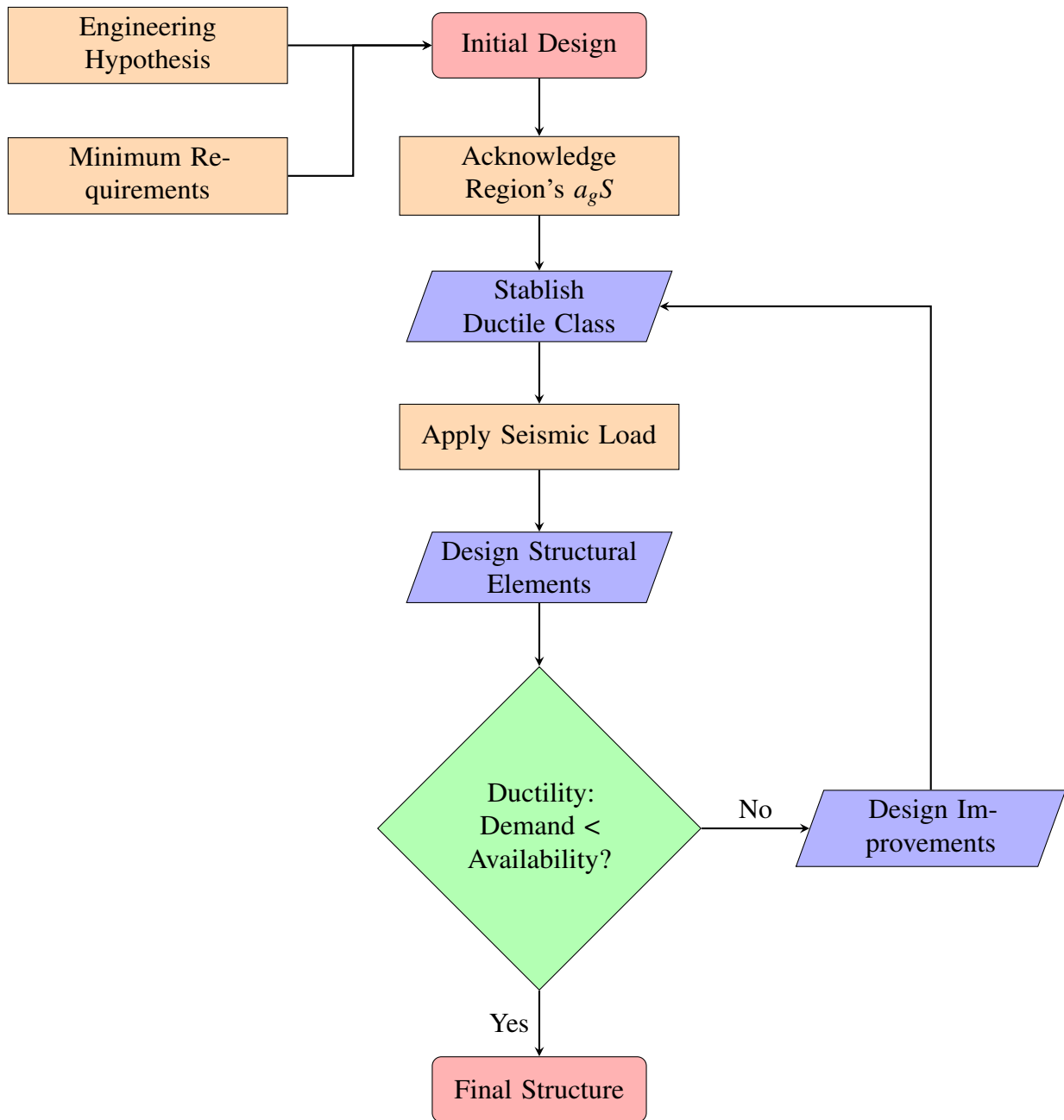


Figure 3.5 – Eurocode 8 designing scheme.

One important topic in building design under seismic action is the inter-storey drift, described as the difference occurring between two consecutive pavements (BHATT, 2020). EC8 presents the following Equation 3.10 as a limitation:

$$d_r \leq \lambda_s h_s, \quad (3.10)$$

where  $\lambda_s$  is a coefficient referring to drift limitation, given accordingly to the structure material, considered 0.0020 for timber moment-resisting frames (EN 1998, 2021);  $h_s$  is the interstorey

height, that is, the distance between adjacent floors.

The horizontal component of the response spectrum shall be calculated by complying with:

$$S_e(T) = \begin{cases} \frac{S_\alpha}{F_a} & 0 \leq T \leq T_A \\ \frac{S_\alpha}{T_B - T_A} \left[ \eta(T - T_A) + \frac{T_B - T}{F_A} \right] & T_A \leq T \leq T_B \\ \eta S_\alpha & T_B \leq T \leq T_C \\ \eta \frac{S_\beta T_\beta}{T} & T_C \leq T \leq T_D \\ \eta T_D \frac{S_\beta T_\beta}{T^2} & T \geq T_D \end{cases} \quad (3.11)$$

where, accordingly to EN 1998 (2021):

$S_e(T)$  is the elastic response spectrum;

$T$  is the vibration period of a linear SDOF;

$S_\alpha$  is the maximum response spectral acceleration (for 5% dumping) corresponding to the constant acceleration range of the elastic response spectrum, calculated with amplification factors;

$S_\beta$  is the 5% damped response spectral acceleration at the vibration period  $T_\beta$ , also given with amplification factors;

$T_\beta$  is equal to 1 s;

$T_A$  is the short-period cut-off associated with the zero-period spectral acceleration;

$F_A$  is the ratio of  $S_\alpha$  with respect to the zero-period spectral acceleration;

$T_C = \frac{S_\beta T_\beta}{S_\alpha}$  is the upper corner period of the constant spectral acceleration range;

$T_B$  is the lower corner period of the constant spectral acceleration range;

$T_D$  is the corner period at the beginning of the constant displacement response range of the spectrum; and

$\eta$  is the damping correction factor, with a reference value  $\eta = 1$  for 5% damping ratio.

With that in mind, EC8 established a pattern to build the elastic response spectrum to find values to the structural design. It is presented in Figure 3.6.

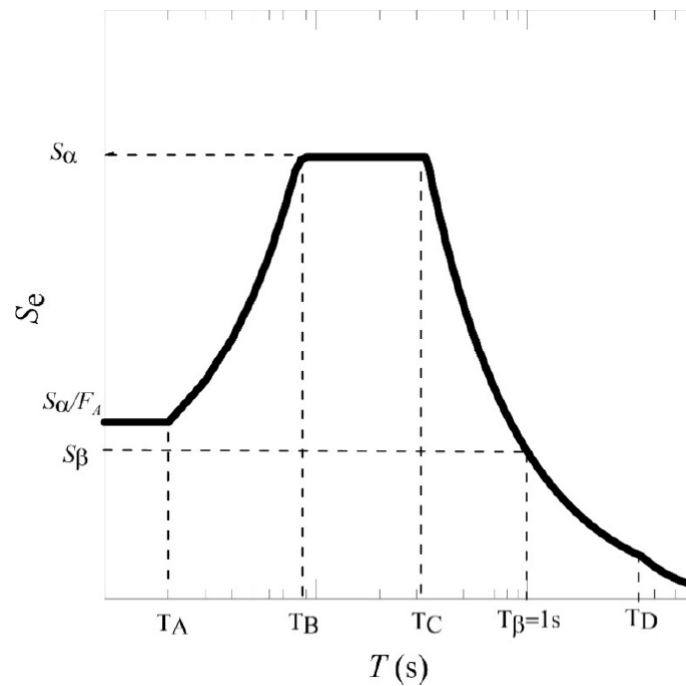


Figure 3.6 – EC8 elastic response spectrum pattern (EN 1998, 2021).

The new version of EC8, currently a draft of 2021, makes progress in amplification factor categorisation to avoid continuity issues, as previously mentioned (PAOLUCCI et al., 2021). These factors can be used accordingly to Table 3.4.

Table 3.4 – Site amplification factors (Adapted from EN 1998 (2021)).

Site Category	$F_\alpha$		$F_\beta$	
	$H_{800}$ and $v_{s,H}$ available	Default Value	$H_{800}$ and $v_{s,H}$ available	Default Value
A	1.0	1.0	1.0	1.0
B	$\left(\frac{v_{s,H}}{800}\right)^{-0.40r_\alpha}$	$1.3(1 - 0.1S_{\alpha,RP}/g)$	$\left(\frac{v_{s,H}}{800}\right)^{-0.70r_\beta}$	$1.6(1 - 0.2S_{\beta,RP}/g)$
C		$1.6(1 - 0.2S_{\alpha,RP}/g)$		$2.3(1 - 0.3S_{\beta,RP}/g)$
D		$1.8(1 - 0.3S_{\alpha,RP}/g)$		$3.2(1 - S_{\beta,RP}/g)$
E	$\left(\frac{v_{s,H}}{800}\right)^{-0.40r_\alpha} \frac{H}{30} \left(4 - \frac{H}{10}\right)$	$2.2(1 - 0.5S_{\alpha,RP}/g)$	$\left(\frac{v_{s,H}}{800}\right)^{-0.70r_\beta} \frac{H}{30}$	$3.2(1 - S_{\beta,RP}/g)$
F	$0.90 \left(\frac{v_{s,H}}{800}\right)^{-0.40r_\alpha}$	$1.7(1 - 0.3S_{\alpha,RP}/g)$	$1.25 \left(\frac{v_{s,H}}{800}\right)^{-0.70r_\beta}$	$4.0(1 - S_{\beta,RP}/g)$

Both  $r_\alpha$  and  $r_\beta$  can be calculated as follows:

$$r_\alpha = \frac{S_{\alpha,RP}/g}{V_{s,H}/150} \quad (3.12)$$

$$r_\beta = \frac{S_{\beta,RP}/g}{V_{s,H}/150} \quad (3.13)$$

The presented equations are valid for topographies with irregularities smaller than 30 m and average slopes of less than  $15^\circ$ . Also, it is applied to soil types A and B determined in Table 3.3.



Regarding the seismic hazard zoning, EC8 attributes it as a National Determined Parameter (NDP) to be discussed in each National Appendix. When considering Portugal, NP EN 1998-1 (2010) provides a zoning map considering 2 types of seismic action. The first one is considered to be away from shore, i.e. with epicentre in the Atlantic region, and the second type concerns near the inshore events, in the continental territory or the Azores. It is presented in Figure 3.7 and its values are given in  $\text{cm/s}^2$ .

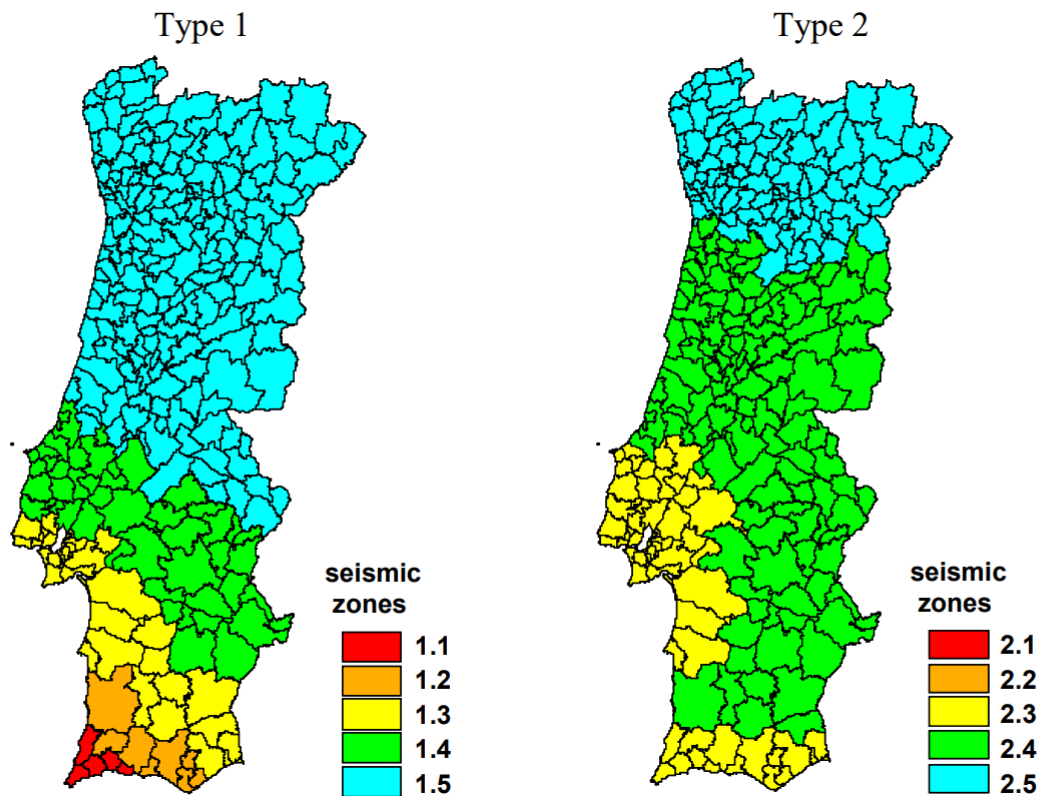


Figure 3.7 – Portuguese seismic zoning (NP EN 1998-1, 2010).

This 2<sup>nd</sup> generation of Eurocode 8 facilitates the integration of ductility considerations within the structural design. Ductile Classes 2 and 3, in comparison to the previous Medium and High established in the first generation, are of simpler implementation to the design. Alongside that, improvements in the homogenisation of seismic zoning, calibration of response spectrum curve generation, development of the displacement-based approach, and others. The latter is better explained in Section 3.8.

An example of the use of this normative to design CLT structures is presented in ??.

### 3.6.1 Ductile Design for Timber Structures

The design procedure of timber structures under medium to high ductile behaviour shall consider that dissipative zones should be located in joints and connections or, if so decided by the designer, outside those bonds when energy dissipation systems are proposed. Hence, one can note that

wood-based elements must remain designed elastically, and the metal connectors are the only source responsible for carrying out energy dissipation. EC8 also states that the ductility should occur by occasion of the flexural yield of metallic connections, being not permitted non-elastic designing to axially loaded fasteners. DC1, on the other side, shall follow non-dissipative designing.

Safety can be verified to the SD limit state for DC2 and DC3 with the use of reduction and modification factors to limit the characteristic value of the strength in dissipative zones ( $F_{Rk,d}$ ). It considers degradation under cyclic loading ( $k_{deg}$ ), duration of the load and moisture content ( $k_{mod}$ ) and material partial factor ( $\gamma_M$ ). It is given by Equation 3.14, where  $F_{Rd,d}$  is the representation of the design strength in the dissipative zone. Concerning the material partial factor, it shall be considered 1.0 in DC2 and DC3 design, unless it is given a different regulation by a National Annex.

$$F_{Rd,b} = k_{deg} \cdot k_{mod} \cdot \frac{F_{Rk,b}}{\gamma_M} \quad (3.14)$$

On the other hand, non-dissipative elements, in DC2 or DC3, and all members of DC1 shall not take under consideration the degradation factor ( $k_{deg}$ ).

Ductile designing within EC8 is treated according to each level of ductility and regards the type of structural party employed in the project. Among the 10 structural types presented by EC8, the present study will bring to attention those recommendations made to Cross-Laminated Timber buildings. So, regarding DC2, structural members and joints should be designed considering Equation 3.15.

$$F_{Rd,b} \geq \frac{\gamma_{Rd}}{k_{deg}} \Omega_d + F_{Ed,E} + F_{Ed,G} \quad (3.15)$$

In this equation, considering the elements already presented in earlier topics, it is introduced  $\gamma_{Rd}$ ,  $\Omega_d$ ,  $F_{Ed,E}$  and  $F_{Ed,G}$ .  $\gamma_{Rd}$  is the overstrength factor, commonly taken as 1.6;  $F_{Ed,E}$  is the action effect in the non-dissipative joint or member due to the design seismic action;  $F_{Ed,G}$  is the action effect of all other actions taking place during the design seismic situation; and, finally,  $\Omega_d$  is the minimum value of all overstrength ratios calculated in each storey, given by:

$$\Omega_{d,i} = \min \left( \frac{\sum_{j=1}^{N_i} |V_{Rd,a,i,j}|}{\sum_{j=1}^{N_i} |V_{Ed,E,i,j}|}, \frac{\sum_{j=1}^{N_i} |M_{Rd,rock,i,j}|}{\sum_{j=1}^{N_i} |M_{Ed,E,i,j}|} \right), \quad (3.16)$$

where  $V_{Rd,a,i,j}$  is the design lateral strength related to shear connection of the  $j^{th}$  shear-wall and the  $i^{th}$  storey;  $V_{Ed,E,i,j}$  is the design global shear of the  $j^{th}$  shear-wall and the  $i^{th}$  storey due to seismic action;  $M_{Rd,rock,i,j}$  is the design rocking strength of the  $j^{th}$  shear-wall and the  $i^{th}$  storey, including the stabilising effect of the vertical load; and  $M_{Ed,E,i,j}$  is the design rocking moment of the  $j^{th}$  shear-wall and the  $i^{th}$  storey, due to seismic action.

When DC2 design is applied, Eurocode 8 recommends the use of the equation:

$$F_{Rd,b} \geq \frac{\gamma_{Rd}}{k_{deg}} \cdot \Omega_d + F_{Ed,E} + F_{Ed,G}, \quad (3.17)$$

where  $F_{Rd,b}$  is the non-dissipative design strength of the analysed joint/member - given by Equation 3.18:

$$F_{Rd,b} = k_{mod} \cdot \frac{F_{Rk,b}}{\gamma_M} \quad (3.18)$$

where  $k_{mod}$  is the modification factor considering the duration of the load and moisture;  $F_{Rk,b}$  is the characteristic value of the strength of the non-dissipative members; and  $\gamma_M$  is the material partial factor.

Seismic excitation modelling can be performed, using EC8, in three different ways: force- and displacement-based approaches, and response history analysis.

Regarding the seismic excitation modelling, the EC8 proposes the use of an inelastic response spectrum. This curve is simply done by dividing the elastic response spectrum, previously presented in Section 3.4 by a behaviour factor defined according to the geometry and to the ductility class of design. Considerations are made for different structural systems in the code, including the Cross-Laminated Timber. This reduction in elastic spectrum considers the overstrength, due to the redistribution of seismic action effects ( $q_R$ ) and other sources ( $q_S$ ), deformation capacity and energy dissipation capacity, taken both in one component ( $q_D$ ). To determine the behaviour factor, Equation 3.19 shall be used.

$$q = q_{RSD} \quad (3.19)$$

As previously stated, in DC1 design it no energy dissipation or plastic deformation is considered. This is mathematically shown when  $q_D$  is equal to 1 in low ductility structures. Behaviour factors  $q$  may be taken, for regular elevation buildings, according to Table 3.5. However, to take

advantage of the material plastic deformation and its energy dissipation, it is expected that the design implements a better detailing of the structure. EN 1998 (2021) specifies that, aiming to use the DC2 and DC3 behaviour factors, it is necessary to follow a few rules, which are presented in Table 3.6.

Ductility Class	Behaviour Factor ( $q$ )
DC1	1.5
DC2	2.0
DC3	3.0

Table 3.5 – Default values of behaviour factors for regular elevation Cross-Laminated Timber buildings (EN 1998, 2021).

Ductility Class 2 (DC2)		Ductility Class 3 (DC3)	
Elements to be over-designed	Dissipation mechanism	Elements to be over-designed	Dissipation mechanism
All CLT wall and floor panels	Angle brackets at wall base	All CLT wall and floor panels	Angle brackets at wall base
Joints between adjacent floor panels	Hold downs at wall ends	Joints between adjacent floor panels	Hold downs at wall ends
Joints between floors and supporting walls underneath		Joints between floors and supporting walls underneath	Vertical step joints in segmented shear walls
Joints between orthogonal walls		Joints between orthogonal walls	

Table 3.6 – Capacity rules for DC2 and DC3 (EN 1998, 2021).

The new EC8 proposal defines the need that the design strength of brittle elements shall be higher or equal to the design strength of dissipating energy elements multiplied by overstrength and degradation factors, as exemplified in Equation 3.20. These factors are taken as 1.3 and 0.8, respectively.

$$\frac{\gamma_{Rd}}{\beta_{sd}} \cdot F_{Rd,d} \leq F_{Rd,b} \quad (3.20)$$

where  $\gamma_{Rd}$  is the overstrength factor;  $\beta_{sd}$  the degradation factor, due to cyclic loading;  $F_{Rd,d}$  the ductile design strength; and  $F_{Rd,b}$  the brittle design strength.

On the other hand, adopting EC8 recommendations, a nonlinear static analysis can be performed using pushover analysis by means of an equivalent single-degree-of-freedom model. This methodology is presented in the literature as the N2 method (FAJFAR, 2000). Initially, it is necessary to establish a modal pattern of lateral loads to apply it to the structure and generate the capacity curve based on the total shear force ( $F_b$ ) and the displacement of a control node.

The incremental load must persist until a brittle failure, an instability or achievement of ultimate local deformation in a ductile post-elastic mechanism (EN 1998, 2021). Regarding the studied model, it was proposed a linear load alongside each floor, as further explained in 3.8.

### 3.7 ABNT NBR 15421:2023

Regulations concerning seismic activity in Brazil are relatively new and still unknown to many designers, which is why it is not broadly used yet. The first edition of the Brazilian code, NBR 15421 by *Associação Brasileira de Normas Técnicas* (ABNT, in English: Brazilian Association of Technical Standards), was published in 2006 and follows the common methodology used in other normative, such as the Eurocode 8 itself. Its second edition, and the one taken as a reference to this dissertation, was recently published, in 2023. Initially, it consists of region definition, aiming to establish zoning influence on accelerations and loadings. To do so, NBR 15421 uses an isopleth map with 5 zones, which can be seen in Figure 3.8, used for rocky soils, and recommends usage of 475 years of earthquake recurrence time.

Alongside with region of analysis, it is necessary to determine terrain class, obtained similarly to the Eurocode 8 methodology. They are divided into classes from A to F, accordingly to Table 3.7, where  $\bar{v}_s$  is the propagation average velocity of shear waves and  $\bar{N}$  is the average number of SPT blows.

Table 3.7 – Standard site categorisation (Adapted from NBR 15421 (2023)).

Terrain Class	Terrain Class Designation	Upper 30m layer average properties	
		$\bar{v}_s$	$\bar{N}$
A	Unaltered Rock	$\bar{v}_s \geq 1500$ m/s	Not applicable
B	Rock	$1500 \text{ m/s} \geq \bar{v}_s \geq 760$ m/s	Not applicable
C	Altered Rock	$760 \text{ m/s} \geq \bar{v}_s \geq 370$ m/s	$\bar{N} \geq 50$
D	Stiff Soil	$370 \text{ m/s} \geq \bar{v}_s \geq 180$ m/s	$50 \geq \bar{N} \geq 15$
E	Soft	$\bar{v}_s \leq 180$ m/s	$\bar{N} \leq 15$
F	-	Any profile with more than 3 m soft clay	
	-	Soil types that need specific evaluation.	

After obtaining terrain properties, NBR 15421 proposes 2 types of analysis: the first one, more practical, is using equivalent horizontal forces, while the second is the seismic analysis through the spectral method. Concerning the latter, the code does not provide much information about the numerical model which must be used and only determines a few topics that must be observed, such as:

- Vibration modes: it must be considered in the analysis sufficient modes to capture, at least,

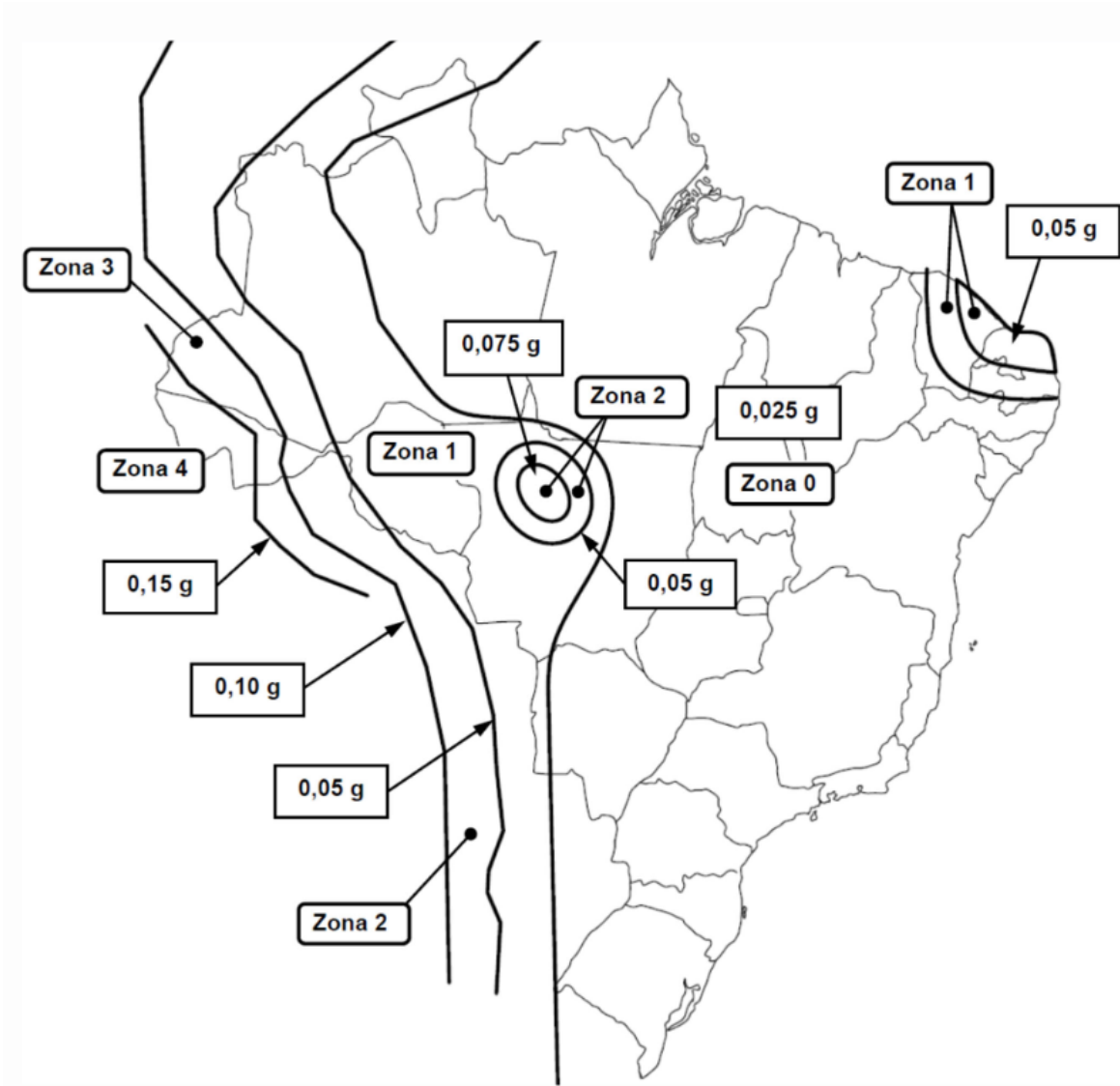


Figure 3.8 – Isopleth map to Brazilian seismic zones (NBR 15421, 2023).

90% of the structure's total mass in each direction orthogonally considered;

- **Modal Response:** all modal responses obtained in terms of force, moments and reactions must be multiplied by the ratio between utilisation importance ( $I$ ) and coefficient of response modification ( $R$ ), both parameters established by the code. Considering displacement responses, absolute or relative, they must be multiplied by the ratio between the displacement amplification coefficient ( $C_d$ ) and the coefficient  $I$ . Both  $R$  and  $C_d$  are parameters obtained when observing the constituent material and geometry of the structure, while  $I$  considers the usage of the building under analysis, aiming to reach more conservative values for buildings of higher importance, such as emergency centres, health institutions, National Defense, etc;
- **Modal Response Combination:** the code suggests the usage of squared sum square root rule for modes not separated by natural frequency values higher than 10% among themselves.

However, it leaves it open to the designer to use a more precise modal superimposition.

The first suggested method is based on the static equivalent load of the seismic activity. It is done using the Equations 3.21 and 3.22:

$$C_s = \frac{2.5 \left( \frac{a_{gs0}}{g} \right)}{\frac{R}{T}} \quad (3.21)$$

$$H_b = C_s \cdot W \quad (3.22)$$

where  $C_s$  represents the seismic response coefficient;  $W$  is the total weight of the structure and  $H_b$  is the horizontal force at the base of the structure in a determined direction. The spectral acceleration  $a_{gs0}$  is determined by the region characteristic acceleration for 0 s period, as presented in Figure 3.8, multiplied by a seismic amplification coefficient determined as a function of  $a_g$ , as presented in:

$$a_{gs0} = C_a \cdot a_g \quad (3.23)$$

It is also possible to reach the acceleration for 1s period, as given in:

$$a_{sg1} = C_v \cdot a_g \quad (3.24)$$

being both values,  $C_a$  and  $C_v$  obtained as function of the soil region.

From  $H_b$  it is possible to use a distribution model among all seismic-resistant vertical elements, taking into consideration the relative stiffness of these elements. It can be carried out by employing:

$$F_i = C_{v,i} H_b, \quad (3.25)$$

being  $F_i$  the characteristic force applied in a  $i$  elevation; and  $C_{v,i}$  determined with:

$$C_{v,i} = \frac{w_i h_i^k}{\sum_{j=1}^n w_j h_j^k}, \quad (3.26)$$

where  $C_{v,i}$  is the vertical distribution coefficient;  $w$  is the weight portion of the respective elevation pointed out as sub-index;  $h$  is the height of the respective elevation; and  $k$  a distribution exponent, taken as a function of the natural period of the structure. In other words, it considers the amount of mass in each floor and establishes a relation with the elevation of the considered location and the summation of total height and mass.

Seismic analysis can also be done with the linear dynamic spectral method. NBR 15421 determines that the vibration modes used in the analysis shall capture at least 90% of the total mass of the structure in each orthogonal direction. The design response spectrum is numerically defined with Equation 3.27. The graphic construction of the spectrum can be carried out with the usage of the variation provided by the code, given in Figure 3.9.

$$S_a(T) = \begin{cases} a_{gs0}(18.75T\frac{C_v}{C_a} + 1) & 0 \leq T \leq 0.08\frac{C_v}{C_a} \\ 2.5a_{gs0} & 0.08\frac{C_v}{C_a} \leq T \leq 0.4\frac{C_v}{C_a} \\ a_{gs1}/T & T > 0.4\frac{C_v}{C_a} \end{cases} \quad (3.27)$$

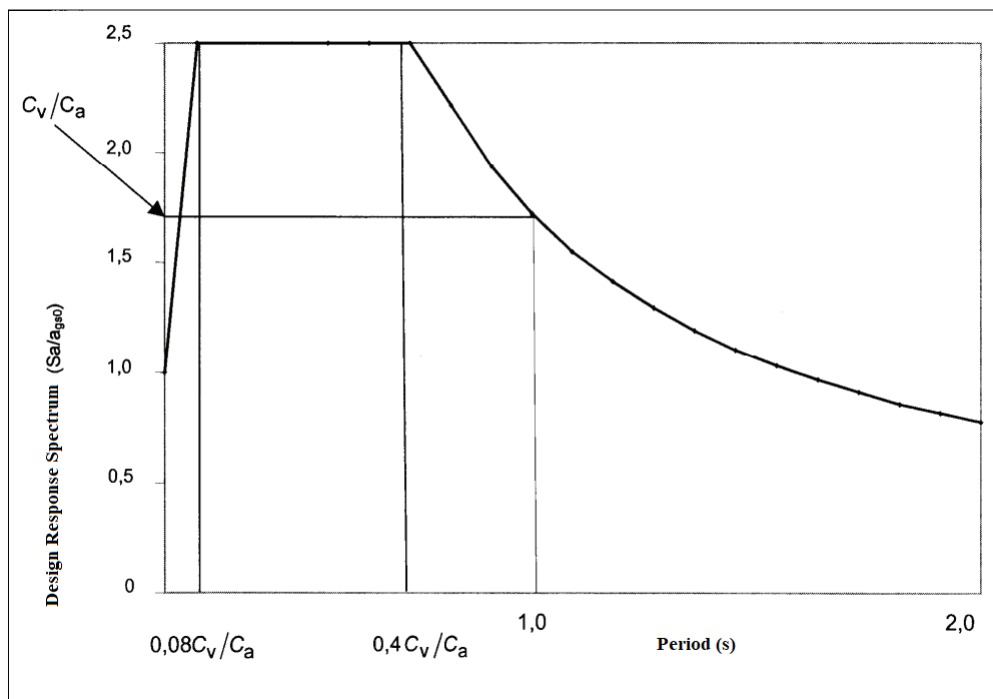


Figure 3.9 – Design response spectrum variation according to the period (T) (Adapted from NBR 15421 (2023)).

With the response spectrum presented in Equation 3.27, it is possible to reach a  $H$  value and apply the same methodology to distribute it along all elevations. Then, it is possible to measure displacement on each pavement and an absolute value given at the roof of the building. With that in mind, it is possible to determine the relative displacement of each storey and compare it to the limit values presented in NBR 15421. These limits are presented in Table 3.8, where



$h_{sx}$  is the distance between the two levels of the pavement in analysis. The usage category is a classification among the activities that will be done within the building. It is similar to the consequence classes of Eurocode 8.

Table 3.8 – Storey drift limitation (Adapted from NBR 15421 (2006)).

Usage Category		
I	II	III
$0.020h_{sx}$	$0.015h_{sx}$	$0.010h_{sx}$

Considering construction materials, NBR 15421 makes no particular recommendations. All design criteria encompass all construction methods, therefore, no specifications are made for timber structures. Moreover, the Brazilian normative makes no considerations concerning the ductility of buildings, resulting in elastic designing.

An example of the use of this normative to design CLT structures is presented in ??.

### 3.8 PUSHOVER ANALYSIS AND N2 METHOD

The pushover analysis is a valuable tool in seismic engineering to assess the structural performance of buildings under lateral loads. It is a complementary approach to the traditional linear dynamic analysis, in this study presented as the Response Spectrum Curves method, and provides a better understanding of the behaviour during seismic events.

In this type of analysis, the structure is subjected to an incremental lateral load distributed as an approximation of the loads that are experienced in an earthquake. The main advantage of this method is the ability to capture the nonlinear behaviour of the structure when metallic fasteners surpass its yield point. Accordingly to Fajfar (2021), strong seismic activity provides, in most buildings, significant inelastic deformations. However, codes only had assessments on ductility and nonlinear analysis after a long period of waiting. Nowadays, most advanced codes have in their methodologies the regulation of the nonlinear response history analysis, the most advanced dynamic analysis available for deterministic models. Still, its implementation bumps into a lot of complexities which makes this method only commonly applied to more complex structures, since simpler methodologies can carry out similar results. Among the available possibilities, one of the methods with a good equilibrium between good reliability and everyday design use applicability is the pushover analysis combined with the N2 method.

The loading procedure must follow the displacement shape of the most important vibration mode, typically the first one for regular structures. The vertical distribution of lateral forces is done through Equation 3.28. The result of this first step is commonly shown as the base shear versus

the average top displacement to have the capacity diagram.

$$P_i = m_i \Phi_i \quad (3.28)$$

where  $\Phi$  is taken as unitary at the roof level and proportional to that in the other floors.

Alongside that, it is needed to build the single-degree-of-freedom (SDOF) model to determine the seismic demand in the structure. This idealisation of the system, reduction of the multi-degree-of-freedom (MDOF) structure to an SDOF oscillator, is called the transformation of quantities and aims to calibrate the SDOF model. Initially, it is needed to calculate the total mass of the oscillator, being the same as the total mass of the structure and, in the present case, the extra permanent load. It can be mathematically written as Equation 3.29. The transformation factor can be obtained employing Equation 3.30.

$$m^* = \sum m_i \Phi_i \quad (3.29)$$

$$\Gamma = \frac{m^*}{\sum m_i \Phi_i^2} \quad (3.30)$$

where  $m^*$  is the equivalent mass of the SDOF system;  $m_i$  is each mass considered in the model;  $\Phi_i$  is the proportional component of the assumed shape; and  $\Gamma$  is the transformation factor, *i.e.*, the variable used to create the relation between SDOF and MDOF.

After the determination of the previous modal parameters, it is necessary to define the bilinear capacity curve of the SDOF system. This curve is created using the pushover data considering the equivalency of energy of both capacity curves. To do so, it is necessary to determine two parameters: yielding displacement of the equivalent SDOF system ( $d_y^*$ ); and period of the equivalent SDOF system ( $T^*$ ), which are presented in Eqs. 3.31 and 3.32, respectively.

$$d_y^* = 2 \left( d_y^* - \frac{E_u^*}{F_y^*} \right) \quad (3.31)$$

$$T^* = 2\pi \sqrt{\frac{m^* d_y^*}{F_y^*}} \quad (3.32)$$

Then, it is needed to determine the performance point by intersecting the equivalent bilinear curve obtained with the capacity curve of the pushover analysis with the elastic response spectrum

determined by the respective code. To do so, both curves must be under the same units. Thus, it is necessary to transform the equivalent capacity force into elastic acceleration and the period axis of the response spectrum into spectral displacement. These transformations can be done by means of, respectively, Eqs. 3.33 and 3.34.

$$S_e = \frac{F^*}{m^*} \quad (3.33)$$

$$d_e^* = S_e(T^*) \left[ \frac{T^*}{2\pi} \right] \quad (3.34)$$

Finally, the period is compared to the  $T_c$  of the construction of the response spectrum curve (see Figure 5.2) and determine if the period of the SDOF equivalent system is shorter than the corner period  $T_c$ , the value used to build the Response Spectrum Curve (RSC) - comparison of periods presented in Figure 3.10. This is done to determine the way of calculating the displacement of the equivalent system. Considering the medium to long period range, the target displacement is defined by Equation 3.35, defined as:

$$d_t^* = d_{et}^* = S_{De}(T^*) \quad (3.35)$$

where  $S_{De}(T^*)$  is the elastic displacement response spectrum at period  $T^*$ .

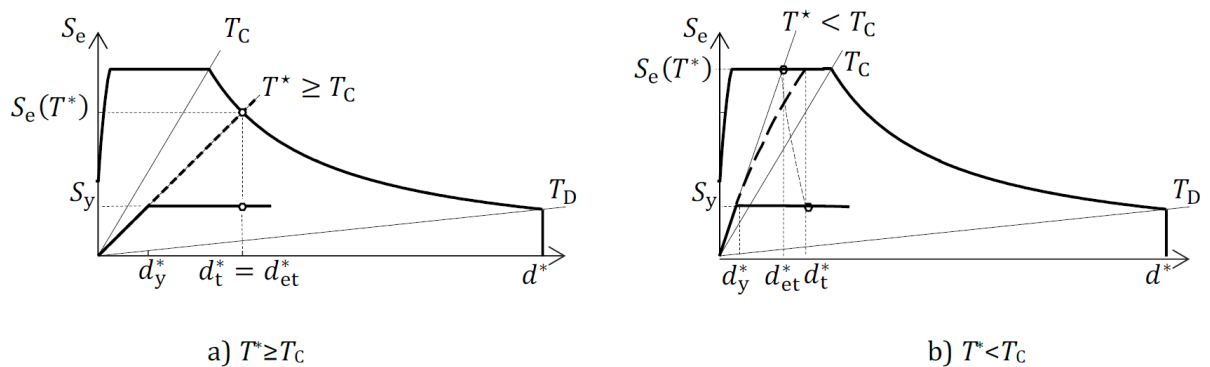


Figure 3.10 – Determination of the target displacement for the equivalent SDOF system (EN 1998, 2021).

## 4 METHODOLOGY

In this chapter, it will be presented all methods considered to implement the numerical solution proposed. It is important to specify the steps used in the generation of artificial seisms, the obtained signals from the database and explain the modelling of the building itself.

### 4.1 CALCULATION PARAMETERS

This section aims to provide information about the calculation carried out in RFEM 5 (DLUBAL SOFTWARE GMBH, 2020). It is proposed to explain the methods used and the assumptions made during the modelling process. The numerical simulation was performed using both linear and nonlinear static analysis concerning the behaviour of supports, elastic foundations, member hinges and releases.

Initially, the structural model must be discretized to create smaller elements to be able to approximate the continuous behaviour of an edification. This process creates elements with known mechanical properties, which are assembled in a global stiffness matrix. Then, it is introduced boundary conditions to define constraints and restrictions of the structure. During this phase, the whole stiffness matrix and load vector are modified to take into consideration the physical behaviour of the structure.

With the system of equations, the solution was carried out using the direct method. It was chosen instead of the iterative method available to reduce computational effort and, consequently, processing time. The direct method typically uses Gaussian Elimination, LU decomposition or Cholesky decomposition, depending on the geometry of the structure to optimise the solution. In the software used in the present study, there are two options to be chosen by the user: direct linear solver and iterative linear solver for symmetric sparse matrices. During the present study, the linear solver used was the direct one, which used the Cholesky decomposition. This method is presented in Equation 4.1 and was used to reduce processing time.

$$A = LL^T, \quad (4.1)$$

where  $L$  is a lower triangular matrix and  $L^T$  is the conjugate transpose of  $L$ . For the solution to be possible,  $A$  must be a positive-definite matrix.

The solution of nonlinear equations of the problem was solved using the Newton-Raphson method, in which the main function is presented in Equation 4.2.

$$x_{n+1} = x_n - [J(x_n)]^{-1} F(x^n), \quad (4.2)$$

where  $J(x)$  is the partial derivative matrix with respect to  $x$ . This matrix is also called the Jacobian Matrix. It is mathematically given by Eq. 4.3.

$$J_{ij}(x^n) = \frac{\partial F_i(x^n)}{\partial x_j} \quad (4.3)$$

During the modelling further presented, the building was computationally reproduced for the numerical analysis using bar elements to represent the metallic connectors and plates to represent the CLT walls and floors. Concerning plate modelling, the plate theory of Reissner-Mindlin plate theory was employed (LIU; QUEK, 2014; AWRUCH; LINN; MORSCH, 2018). The lamination was considered according to each lamella thickness and mechanical property. Since they were produced out of the same wood species, there were no differences despite the grain direction. When observing the hybrid CLT-concrete panel, a new layer was introduced with the proper properties of the concrete to the CLT panel. After this configuration, it is created by the software a local overall stiffness matrix for each surface. The Reissner-Mindlin theory is also known as the First Order Shear Deformation Theory (FSDT) and it is considered an extension of the Classical Plate Theory. FSDT considers the shear deformations along the thickness of the plate in a way that the straight fibres orthogonality to the middle surface are not imposed after the deformation (SANTOS, 2023).

## 4.2 NUMERICAL MODEL

The creation of the numerical model follows the same configuration elaborated by De Matos (2020). The building used during the numerical analysis and experimental campaign was built to simulate a real house with practical use. The ground and second pavement plans are presented in Figure 4.1. To fully understand the architecture of the building, the façades are presented in Figure 4.2.

Despite other ways to represent CLT-constructed buildings proposed in the literature, the numerical model used in the present study was created to represent the experimental campaign performed at the University of Minho and is marked to have a storey separation and the usage of bars to emulate metallic connectors. Unlinking floors is done to better represent fastener

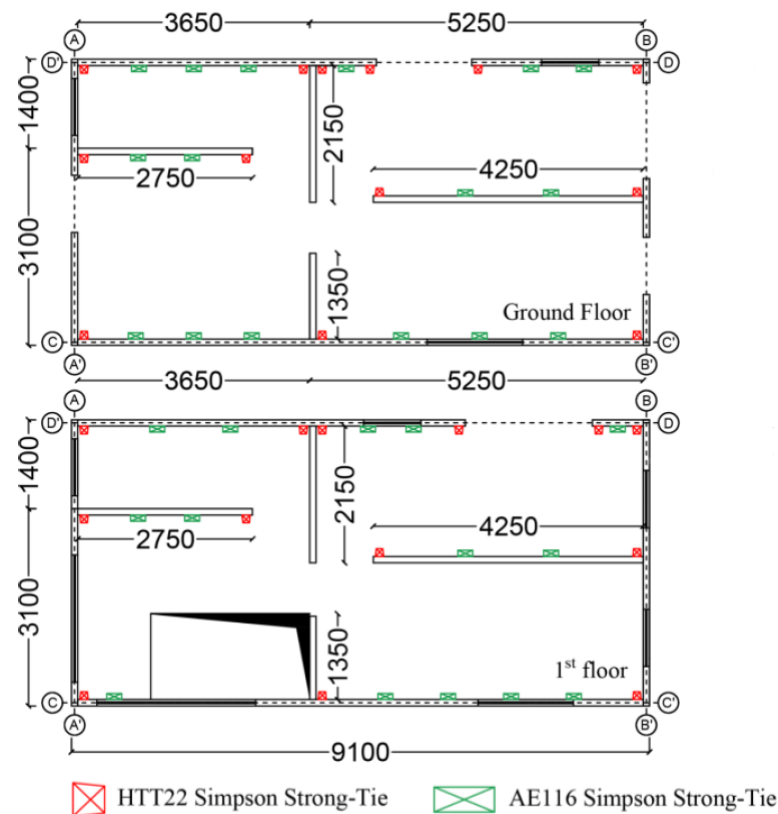


Figure 4.1 – Geometry of the analysed building - ground and second pavements (dimensions in mm) (De MATOS, 2020).

behaviour. The study carried out by De Matos (2020) used the gap between the diaphragm and the base of wall panels of 0.1 m, as presented in Figure 4.3. Concerning the load transfer to the ground, it was used a line hinge to recreate the metallic beam used to anchor the building to the soil.

The numerical modelling of the CLT panels was done using the RF-LAMINATE add-on module of the RFEM software. This consideration takes into account the lamellae configuration informed by the user and creates an equivalent stiffness matrix to the surface. During this study, the CLT panels were considered with linear and elastic behaviour, without any energy dissipation carried out in these elements.

Regarding connectors modelling, it was used nodal supports with nonlinear behaviour and rigid lines anchored into each CLT panel of 0.1 m in the geometry to represent hold-downs and angle brackets. As for their mechanical behaviour, they were characterised using load-displacement curves obtained according to cyclic loading procedures specified in CEN EN 12512 (2006) by De Matos (2020). This campaign used 3 different curves in the study, aiming to evaluate performance and establish the best fit for the proposed analysis. The curves are presented in Figure 4.5. The present study, due to the results shown in the numerical analysis of De Matos (2020), used as reference the 1<sup>st</sup> Load Envelope Curve (1<sup>st</sup> LEC).

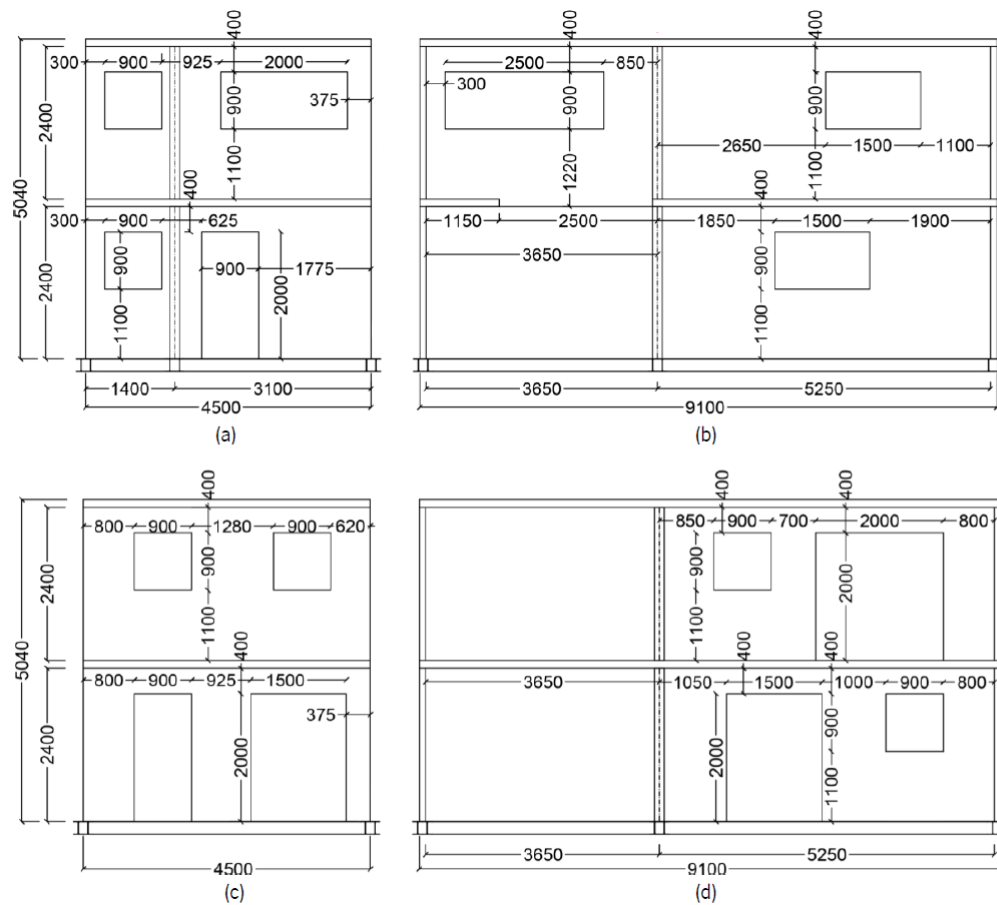


Figure 4.2 – Building façades (dimensions in mm). (a) AA' façade; (b) CC' façade; (c) BB' façade; and (d) DD' façade.

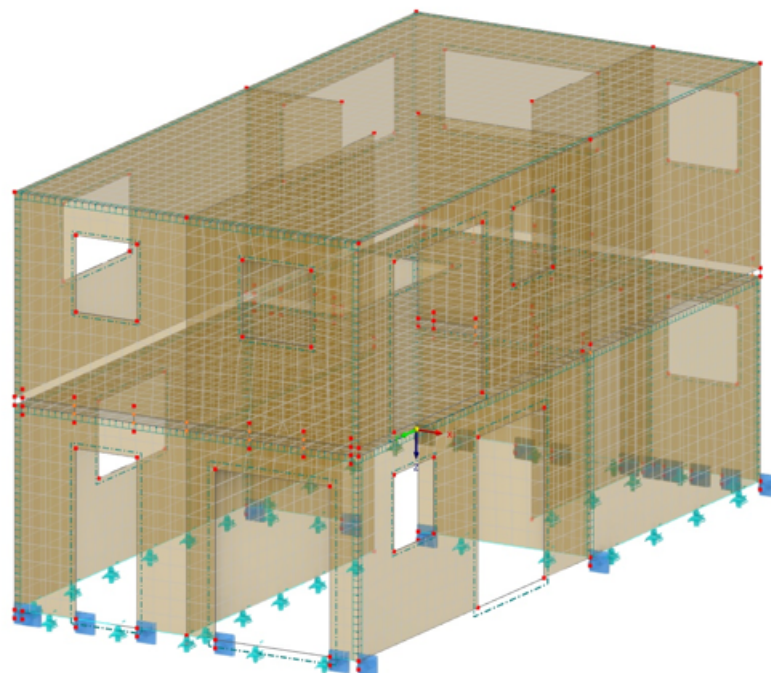


Figure 4.3 – Numerical model used in the present study.

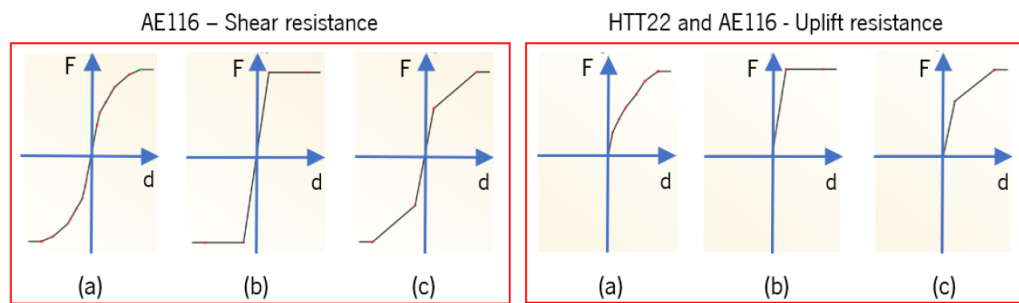


Figure 4.4 – Force versus displacement curves. (a) 1<sup>st</sup> LEC; (b) Equivalent Energy Elastic-plastic; and (c) bilinear curve (De MATOS, 2020);

The 2-storey building model was built in RFEM, a commercial analysis software from Dlubal Software (DLUBAL SOFTWARE GMBH, 2020). It is equipped with a graphic interface and tools that enable the user to fully characterise structural elements. Furthermore, RFEM is considered appropriate to model from simple reticulated to complex three-dimensional structures with its particularities. The solution is achieved with the employment of the Finite Elements Method, a methodology broadly used in Engineering, and, considering its vast discussion in the literature, its formulation shall not be further presented in the present study.

Connections between wall panels were considered rigid, as specified in De Matos (2020). The connections were considered as elements to dissipate energy during the excitation. To do so, their mechanical behaviour were specified as presented in the experimental campaign conducted in the study of De Matos (2020). The representation of these connectors are presented in Figure ???. This characterisation fulfils the requirements presented in Table 3.6. As the model used in the present study was already with a good level of detailing to consider DC2, the only specification that needed to be done was the joints between orthogonal walls. In the literature, it is possible to note a big variety of connections of this nature, such as nailed (BELLINI et al., 2020), screwed (GRAVIC; FRAGIACOMO; CECCOTTI, 2015; BROWN et al., 2021), dowelled (BROWN; LI, 2021) or even glued (AYANSOLA; TANNERT; VALLEE, 2022). In the present study, the screwed connection was adopted, since it has a higher capacity when compared to other connection types with good efficiency when submitted to lateral or axial loads (EINI; ZHOU; NI, 2022).



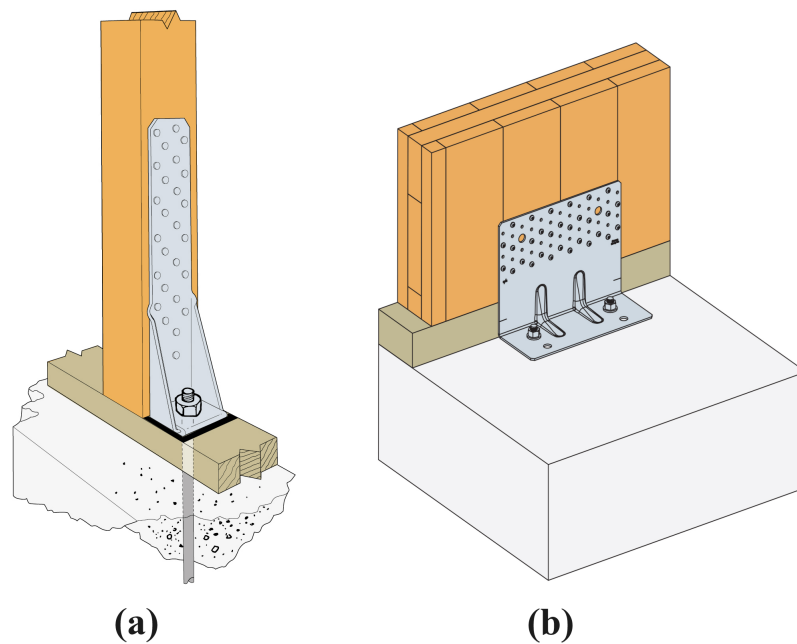


Figure 4.5 – Metallic connectors: (a) Hold-down; and (b) Angle Bracket.  
Adapted from Tie (2020);

The modelling of these connections was performed using the tool of line hinges of RFEM 5. The software considers every connection between surfaces as being rigid – the desired hypothesis in Ductile Class 1. However, to implement Ductile Class 2, it is needed to describe its mechanical behaviour. The line hinge tool makes it possible for the designer to choose between the degrees of freedom and exclude the restriction or, as in the proposed case, consider it as a spring. Therefore, the restoring force of similar connections published in the literature was used to determine the spring constant by means of Hooke's Law. Since there's no energy dissipation in these elements, only the elastic range of the force-displacement curves will be taken into consideration. If it is intended to perform a non-linear analysis on these elements, different modelling in RFEM 5 is needed in the face of its limitations. Experimental self-tapping screw (STS) connection behaviour is presented in Brown et al. (2021) and the reference test is also presented in Figure 4.6. This connection is represented in Figure 4.7 and is constituted of 8 fully-threaded (FT) with 8 mm of diameter. The material used to manufacture STS is hardened steel with strength up to 1000 MPa (BROWN et al., 2021).

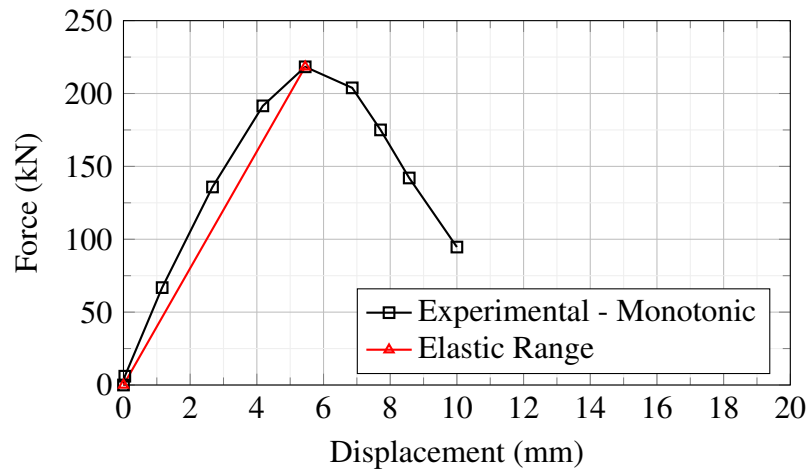


Figure 4.6 – Load-slip curve under shear for 16X-400 configuration.

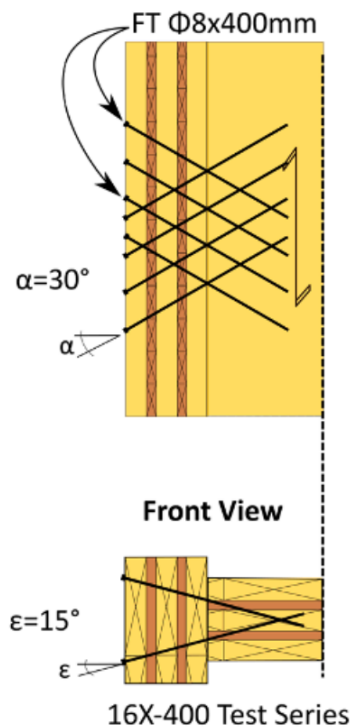


Figure 4.7 – Detailing of 16X-400 STS connection. Elevation and plan view, respectively. (BROWN et al., 2021)

From the presented data, it is possible to obtain the elastic stiffness of the connection using Hooke's Law. Hence, the spring constant used to describe the 16X-400 STS connection in orthogonal panels was 40.057 kN/m.

For this modelling, two types of elements were used: one-dimensional and two-dimensional. There were no solid elements used. A total of 449 1D finite elements and 2560 2D finite elements were implemented. The length of the elements was set to 0.5 m, which was consistent with the configuration used in the De Matos (2020) study. A simple convergence test was conducted,

and it was found that there were no significant productivity gains by using a higher number of elements than the one used in De Matos (2020).

In order to accurately represent the fasteners used in the real configuration, one-dimensional members were used. Rigid beam elements were introduced and all degrees of freedom were taken into consideration during the analysis. The rigidness consideration is done using the penalty method, with a couple of orders higher than the surrounding aiming to set the rigid behaviour as well as the stability of the analysis. The element can be visually depicted in Figure 4.8.

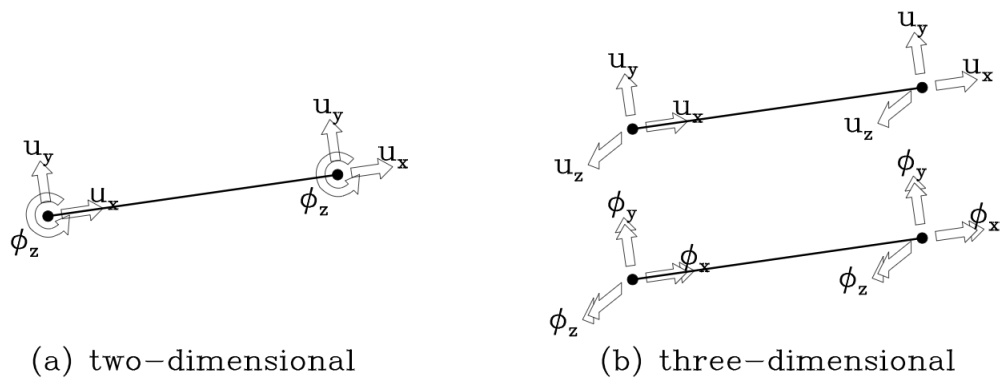


Figure 4.8 – Representation of a beam element. (DIANA, s.d.).

On the other side, considering the two-dimensional elements, the mixed interpolation of tensorial components (MITC) approach was used with quadrangles (4 nodes) and triangular (3 nodes) elements - MITC4 (see Figure 4.9) and MITC3 (see Figure 4.10), respectively. MITC3, as presented in Lee and Bathe (2004), was used in RFEM 5 in replacement of the Lynn-Dhillon element aiming to avoid shear locking error when Reissner-Mindlin theory is applied. The same occurs with MITC4, which is used as nonlinearities can lead to instabilities in Lynn-Dhillon, and as a consequence, the software uses this more robust element. In bar elements, to linear cases the analytical integration is performed and to nonlinear the Gaussian quadrature. To plates, both methods are used, the first one in triangular elements (MITC3) and the latter in quadrangle elements (MITC4).

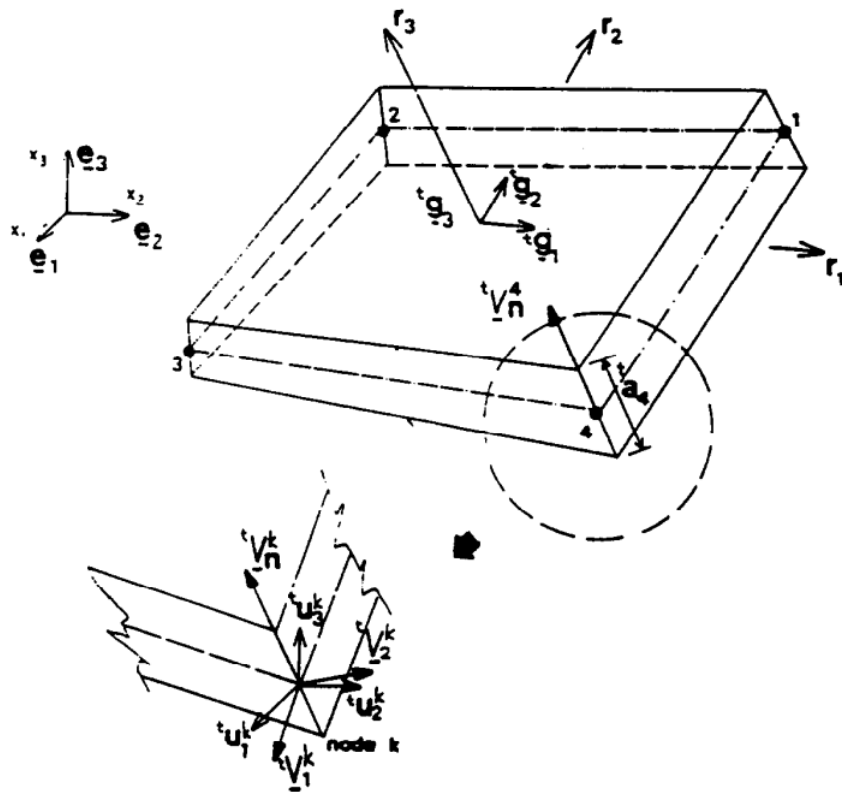


Figure 4.9 – Representation of the MITC4 element. (DVORKIN; PANTUSO; REPETTO, 1995)

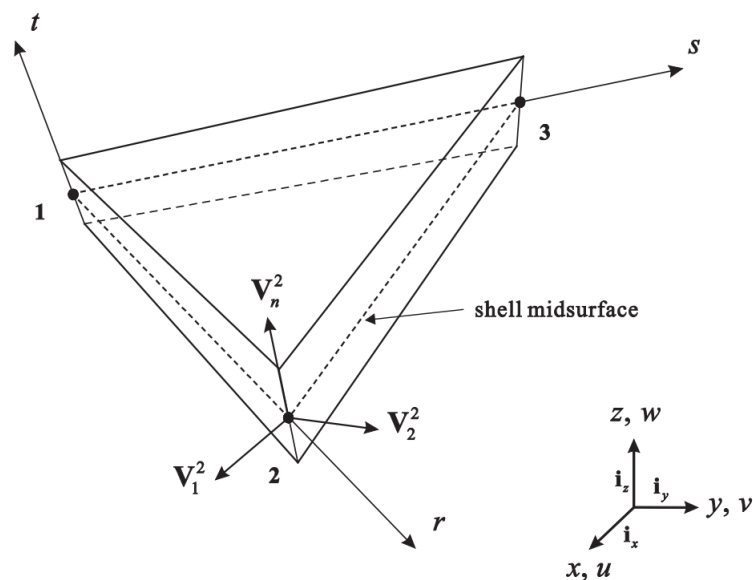


Figure 4.10 – Representation of the MITC3 element. (LEE; LEE; BATHE, 2014)

### 4.3 MODEL VALIDATION

The numerical model validation was done by means of the experimental campaign carried out by De Matos (2020). In this study, the building was submitted to hydraulic jack action at two different points, one of them located at the top of the first floor and the other at the top of the second floor. Both were located in a plane that contains the centre of the building. Two protocols were established during these tests: quasi-static monotonic and cyclic tests. The former consisted on the application of displacement at a constant rate, being 0.08 mm/s for the second and 0.04 mm/s for the first floor. The latter procedure was based on force control when it was prescribed 0.90 kN/s for the first floor and 1.80 kN/s for the second one. Both protocols were carried observing prescriptions made in ISO/FDIS 21581 (2010).

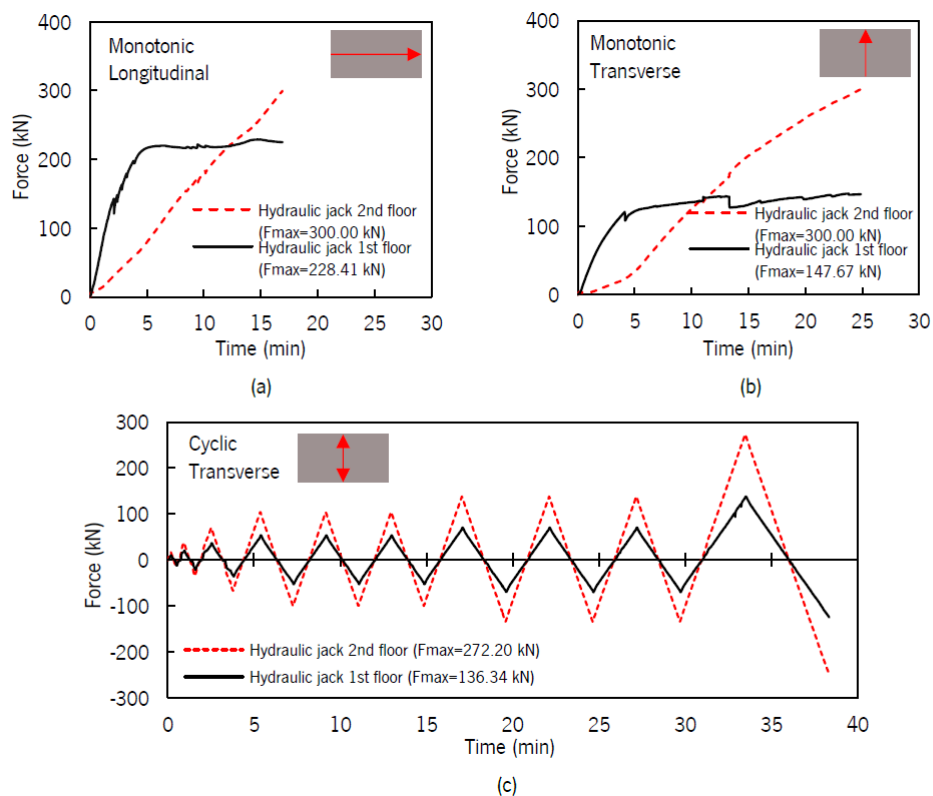


Figure 4.11 – Hydraulic jack action over time during the tests: (a) monotonic test in the longitudinal direction; (b) monotonic test in the transverse direction; and (c) cyclic test in the transverse direction. (De MATOS, 2020).

Figure 4.11 presents the structural response of the building due to the hydraulic jack excitation, according to the protocol observed. These protocols were not possible to be replicated under RFEM 5 availability of loads types. For this reason, the model was submitted to the maximum load achieved in each jack and compared to the displacements obtained in the monotonic experimental test. The values of these loads considering the transverse direction are also presented in Figure 4.11, being 300 kN and 147.67 kN to the second and first floors, respectively. Maximum

displacements obtained during the experimental campaign can be observed in Figure 4.12.

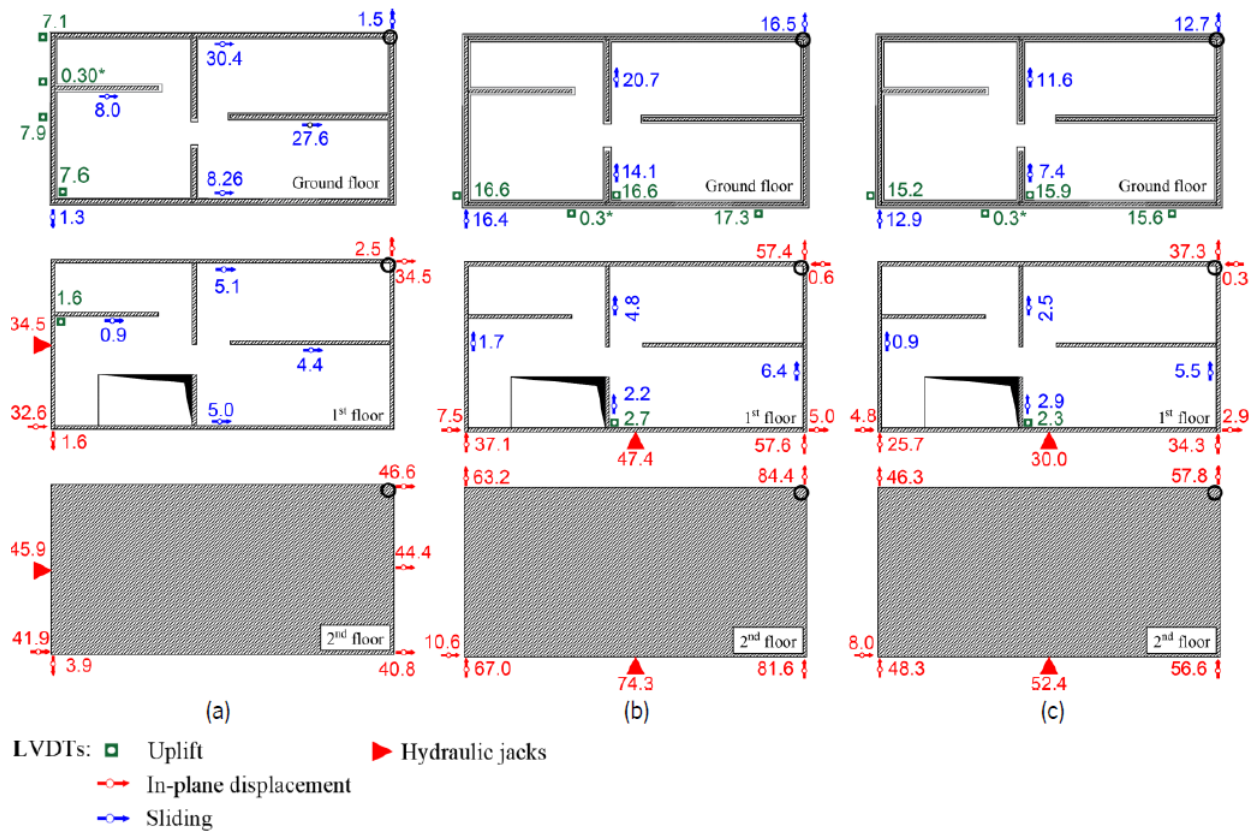


Figure 4.12 – Maximum displacements in mm: (a) monotonic test in the longitudinal direction; (b) monotonic test in the transverse direction; and (c) cyclic test in the transverse direction. (De MATOS, 2020).

These displacements were used as a parameter of comparison in order to establish the model validation. Considering the results presented in De Matos (2020) (Experimental), the longitudinal direction model ended up being stiffer and, however, less interesting in the present study. Thus, the transverse direction results were compared to the numerical model and are presented in Table 4.1. This table presents the comparison between the available results due to the experimental campaign and the numerical analysis carried out to validate the model in the present study.

As one can note, the structural behaviour of the numerical model is very similar to the experimental tests. This difference is considered a good approximation when taking into consideration the loading difference and the simplifying hypothesis. The average relative difference, taken as the arithmetic mean of the nodal relative difference, resulted in a value of 11%, without the consideration of friction influence.

Table 4.1 – Experimental and numerical displacement in transverse direction results in comparison.

Floor	Node	Experimental De Matos (2020) (mm)	Present Study (mm)	Abs. Dif. (mm)	Rel. Dif. (%)
1 <sup>st</sup>	1	57.6	49.5	8.1	14
	2	37.1	42.2	5.1	14
	3	57.4	47.1	10.3	18
2 <sup>nd</sup>	1	81.6	72.8	8.8	11
	2	67.0	65.9	1.1	2
	3	84.4	72.9	11.5	14
	4	63.2	65.9	2.7	4

Concerning the story drift, results are shown in Figure 4.13 and the deformed configuration is illustrated in Figure 4.14. It showed a good agreement on the behaviour of the numerical model when compared to the experimental data. The point of the presented analysis is the centre of the building, *id est*, the point of application of the hydraulic jack load. The numerical model presents a higher slip between floors when compared to the experimental results. This slip is measured as the difference between the top of wall panels in the ground pavement and the bottom of the panel in the second pavement. It can be interpreted as the influence of the method of storey separation and the simplifying hypothesis of zero friction between CLT panels.

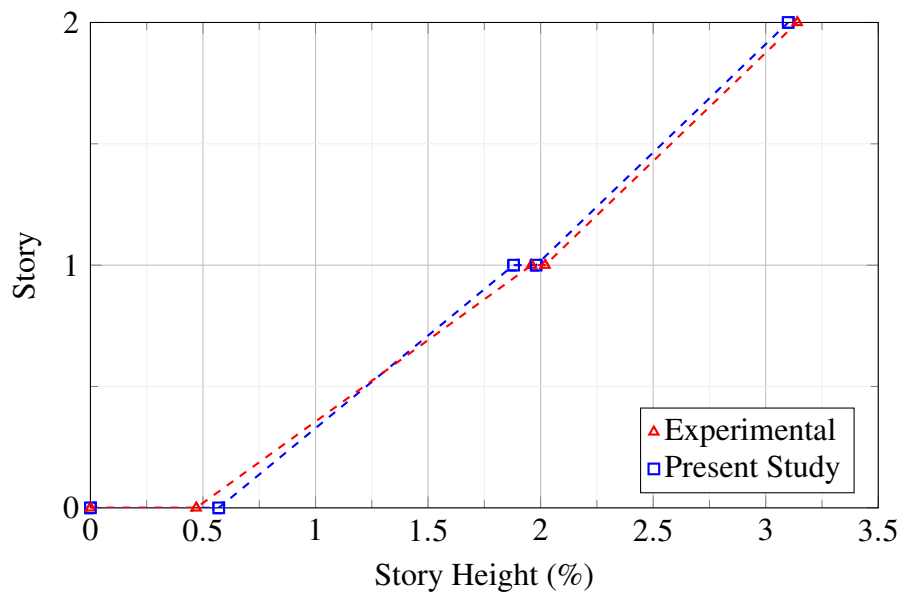


Figure 4.13 – Story Drift comparison: experimental and numerical model results.

Another critical parameter of the model is due to the comparison in order to evaluate the global stiffness and ductility of the model is the base shear force versus the displacement at the top. Figure 4.15 shows both experimental and numerical curves obtained. To do so, it was necessary to introduce another method of calculation to achieve the presented diagram. As previously mentioned, forces were introduced instantly to the model and obtained displacements were

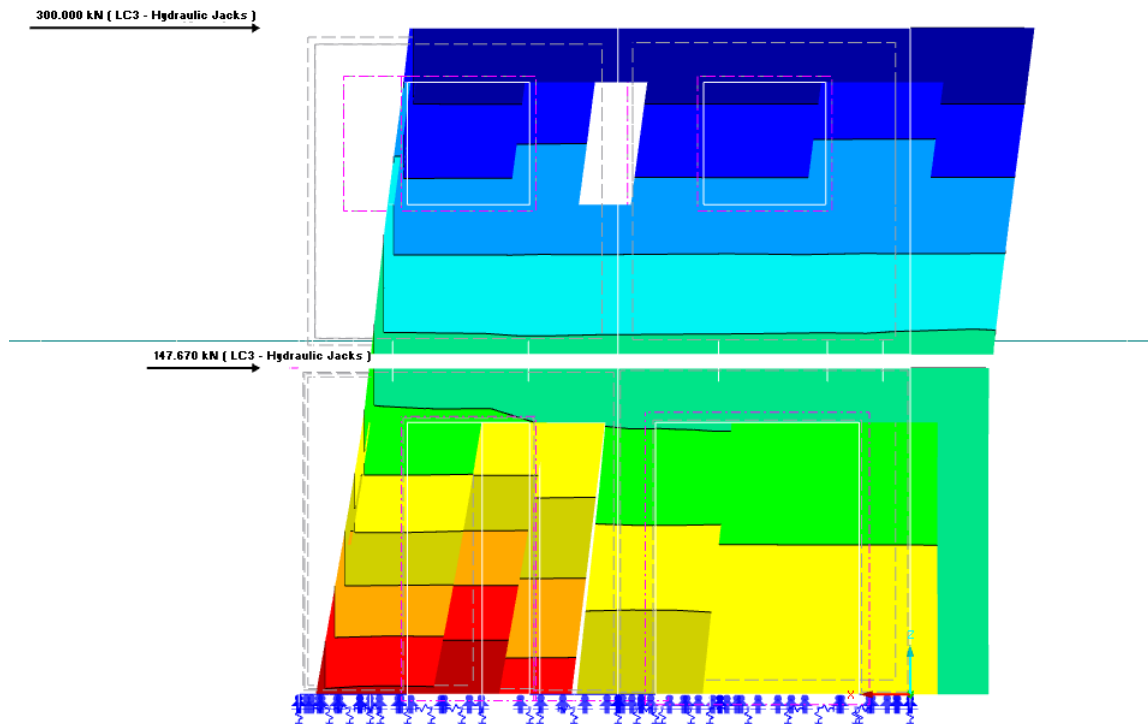


Figure 4.14 – Deformed configuration after hydraulic jack load application.

compared in Table 4.1 and Figure 4.13. However, it was not possible to study the building behaviour during the loading with this methodology. Thus, the load was gradually introduced at a rate of 5% in each application until it reached the full load previously presented. No difference was noticed when comparing displacements of instantaneous application and stepped load.

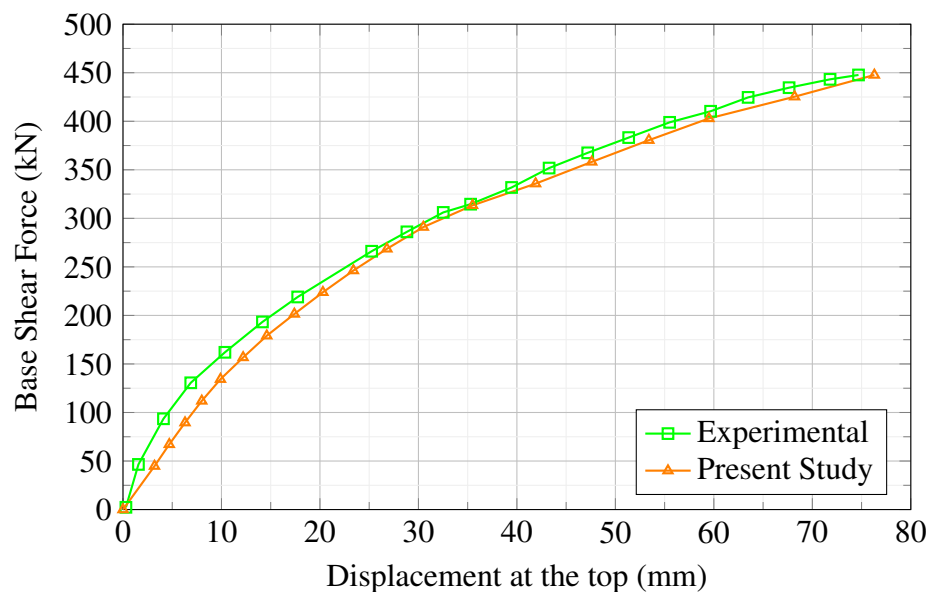


Figure 4.15 – Experimental and numerical model comparison of base shear forces versus displacement at the top.

One can note the existing difference in initial stiffness when comparing the experimental results



and those obtained in the present study. This discrepancy can be attributed to the lack of elasticity tests carried out on the material used to calibrate the model. In the present study, the data was provided by the manufacturer. However, despite this, the results above made it possible to consider the model calibrated and suitable to be used in parametric studies on the seismic response of the type of CLT building evaluated by De Matos (2020).

## 4.4 LOAD CASES

During the present study, different load cases were used to evaluate the building behaviour under seismic activity. As previously presented, the assessment under EC8 and NBR 15421 can be performed with the aid of Response Spectrum Curves, which shall be the first load case used due to its large applicability in designing. Alongside that, it was intended to establish a comparison of both codes and real events data, which was only possible to European locations for instance. To balance this lack of Brazilian seismic data, it was proposed the usage of the Kanai-Tajimi filtering method (CHIESA; MIGUEL, 2017) to generate artificial stationary accelerograms and evaluate behaviour.

The following topics will present the specified locations of the events chosen, as well as the formulation carried out in the signal generation process.

### 4.4.1 Seismic Data

Seismic data will be used to analyse building behaviour compared to response spectrum curves. The database used, the Engineering Strong-Motion Database (ESM), in this study is available online and is made public by Luzi et al. (2016) and Lanzano et al. (2021). These authors developed a strategy to encompass all previous European databases to simplify the access to strong-motion data, *i.e.* earthquakes with higher magnitude than 4, since there was no unified and reliable database for long-term usage. This database compiles information from 1969 up to nowadays on the Pan-European region.

Data collection was initially formed with regional databases of Greece, the Unified Hellenic Accelerogram Database (HEAD), Italy, the Italian Accelerometric Archive (ITACA), Turkey, the National Strong-Motion Network of Turkey and the European Strong-Motion Database (ESD), used to recover pan-European data. Further, it introduced new databases and continuous data services, linked with Incorporated Research Institutions for Seismology (IRIS) and European Integrated Data Archive (EIDA). Nowadays, the platform has 45,685 different waveforms in its archive and is fully available online. ESM processed all data used in the present study with the procedure described in Paolucci et al. (2011).

Regarding the data retrieved to use in the study, it was considered 2 locations: Villacollemantina, in Italy, and Manteigas, in Portugal. The proposed events were chosen based on the seismic region- Portugal is the original place where the experimental campaign was carried out and Italy is a country with high seismicity. Both accelerograms are presented in Figures 4.16 and 4.17 and are representative of recent earthquakes of a magnitude of approximately 4 points, presented in Richter Scale. Considering the date of the seisms, it is possible to infer that the ESM database complies with the proposed objectives to simplify and provide normalised up-to-date data. The time discretisation adopted was 0.005 s, reaching approximately 16 and 33 thousand values, respectively.

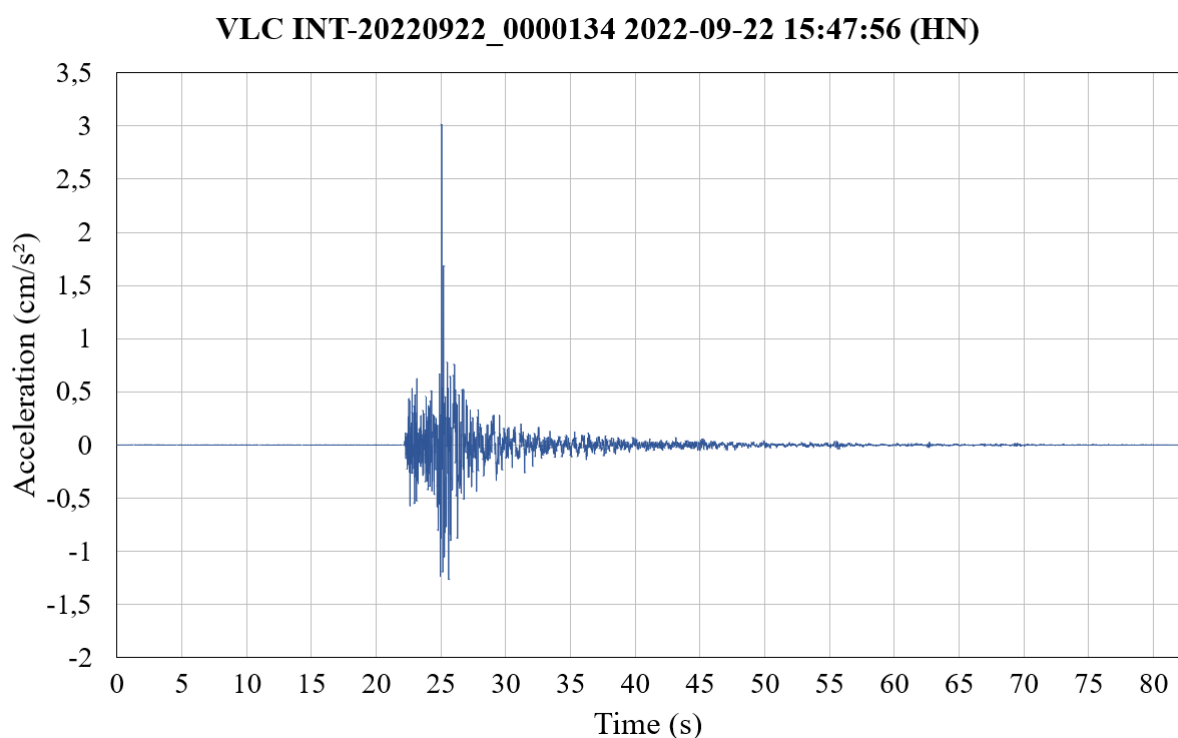


Figure 4.16 – Accelerogram of an event in Villacollemantina, Italy - 22nd September 2022 (Adapted from Luzi et al. (2016)).

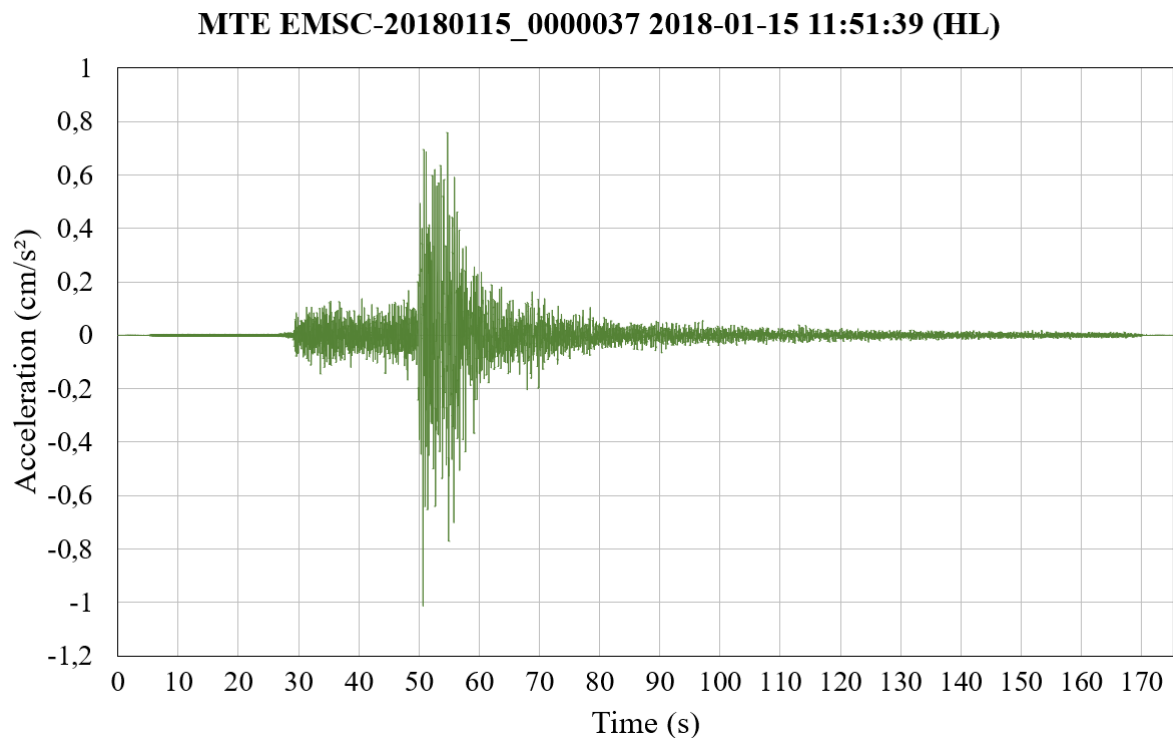


Figure 4.17 – Accelerogram of an event in Manteigas, Portugal - 15th January 2018 (Adapted from Luzi et al. (2016)).

As the numerical model is duly implemented, it is possible to resort to other events with higher magnitudes and intensities. Initially, it was intended to use recent data with relevant impact, in order to evaluate and assess the building behaviour.

Differently from Europe, the availability of seismic data in Brazil is limited to those who do not have direct access to the seismographic network internal system, since it is not provided publicly. After a few attempts, it was not possible to reach out to any of the members of the *Rede Sismográfica Brasileira* (RSBR, in English: Brazilian Seismographic Network), the main joint effort coordinated by the Brazilian government that compiles data provided by stations in all regions of the country. Due to that, an alternative using Kanai-Tajimi filtering was proposed and is presented in the next subsection.

Data presented in Figures 4.16 and 4.17 are the compilation of full events, comprehending since and until the rest of the seismograph. Considering the computational usage of the available data, it is recommended to discard the instants without relevant information, such as initial and final null values, reducing the computational effort.

#### 4.4.2 Kanai-Tajimi Spectrum

Kanai (1961) and Tajimi (1960) proposed a method to create an accelerogram of an artificial seismic excitation by means of a stochastic process. This random process is used to generate a filtered Gaussian white noise using soil properties and is broadly used in Seismic Engineering (SILVA, 2021; FAN; AHMADI, 1990). The white noise is defined by Azevedo (2020) as being a stationary process with equal contribution of all frequencies in the signal obtained as a result. Considering that the acceleration in a real event of earthquake is not stationary, there are methods presented in the literature to simulate this behaviour. The most common is the implementation of an envelope function to recreate the real phases of seisms in time: initial ground acceleration growth, peak region and return to rest. However, due to simplicity since this is not the main point of analysis, the stationary accelerogram will be used. Kanai-Tajimi filtering scheme is presented in Figure 4.18.

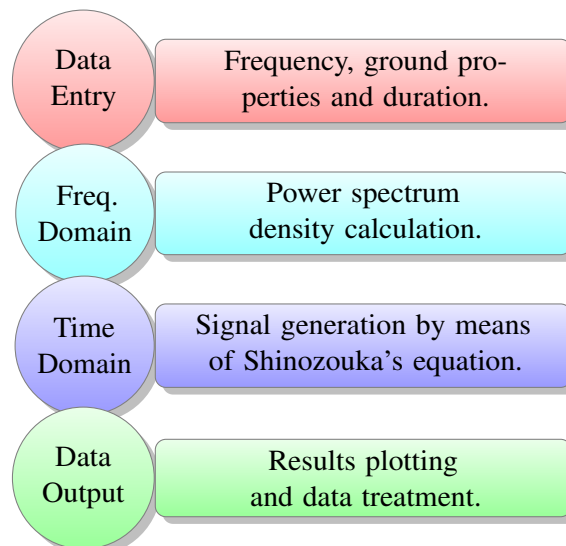


Figure 4.18 – Computation routine to generate accelerogram.

Initially, the stochastic process is defined to be a collection of  $N$  sample functions that define a random experiment repeated also  $N$  times (CHIESA; MIGUEL, 2017). Considering this definition, a phenomenon defined by a random process has known properties in each instant of time, taken as the average in the specific observed time of all sample functions. It can be mathematically translated in Equation 4.4.

$$\mu_p(t_s) = \lim_{N \rightarrow \infty} \frac{1}{N} \sum_{m=1}^N p_m(t_s), \quad (4.4)$$

where  $\mu_p(t_s)$  represents the mean value of  $p(t)$  in instant  $t_s$  and  $N$  is the number of samples, or, in other words, the amount of times the phenomenon was repeated (CHIESA; MIGUEL, 2017). Kanai-Tajimi spectrum is calculated by means of Equation 4.5.

$$S(\omega) = S_0 \left[ \frac{\omega_g^4 + 4\omega_g^2 \xi_g^2 \omega^2}{(\omega^2 - \omega_g^2)^2 + 4\omega_g^2 \xi_g^2 \omega^2} \right] \quad (4.5)$$

$$S_0 = \frac{0.03 \xi_g}{\pi \omega_g (4 \xi_g^2 + 1)} \quad (4.6)$$

where  $\omega_g$  is the ground's natural frequency in *rad/s*;  $\xi_g$  is the soil damping;  $\omega$  is the frequency vector, also in *rad/s*; and  $S_0$  is the spectral density constant, given by Equation 4.6. Concerning  $\omega_g$  and  $\xi_g$ , their values are taken as in Table 4.2.

Table 4.2 – Properties used in Kanai-Tajimi's method (SEYA; TALBOTT; HWANG, 1993).

Soil Type	$\omega_g$ (rad/s)	$\xi_g$	Total duration (s)
Rock	$8\pi$	0.60	15
Stiff soil	$5\pi$	0.60	20
Soft soil	$2.4\pi$	0.85	25

The spectrum creation routine used in the present study was computationally done using MATLAB software, presented in Figure 4.19, and the code can be checked in App. A. Modelling validation was carried out with values published in Chiesa and Miguel (2017).

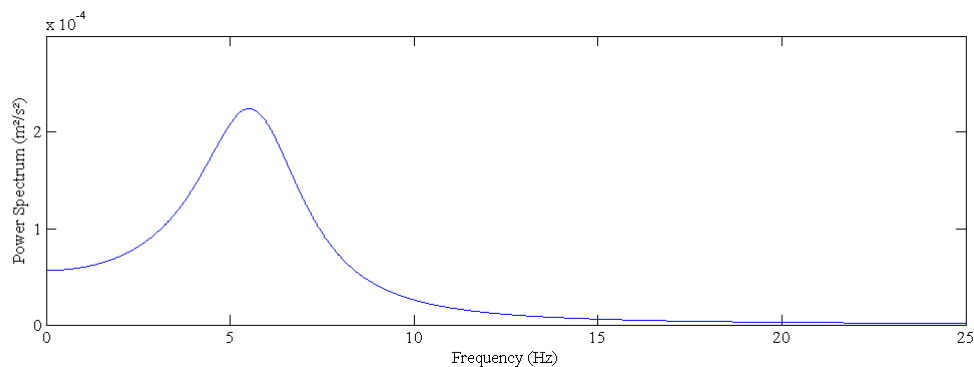


Figure 4.19 – Power Spectrum generated with Kanai-Tajimi filter to  $\omega_s = 37.3$  rad/s and  $\xi_s = 0.3$ .

The solution of Equations 4.5 and 4.6 presented in Figure 4.19, results in a signal in the frequency domain. To use it in structural analysis, it is necessary to obtain ground acceleration in time domain, which is possible with the usage of the equation:

$$\ddot{y}(t) = \sqrt{2} \sum_{k=1}^{N_\omega} \sqrt{S_w(\omega_j) \Delta\omega_j} \cos(\omega_j t + \phi_j) \quad (4.7)$$

where  $N_\omega$  is the amount of intervals of the frequency band;  $\Delta\omega$  is the increment of frequencies and  $\phi_j$  is the phase angle taken randomly with standard uniform distribution from 0 up to  $2\pi$ . The Shinozouka-Jan's equation, Equation 4.7, does a superimposition of amplitudes for each frequency in the same instant of time. This process enables a signal of accelerations over time of the artificial seism. As a final step, it is carried out a normalisation of the values obtained, into which the peak value of the data series is equal to the Peak Ground Acceleration (PGA) for the location studied. The normalised results can be observed um Figure 4.20.

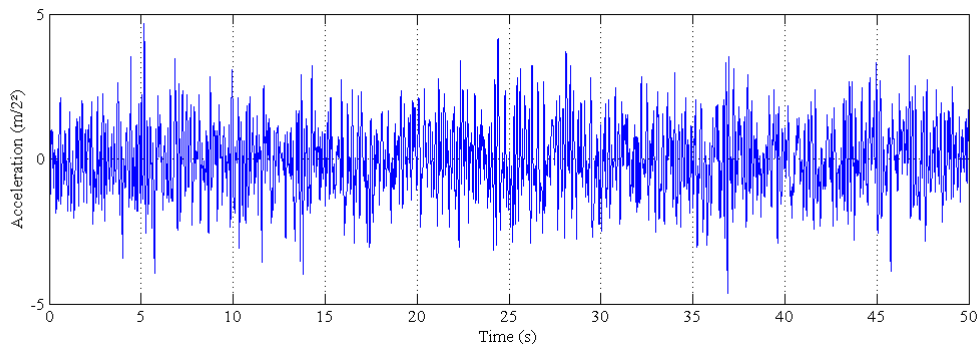


Figure 4.20 – Ground accelerations over time generated using Kanai-Tajimi spectrum -  $\omega_s = 37.3$  rad/s and  $\xi_s = 0.3$ .

After the routine validation, four spectra were generated in order to evaluate the structural behaviour of the CLT building. The first one was considering the average natural frequency of the first vibration mode of all models studied in the parametric assessment as the ground frequency, aiming to induce resonance in the structure due to the similarity of excitation and natural periods. After that, three scenarios were proposed, according to the recommendation presented in Seya, Talbott and Hwang (1993) for rock, stiff soil and soft soil. Considering the PGA normalisation, it was used  $0.15g$  as the peak value, since it is the higher acceleration in the Brazilian code. The resulting accelerograms are presented in Figures 4.21, 4.22, 4.24 and 4.23.

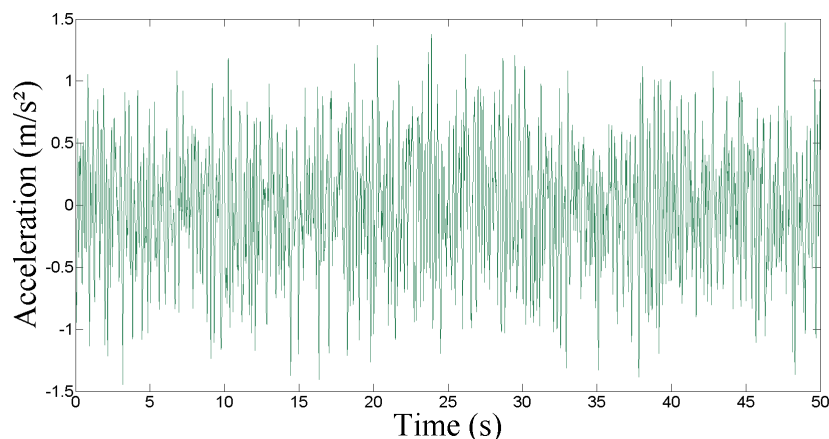


Figure 4.21 – Ground accelerations over time generated using Kanai-Tajimi spectrum -  $\omega_s = 30.33$  rad/s,  $\xi_s = 0.3$  and PGA =  $0.15g$ .

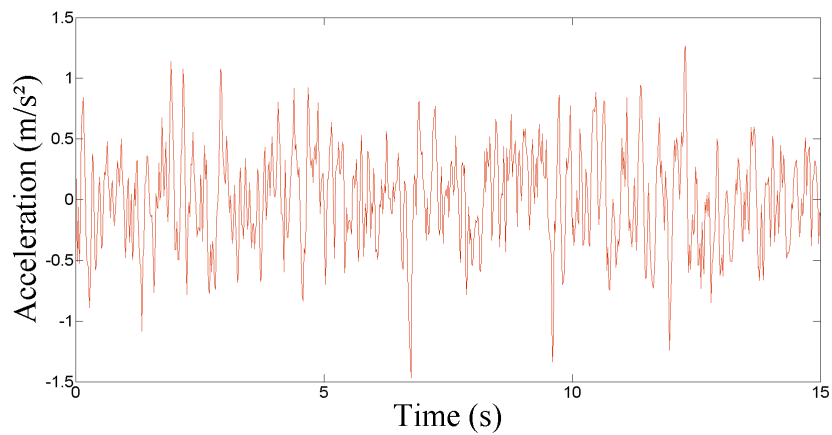


Figure 4.22 – Ground accelerations over time generated using Kanai-Tajimi spectrum - Rock -  $\omega_s = 8\pi$  rad/s,  $\xi_s = 0.6$  and PGA = 0.15g.

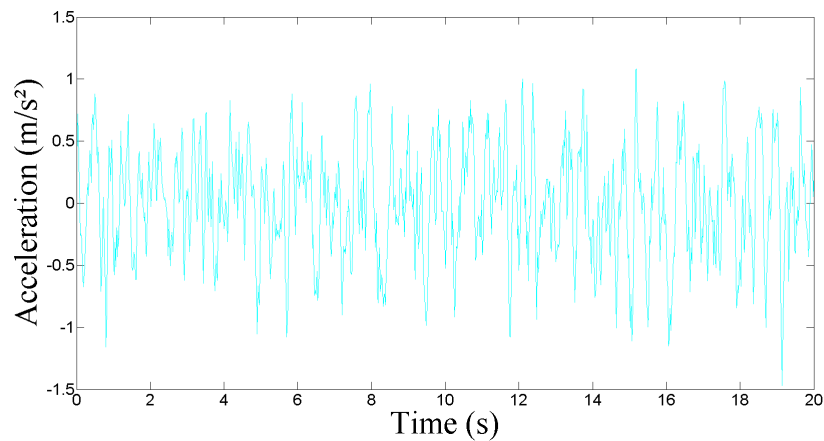


Figure 4.23 – Ground accelerations over time generated using Kanai-Tajimi spectrum - Stiff Soil -  $\omega_s = 5\pi$  rad/s,  $\xi_s = 0.6$  and PGA = 0.15g.

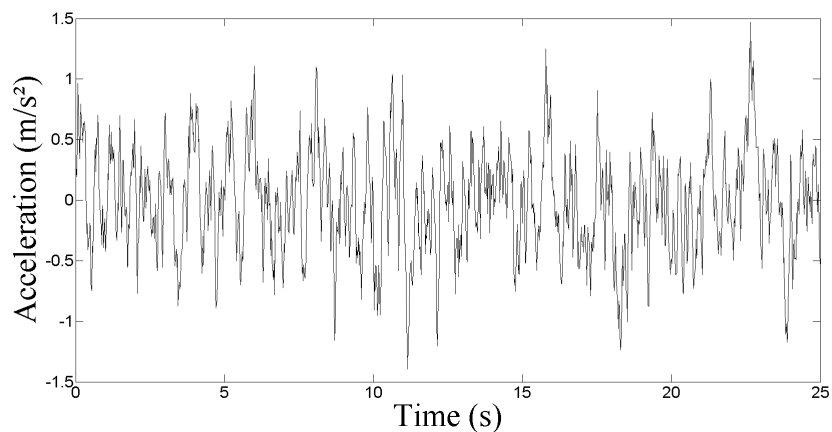


Figure 4.24 – Ground accelerations over time generated using Kanai-Tajimi spectrum - Soft soil -  $\omega_s = 2.4\pi$  rad/s,  $\xi_s = 0.85$  and PGA = 0.15g.

## 5 RESULTS AND DISCUSSION

In this chapter, the results obtained after the implementation of the methodology previously established are presented. The sections are divided by type of load, firstly the obtained results considering the two codes under evaluation are discussed. Then, real and artificial events are compared to the normative prescription. In a second moment, a parametric study is conducted in order to enhance design through the energy dissipation in metallic connectors during seismic load.

### 5.1 RESPONSE SPECTRUM CURVES

As previously presented, the response spectrum method represents an envelope curve of a great variety of events observed in a determined location. To do so, it is important to take into consideration site characterisation and seismic hazard - see Tables 3.3 and 3.7 and Figs. 3.7 and 3.8. The evaluation carried out in this section aimed to generate response spectrum curves from each code, respecting its prescriptions, however normalising site effects into the results.

The location was arbitrarily created, taking as a parameter Brazilian higher seismic hazard, since due to its low seismicity, the higher region is considered as medium activity in European code. With that in mind, the analysed site was located in the Brazilian state of Acre, in the west Amazon region. Accordingly, to the isopleth map presented by NBR 15421 (2023), it is inserted in Zone 4 with a *PGA* of 0.15g and a medium stiffness soil was chosen with a *SPTN*-value of 25 blows - being characterised as D site category, C seismic category and I structural category. With this information, it was possible to build the response spectrum curve out of the prescription of NBR 15421 (2023), which can be seen in Figure 5.1. It is important to point out that there is no ductility assessment in this code.



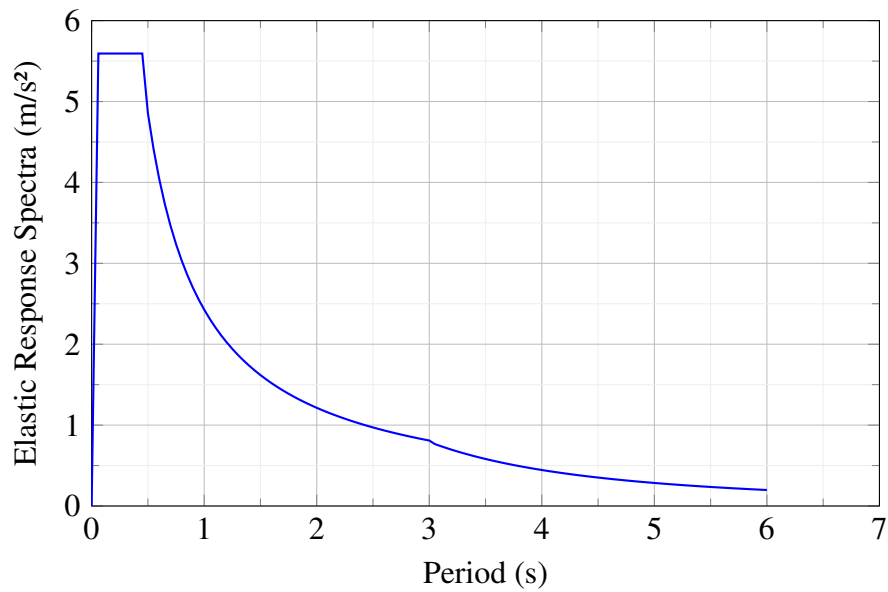


Figure 5.1 – NBR 15421 (2023) elastic response spectrum.

Following the similar parameters previously used to create the Brazilian respective response spectrum curve, with the aid of the site categorisation methodology presented in Chapter 4, the EC8 curves for the proposed regions in Europe are presented in Figures 5.2 and 5.3. Both curves took into account the National Determined Parameters, available in the respective National Annexes of each country (NP EN 1998-1, 2010; UNI EN 1998-1, 2007).

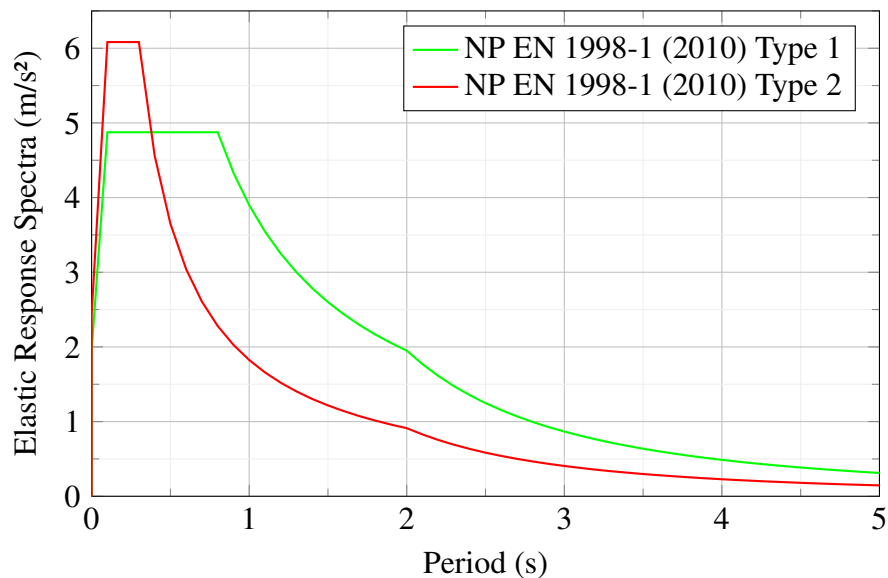


Figure 5.2 – Portuguese elastic response spectrum.

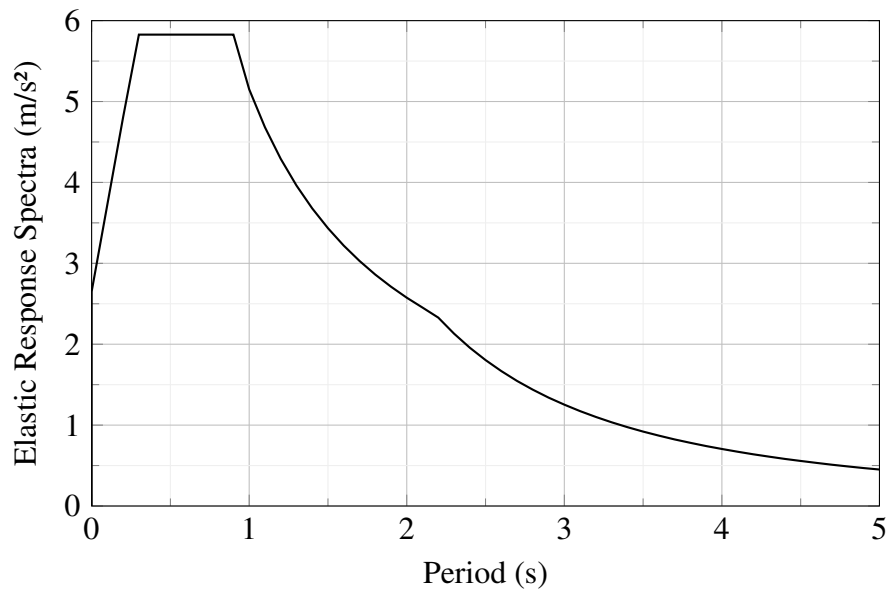


Figure 5.3 – Italian elastic response spectrum.

After the curve characterisation, it is possible to introduce it into the RFEM 5 software in order to create a Dynamic Load Case, with the aid of the RF-DYNAM Pro add-on module. The obtained results are presented in Table 5.1. It is important to point out that the given curves concern the elastic response, EC8 enables the designer to take advantage of the structure's capacity to dissipate energy even in low ductility class (DC1) by means of a behaviour factor. Due to that, the presented curves shall be reduced by 1.5, the proposed behaviour factor value for DC1. This configuration is performed directly in RFEM 5, which has a field to take into account this coefficient. It is important to highlight that the presented values do not represent story drift, since they are the average absolute displacement at the top of the first and second pavements. Relative displacement is the percentage of the displacement compared to the height of the story.

Table 5.1 – Average displacements, maximum base shear and average stiffness by load case.

Description	1 <sup>st</sup> floor		2 <sup>nd</sup> floor		Base Shear (kN)	K (kN/m)
	Avg. d (mm)	Rel. d (%)	Avg. d (mm)	Rel. d (%)		
NBR 15421 (2023)	4.3	0.1780%	5.6	0.2340%	183	32565
NP EN 1998-1 (2010) Type 1	3.1	0.1292%	4.1	0.1688%	133	32748
NP EN 1998-1 (2010) Type 2	3.1	0.1292%	4.1	0.1688%	133	32810
UNI EN 1998-1 (2007)	2.7	0.1104%	3.4	0.1427%	114	33285

It is interesting to highlight the proximity of NBR 15421 (2023) displacement results to both types of the Response Spectrum Curve of NP EN 1998-1 (2010). In terms of absolute values, the difference was 0.5 mm. This similarity is important to draw attention to because, despite Brazilian seismic activity being considered low, the current regulation, under the same conditions, presents a methodology very close to the one used in countries with medium to high seismic

hazards. However, this comparison can only be made considering the Ductile Class 1 of the European code, since ductile designing is not viable under NBR 15421 (2023). When looking at the results obtained through Italian methodology, however, the opposite is observed since it is an earthquake-prone territory. The difference between Italian and Brazilian demand reached approximately 160%, which represents a clear normative disparity in this matter.

As evident from the results, the proposed building exhibited excellent performance across all regulations. This conclusion is drawn based on the observation that all relative inter-storey displacements remained below the regulatory storey drift limit of 2.0%, to the Brazilian case, and of 1.5%, to the European one. Given the context of the tests being conducted in Portugal, an opportunity exists to enhance the building's design to achieve even more favourable outcomes. Consequently, two types of structural improvements are proposed: firstly, a reduction in the number of metallic fasteners; and secondly, the adoption of less rigid connectors, allowing for enhanced energy dissipation within the building.

### 5.1.1 Parametric Study on Angle Bracket Sizing

The initial parametric analysis focused on reducing metallic fasteners within the structure. This specific variation was chosen due to its substantial influence on ductility, making it the primary modification examined in these tests. The reduction of angle brackets was undertaken with the objective of decreasing lateral resistance and facilitating the attainment of plastic deformation. Three distinct models were analysed to represent reductions of 25%, 50%, and 75% of the angle brackets used for panel fixation on each floor. Table 5.2 shows the models used for this comparison.

The results of the models subject to the seismic demand prescribed in the regulations under study is presented in Tables 5.3 up to 5.11. These tables present the Average Displacement (Avg. d), taken as the arithmetic average of displacements of 4 nodes located in the extremities of the building; the Relative Displacement (Rel. d), taken as the ratio between average displacement and storey height; the base shear, which is calculated as the sum of all reaction forces in determined direction; and stiffness (K), which is taken as the ratio between the average displacement at the top and the base shear.

Table 5.2 – Modified models with AE116. Percentage of metallic connectors kept in the model.

Model	1 <sup>st</sup> floor (%)	2 <sup>nd</sup> floor (%)
0	100	100
1	100	75
2	100	50
3	100	25
4	75	75
5	75	50
6	75	25
7	50	50
8	50	25
9	25	25

Table 5.3 – Average displacements, maximum base shear and average stiffness by load case for model 1.

Description	1 <sup>st</sup> floor		2 <sup>nd</sup> floor		Base Shear (kN)	K (kN/m)
	Avg. d (mm)	Rel. d (%)	Avg. d (mm)	Rel. d (%)		
NBR 15421 (2023)	4.2	0.1781%	5.6	0.2333%	183	32957
NP EN 1998-1 (2010) Type 1	2.5	0.1042%	3.3	0.1344%	106	32958
NP EN 1998-1 (2010) Type 2	3.1	0.1292%	4.1	0.1688%	133	32738
UNI EN 1998-1 (2007)	2.7	0.1104%	3.4	0.1427%	114	33203

Table 5.4 – Average displacements, maximum base shear and average stiffness by load case for model 2.

Description	1 <sup>st</sup> floor		2 <sup>nd</sup> floor		Base Shear (kN)	K (kN/m)
	Avg. d (mm)	Rel. d (%)	Avg. d (mm)	Rel. d (%)		
NBR 15421 (2023)	4.2	0.1760%	5.5	0.2302%	181	32702
NP EN 1998-1 (2010) Type 1	2.5	0.1021%	3.3	0.1354%	105	32305
NP EN 1998-1 (2010) Type 2	3.1	0.1271%	4.0	0.1677%	113	32544
UNI EN 1998-1 (2007)	2.7	0.1104%	3.4	0.1438%	112	33577

Table 5.5 – Average displacements, maximum base shear and average stiffness by load case for model 3.

Description	1 <sup>st</sup> floor		2 <sup>nd</sup> floor		Base Shear (kN)	K (kN/m)
	Avg. d (mm)	Rel. d (%)	Avg. d (mm)	Rel. d (%)		
NBR 15421 (2023)	4.2	0.1750%	5.5	0.2281%	179	32760
NP EN 1998-1 (2010) Type 1	2.5	0.1021%	3.3	0.1354%	104	32569
NP EN 1998-1 (2010) Type 2	3.1	0.1271%	4.0	0.1667%	130	32505
UNI EN 1998-1 (2007)	2.6	0.1083%	3.4	0.1417%	111	32821

Table 5.6 – Average displacements, maximum base shear and average stiffness by load case for model 4.

Description	1 <sup>st</sup> floor		2 <sup>nd</sup> floor		Base Shear (kN)	K (kN/m)
	Avg. d (mm)	Rel. d (%)	Avg. d (mm)	Rel. d (%)		
NBR 15421 (2023)	5.3	0.2208%	6.6	0.2740%	190	28966
NP EN 1998-1 (2010) Type 1	3.1	0.1271%	3.9	0.1604%	111	28743
NP EN 1998-1 (2010) Type 2	3.8	0.1594%	4.8	0.1979%	138	29067
UNI EN 1998-1 (2007)	3.4	0.1396%	4.2	0.1750%	121	28693

Table 5.7 – Average displacements, maximum base shear and average stiffness by load case for model 5.

Description	1 <sup>st</sup> floor		2 <sup>nd</sup> floor		Base Shear (kN)	K (kN/m)
	Avg. d (mm)	Rel. d (%)	Avg. d (mm)	Rel. d (%)		
NBR 15421 (2023)	5.2	0.2167%	6.6	0.2729%	189	28869
NP EN 1998-1 (2010) Type 1	3.1	0.1271%	3.8	0.1573%	106	28156
NP EN 1998-1 (2010) Type 2	3.8	0.1573%	4.8	0.1979%	137	28861
UNI EN 1998-1 (2007)	3.3	0.1365%	4.1	0.1708%	119	2915

Table 5.8 – Average displacements, maximum base shear and average stiffness by load case for model 6.

Description	1 <sup>st</sup> floor		2 <sup>nd</sup> floor		Base Shear (kN)	K (kN/m)
	Avg. d (mm)	Rel. d (%)	Avg. d (mm)	Rel. d (%)		
NBR 15421 (2023)	5.2	0.2167%	6.6	0.2729%	189	28869
NP EN 1998-1 (2010) Type 1	3.1	0.1271%	3.8	0.1573%	110	29105
NP EN 1998-1 (2010) Type 2	3.8	0.1573%	4.8	0.1979%	137	28861
UNI EN 1998-1 (2007)	3.3	0.1365%	4.1	0.1708%	119	29153

Table 5.9 – Average displacements, maximum base shear and average stiffness by load case for model 7.

Description	1 <sup>st</sup> floor		2 <sup>nd</sup> floor		Base Shear (kN)	K (kN/m)
	Avg. d (mm)	Rel. d (%)	Avg. d (mm)	Rel. d (%)		
NBR 15421 (2023)	6.3	0.2594%	7.6	0.3146%	193	25539
NP EN 1998-1 (2010) Type 1	3.6	0.1500%	4.4	0.1833%	112	25461
NP EN 1998-1 (2010) Type 2	4.6	0.1896%	5.5	0.2271%	140	25649
UNI EN 1998-1 (2007)	4.1	0.1677%	4.9	0.2042%	124	25308

Table 5.10 – Average displacements, maximum base shear and average stiffness by load case for model 8.

Description	1 <sup>st</sup> floor		2 <sup>nd</sup> floor		Base Shear (kN)	K (kN/m)
	Avg. d (mm)	Rel. d (%)	Avg. d (mm)	Rel. d (%)		
NBR 15421 (2023)	7.1	0.2948%	8.4	0.3500%	195	23174
NP EN 1998-1 (2010) Type 1	4.1	0.1708%	4.9	0.2031%	113	23202
NP EN 1998-1 (2010) Type 2	5.2	0.2146%	6.1	0.2542%	141	23134
UNI EN 1998-1 (2007)	4.6	0.1927%	5.5	0.2292%	127	23093

Table 5.11 – Average displacements, maximum base shear and average stiffness by load case for model 9.

Description	1 <sup>st</sup> floor		2 <sup>nd</sup> floor		Base Shear (kN)	K (kN/m)
	Avg. d (mm)	Rel. d (%)	Avg. d (mm)	Rel. d (%)		
NBR 15421 (2023)	11.0	0.4594%	12.3	0.5115%	197	16083
NP EN 1998-1 (2010) Type 1	6.4	0.2667%	7.1	0.2958%	115	16159
NP EN 1998-1 (2010) Type 2	8.0	0.3323%	8.9	0.3688%	143	16174
UNI EN 1998-1 (2007)	7.6	0.3156%	8.5	0.3521%	136	16109

As expected, changes in the model's mechanical properties result in varied responses to seismic excitation. The primary objective of the proposed parametric evaluation is to reduce the reliance

on connectors, leading to a less stiff structure, as they play a crucial role in providing strength during lateral load scenarios. Furthermore, the introduced geometric modifications affect the structure's natural frequency, causing it to display slightly higher vibration modes. Importantly, as the natural frequency increases, the structure moves away from the dominant frequencies in seismic excitation. This behaviour indicates reduced susceptibility to resonance effects and an enhanced capacity to dissipate incoming seismic forces, contributing to improved seismic performance. Consequently, considering the response spectrum curves, a higher natural frequency of the structure corresponds to reduced vulnerability to seismic impacts.

On the other hand, the differences observed in the presented results are not relevant enough to provide a great natural frequency change that may cause the previously highlighted. Figure 5.4, in this way, presents the differences in stiffness as reductions on angle brackets are conducted. Nevertheless, it is necessary to discuss not only overall stiffness but also the relative difference to the previous one to evaluate the obtained gains while reducing metallic connectors. Losses in performance are tolerable when they represent gains in a more economical design without safety or maintenance issues. That being said, major stiffness reductions were observed in the reduction of angle brackets in the base, as one can note in the differences from models 3 to 4 and 6 to 7. Models 8 and 9 showed an advanced loss in stiffness, being not viable options for enhancement of the structure.

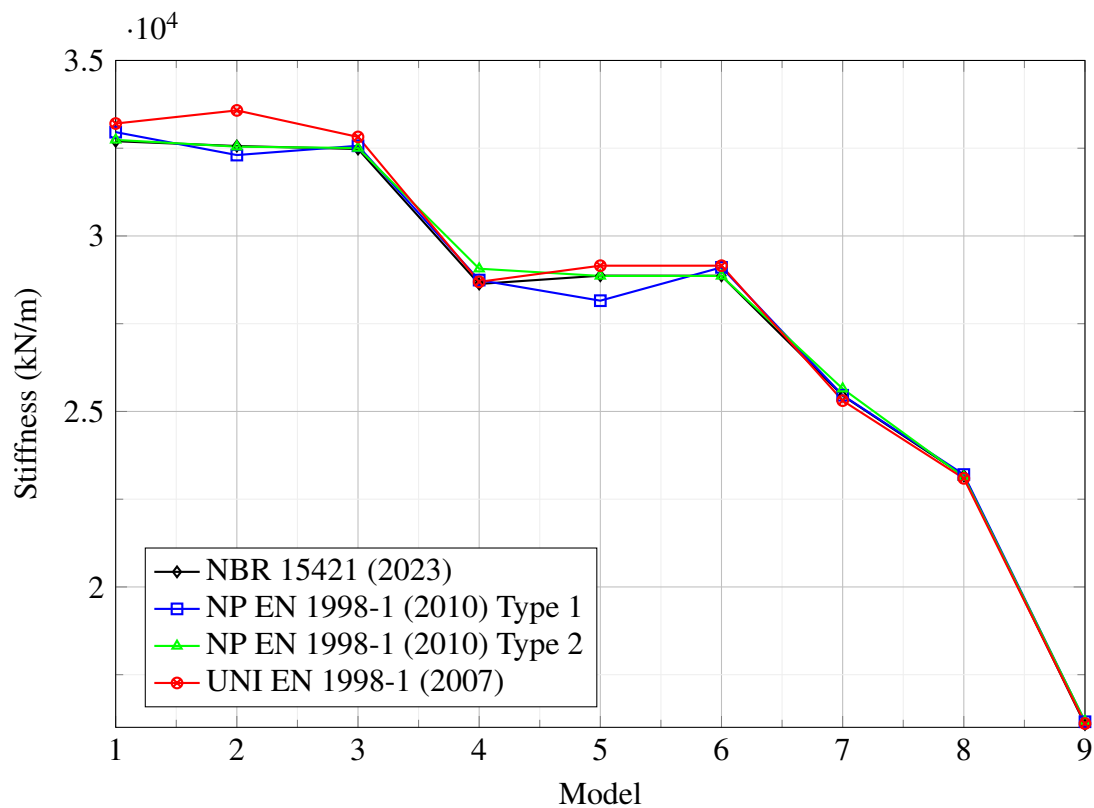


Figure 5.4 – Stiffness changes through models.

The reduction observed from models 3 to 6 is interesting to study since it may not be representative of a global stability hazard and may be a great outcome in economic design. Regarding the reduction in angle brackets, model 3 proposed a reduction of 37.5% of the total quantity while 6 proposed a reduction of 50%. When compared to the original structure stiffness, model 3 reached an average, considering all load cases, of 32,664 kN/m while model 6 reached 28,997 kN/m. This is a representation of less than 1% change and of -13%, respectively, when compared to the original configuration with all angle brackets. With that, it is possible to conclude that, considering that both situations comply with normative limits when the two scenarios are compared model 6 represents a more economic design and a better option when solely observed the seismic excitation criteria.

### 5.1.2 Parametric Study on Angle Bracket Mechanical Behaviour

This item aims to evaluate the mechanical behaviour of angle brackets in CLT building modelling. As previously referenced in the literature and shown in previously presented results, these elements play an important role in structural stiffness, and, with that in mind, the parametric evaluation of its mechanical behaviour is proposed to establish the relation to the lateral load demands. The proposed approach consists of evaluating the same models created in Table 5.2 considering the differences in mechanical properties.

For the purpose of attending to the established objective, the angle brackets used in the building's construction were changed to a less stiff one, from another manufacturer. Hence, the Rothoblaas' WBR075 was chosen to be a substitute for the Simpson Strong-Tie's AE116. The mechanical properties differences are presented in Figs. 5.5 and 5.6 (ROTHOBLAAS, s.d.). These mechanical properties are available in the technical brochures of the manufacturer. In both cases, they were obtained following the test protocols of the European Standard EN12512:2006 (CEN EN 12512, 2006). It is important to point out that the presented data is relative to the positioning of angle brackets between two adjacent CLT panels, being not viable for data usage in the base of the building. For this purpose, the connector shall be tested positioned in a CLT panel and anchored in another base, metallic or reinforced concrete.

As one can observe, the connector used in the original experimental campaign had considerably higher resistance under shear and under tension than the proposed one. Considering Eq. 3.6 and 3.1, both connectors can be described as having high ductile behaviour under tension and medium when undergoing shear loads.

The obtained results are shown in Tables from 5.13 to 5.21. One can note that the reduction in lateral stiffness observed in the previous parametric study repeats itself in this analysis. However, displacement values show themselves as being very similar to each other, under the same load case, as the model changes. Higher displacement changes were observed when there were

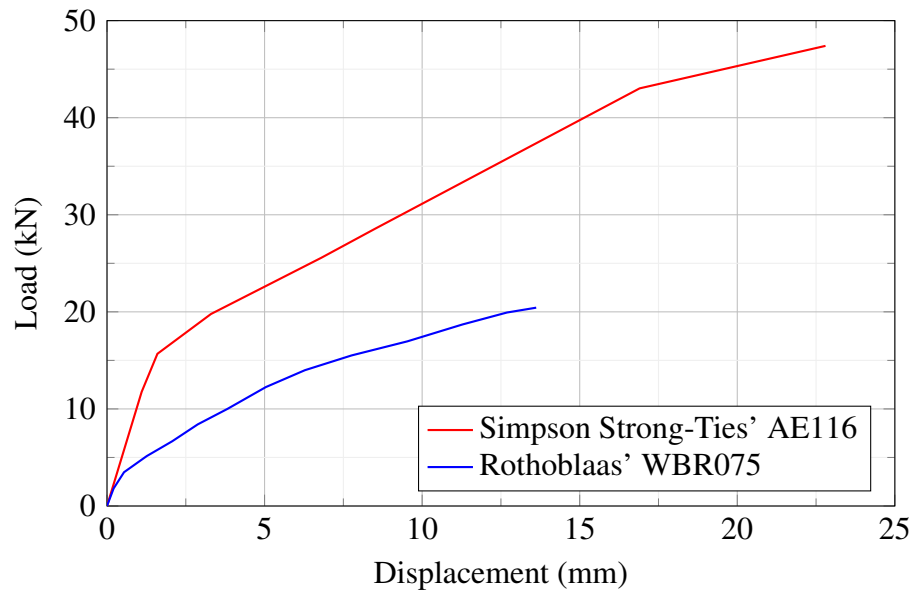


Figure 5.5 – Load-displacement under tension curve comparison (Adapted from Rothoblaas (s.d.)).

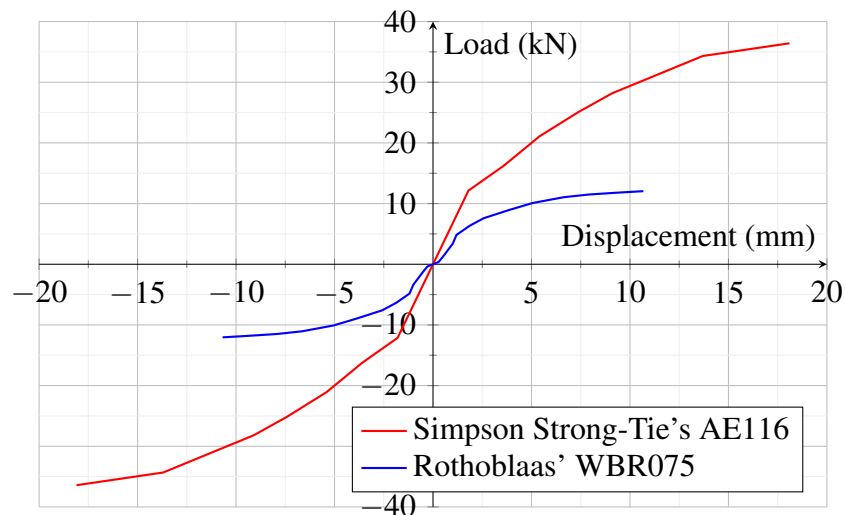


Figure 5.6 – Load-displacement under shear curve comparison (Adapted from Rothoblaas (s.d.)).

removals of angle brackets located on the ground floor. These increases were of, approximately, 0.04% in relative displacement, resulting in 0.96 mm on average. It is considered a suitable alternative to the studied building since it represents an opportunity to use a less stiff and more economical design, considering the possibility of remaining under the sensory acceptability recommended by the codes, under the assessment of the storey drift.



Table 5.12 – Average displacements, maximum base shear and average stiffness by load case for Rothoblaas changed model 0.

Description	1 <sup>st</sup> floor		2 <sup>nd</sup> floor		Base Shear (kN)	K (kN/m)
	Avg. d (mm)	Rel. d (%)	Avg. d (mm)	Rel. d (%)		
NBR 15421 (2023)	4.3	0.1781%	5.6	0.2344%	183	32565
NP EN 1998-1 (2010) Type 1	3.7	0.1542%	4.9	0.2042%	160	32540
NP EN 1998-1 (2010) Type 2	4.6	0.2500%	6.0	0.2500%	160	33160
UNI EN 1998-1 (2007)	2.7	0.1104%	3.4	0.1427%	114	33285

Table 5.13 – Average displacements, maximum base shear and average stiffness by load case for Rothoblaas changed model 1.

Description	1 <sup>st</sup> floor		2 <sup>nd</sup> floor		Base Shear (kN)	K (kN/m)
	Avg. d (mm)	Rel. d (%)	Avg. d (mm)	Rel. d (%)		
NBR 15421 (2023)	4.28	0.23%	5.6	0.18%	183	32700
NP EN 1998-1 (2010) Type 1	2.5	0.1042%	3.3	0.1354%	106	32739
NP EN 1998-1 (2010) Type 2	4.7	0.1938%	6.1	0.2542%	119	32648
UNI EN 1998-1 (2007)	2.7	0.1104%	3.5	0.1458%	114	32549

Table 5.14 – Average displacements, maximum base shear and average stiffness by load case for Rothoblaas changed model 2.

Description	1 <sup>st</sup> floor		2 <sup>nd</sup> floor		Base Shear (kN)	K (kN/m)
	Avg. d (mm)	Rel. d (%)	Avg. d (mm)	Rel. d (%)		
NBR 15421 (2023)	4.23	0.23%	5.6	0.18%	181	32562
NP EN 1998-1 (2010) Type 1	4.2	0.1760%	5.6	0.2313%	181	32562
NP EN 1998-1 (2010) Type 2	4.6	0.1906%	6.1	0.2521%	196	32317
UNI EN 1998-1 (2007)	2.7	0.1104%	3.5	0.1458%	112	32597

Table 5.15 – Average displacements, maximum base shear and average stiffness by load case for Rothoblaas changed model 3.

Description	1 <sup>st</sup> floor		2 <sup>nd</sup> floor		Base Shear (kN)	K (kN/m)
	Avg. d (mm)	Rel. d (%)	Avg. d (mm)	Rel. d (%)		
NBR 15421 (2023)	4.23	0.23%	5.5	0.18%	179	32478
NP EN 1998-1 (2010) Type 1	3.7	0.1521%	4.8	0.2000%	156	32579
NP EN 1998-1 (2010) Type 2	4.6	0.1906%	6.0	0.2500%	195	32520
UNI EN 1998-1 (2007)	2.6	0.1083%	3.4	0.1427%	112	32599

Table 5.16 – Average displacements, maximum base shear and average stiffness by load case for Rothoblaas changed model 4.

Description	1 <sup>st</sup> floor		2 <sup>nd</sup> floor		Base Shear (kN)	K (kN/m)
	Avg. d (mm)	Rel. d (%)	Avg. d (mm)	Rel. d (%)		
NBR 15421 (2023)	5.3	0.2208%	6.7	0.2771%	190	28633
NP EN 1998-1 (2010) Type 1	4.6	0.1927%	5.8	0.2417%	166	28614
NP EN 1998-1 (2010) Type 2	5.8	0.2396%	7.2	0.30000%	207	28759
UNI EN 1998-1 (2007)	3.4	0.1396%	4.2	0.1750%	121	28698

Table 5.17 – Average displacements, maximum base shear and average stiffness by load case for Rothoblaas changed model 5.

Description	1 <sup>st</sup> floor		2 <sup>nd</sup> floor		Base Shear (kN)	K (kN/m)
	Avg. d (mm)	Rel. d (%)	Avg. d (mm)	Rel. d (%)		
NBR 15421 (2023)	5.2	0.2167%	6.6	0.2729%	189	28869
NP EN 1998-1 (2010) Type 1	4.5	0.1885%	5.7	0.2354%	166	29170
NP EN 1998-1 (2010) Type 2	5.7	0.2354%	7.1	0.2958%	206	28962
UNI EN 1998-1 (2007)	3.2	0.1313%	4.2	0.1719%	119	29154

Table 5.18 – Average displacements, maximum base shear and average stiffness by load case for Rothoblaas changed model 6.

Description	1 <sup>st</sup> floor		2 <sup>nd</sup> floor		Base Shear (kN)	K (kN/m)
	Avg. d (mm)	Rel. d (%)	Avg. d (mm)	Rel. d (%)		
NBR 15421 (2023)	5.2	0.2167%	6.6	0.2729%	189	28866
NP EN 1998-1 (2010) Type 1	4.5	0.1885%	5.7	0.2375%	165	28912
NP EN 1998-1 (2010) Type 2	5.7	0.2354%	7.1	0.2958%	206	28959
UNI EN 1998-1 (2007)	3.3	0.1375%	4.2	0.1719%	119	28979

Table 5.19 – Average displacements, maximum base shear and average stiffness by load case for Rothoblaas changed model 7.

Description	1 <sup>st</sup> floor		2 <sup>nd</sup> floor		Base Shear (kN)	K (kN/m)
	Avg. d (mm)	Rel. d (%)	Avg. d (mm)	Rel. d (%)		
NBR 15421 (2023)	6.3	0.2604%	7.6	0.3156%	193	25451
NP EN 1998-1 (2010) Type 1	5.5	0.2271%	6.63	0.2760%	168	25363
NP EN 1998-1 (2010) Type 2	6.8	0.2833%	8.23	0.3427%	210	25489
UNI EN 1998-1 (2007)	4.0	0.1677%	4.9	0.2042%	119	25308

Table 5.20 – Average displacements, maximum base shear and average stiffness by load case for Rothoblaas changed model 8.

Description	1 <sup>st</sup> floor		2 <sup>nd</sup> floor		Base Shear (kN)	K (kN/m)
	Avg. d (mm)	Rel. d (%)	Avg. d (mm)	Rel. d (%)		
NBR 15421 (2023)	7.1	0.2948%	8.4	0.3500%	195	23169
NP EN 1998-1 (2010) Type 1	6.2	0.2573%	7.35	0.3063%	169	23080
NP EN 1998-1 (2010) Type 2	7.7	0.3219%	9.15	0.3813%	212	23131
UNI EN 1998-1 (2007)	4.6	0.1927%	5.5	0.2292%	127	23093

Table 5.21 – Average displacements, maximum base shear and average stiffness by load case for Rothoblaas changed model 9.

Description	1 <sup>st</sup> floor		2 <sup>nd</sup> floor		Base Shear (kN)	K (kN/m))
	Avg. d (mm)	Rel. d (%)	Avg. d (mm)	Rel. d (%)		
NBR 15421 (2023)	11.0	0.4594%	12.3	0.5115%	197	16083
NP EN 1998-1 (2010) Type 1	9.6	0.40%	10.7	0.4458%	172	16091
NP EN 1998-1 (2010) Type 2	11.98	0.4990%	13.98	0.5563%	211	16082
UNI EN 1998-1 (2007)	7.6	0.3156%	8.5	0.3521%	136	16108

The presented data shows the predominance of the base connectors in the overall behaviour of the structure. Since there was no availability of connectors anchored in a steel plate, the change

to the Rothoblaas' angle bracket was only possible on the second pavement. The similarities in the results confirm the previous assessment of the structural reliance on the connectors of the ground floor, since the results are very similar, despite the significant reduction in stiffness carried out in the connectors between floors.

Considering the lateral stiffness of the model, already presented in previous tables, it can be graphically observed in Figure 5.7. The structural behaviour is similar to the previous parametric analysis. When observing the differences in the models previously chosen, 3 and 6, the resulting difference in stiffness was around 1% and 14%, respectively, slightly higher than the previous parametric evaluation, indicating the same behaviour despite the differences in mechanical behaviour.

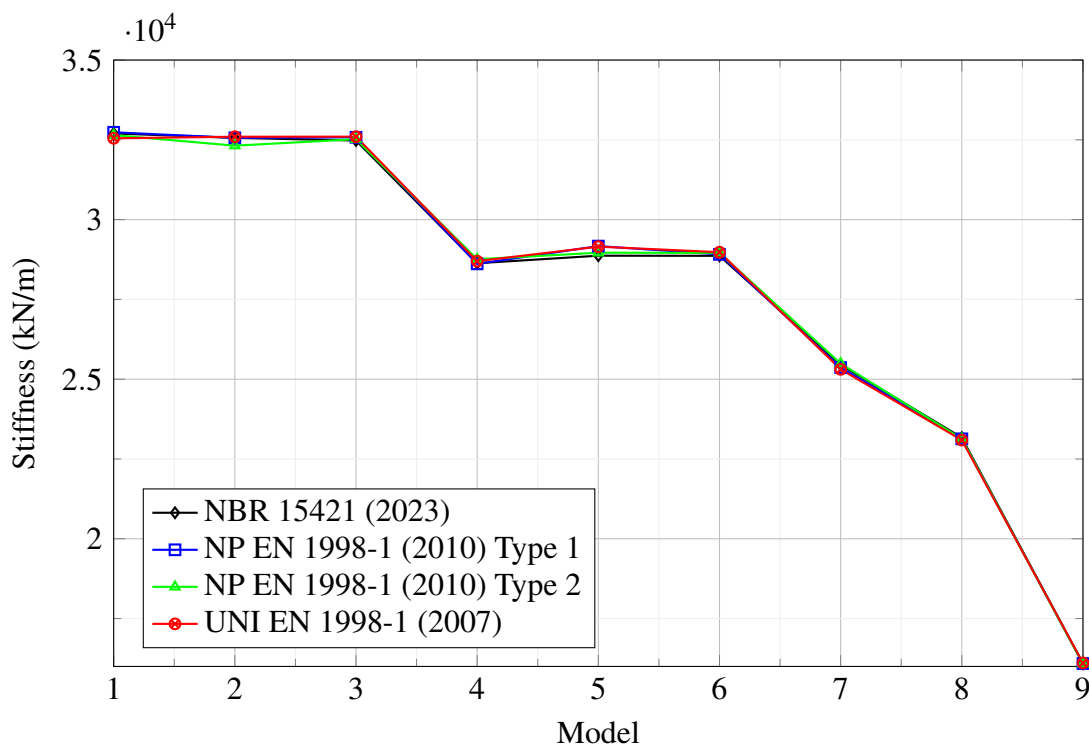


Figure 5.7 – Stiffness changes through Rothoblaas' models.

## 5.2 ARTIFICIAL KANAI-TAJIMI AND REAL EVENT ACCELEROGRAMS

This section was proposed aiming the analysis of frequency content of artificial seisms generated with the methodology combining the Kanai-Tajimi filtering (see Eqs. 4.5 and 4.6) of white noise and the superimposition of modal modes in each instant of time done with Shinozuka-Jan's equation (see Eq. 4.7). Alongside that, it was analysed the results achieved when the structure was submitted to real seismic data. As previously mentioned, the Kanai-Tajimi was applied to induce resonance in the building, combining ground and structural vibration frequencies. The average natural frequencies were taken into consideration to generate the artificial seism and,

initially, the PGA was normalised as the highest isopleth curve of the Brazilian code, of 0.15g. The accelerograms were presented in Figures 4.21, 4.22, 4.23 and 4.24.

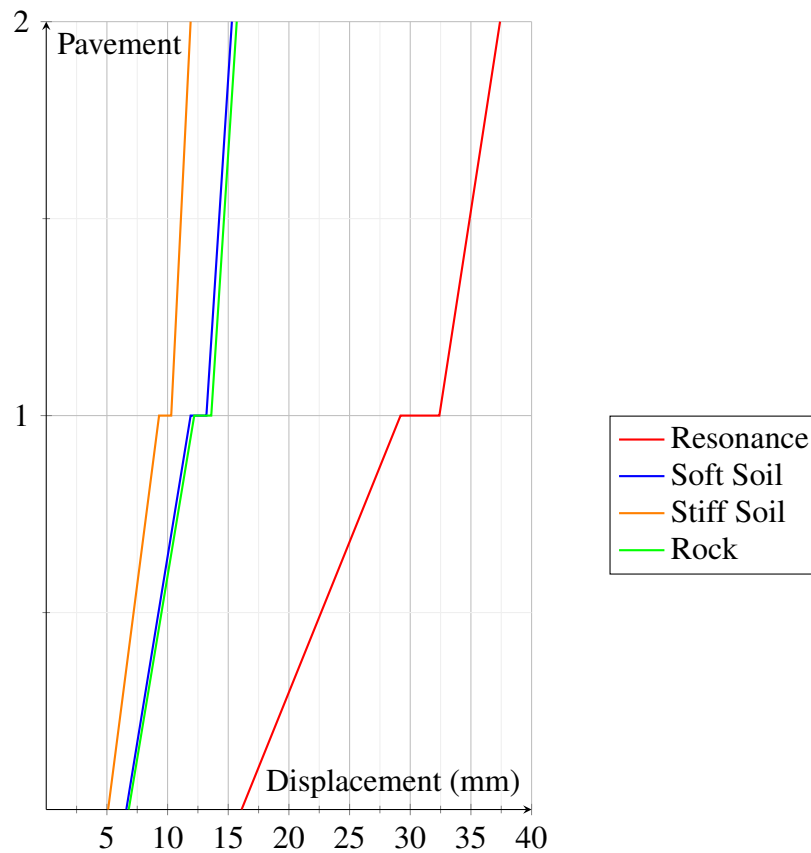


Figure 5.8 – Displacement profile in determined location due to different Kanai-Tajimi loading.

The profile of displacements in one of the corners of the building, model 0, is presented in Figure 5.8. It is possible to infer that the results are consistent with the expected structural response. The resonance excitation, which was built using the building's first vibration mode the ground's natural frequency, resulted in higher displacements, rocking and sliding. On the other side, it is interesting to point out that it was observed almost identical behaviour of the structure when it was simulated under soft soil or over a rocky substrate. Despite the proximity, stiff soil represented a better performance of the structure, as observed in Figure 5.8. Alongside that, the sliding movement has an important impact on the final configuration since it has presented considerable value in the base of the building and also at the connection between adjacent floors. This translational movement is entirely supported by metallic fasteners placed between walls and floors and among orthogonal walls, also with connectors placed to absorb and control these displacements.

It is important to highlight that the previous load case was carried out with a PGA of 0.15g, which has the highest value being 1.4715 m/s<sup>2</sup>. This can be representative of a medium to low

seismicity in Europe, even though this is the highest acceleration presented in the Brazilian code. However, since it is the objective of this study to establish a comparative assessment of both Brazilian and European codes, this was taken as a normalisation factor to reduce regional influence.

Alongside the Kanai-Tajimi spectra, the model was submitted to a load that was normalised and represented two real events, which took place in Portugal and Italy - see Sub-Section 4.4.1. The resultant deformed configuration is depicted in Figure 5.9. As can be graphically observed, both normalised events resulted in displacements under the normative limitations prescribed by both codes. However, the results are much higher than the RSC simulations previously carried out. This difference is attributed to the soil configuration of the region it was recorded and due to the normalisation done in Kanai-Tajimi signal.

Figure 5.10, on the other hand, summarises all obtained profiles after the normalisation of both real events to the same PGA of 0.15g. This comparison is interesting not only to assess soil profile comparison to the established in the literature by empirical methods but also to analyse the frequency content of the events. As one can note, the Kanai-Tajimi situation to emulate resonance effects is by far the most damaging scenario to the structure, resulting in high displacements but yet not exceeding story drift limitations. In addition, it is possible to infer that the MTE-EMSC-20180115 event probably occurred in a rocky region due to its proximity to the respective Kanai-Tajimi version. Concerning the VLC-INT-20220922, no parallels can be drawn to its soil layering, since it is far from any typical pre-defined configuration, being more probably a situation of stiff soil if it is considered the nearest version of Kanai-Tajimi load.

Another typical deformation that is observed through the plotted profiles is the sliding between pavements. Being the connectors the main responsible for absorbing sliding effects in the building, its magnitude is directly attached to the shear resistance of the metallic connectors. Sliding in CLT buildings is only detectable in numerical simulations due of the story separation carried out in the beginning of the present study - see Section 4.2. The numerical analysis benefits itself from the employment of friction between wall panels, since it contributes to reducing the absorption of shear load by the connectors, being partially dissipated in CLT joints.

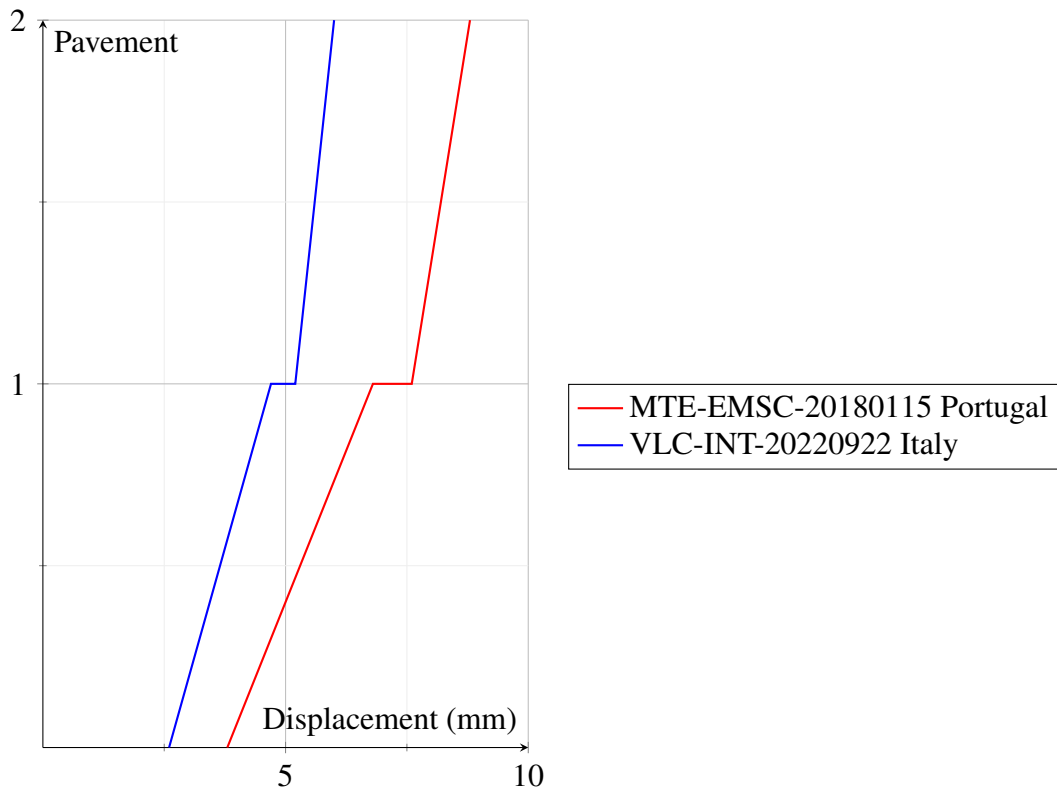


Figure 5.9 – Displacement profile due to real seismic loading.

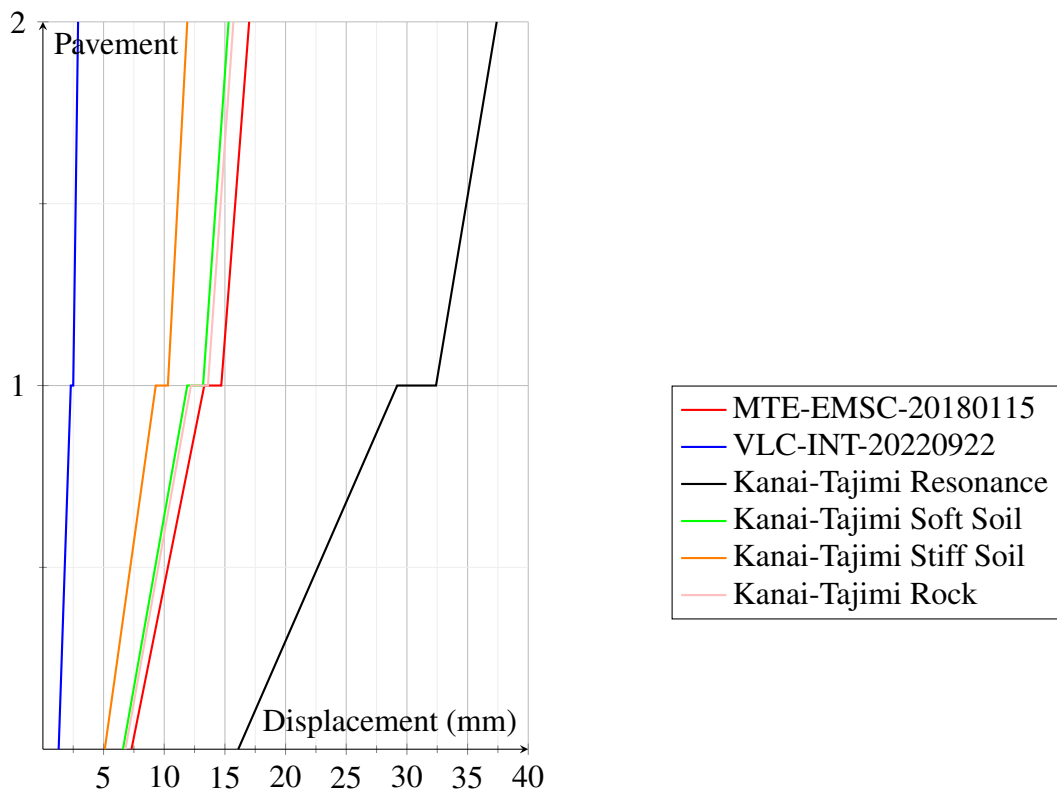


Figure 5.10 – Displacement profile comparison of normalised loadings - PGA = 0.15g.

### 5.3 ANALYSIS UNDER DUCTILE CLASS 2

In this section, it will be presented the structural behaviour of the structure considering Ductile Class 2. As previously stated, the implementation of different ductile classes than 1 implies better detailing of the numerical model in order to take advantage of its energy dissipation. The current study implemented the screwed connections accordingly to values published in the literature. However, this analysis was only carried out on the models chosen previously, following the analysis of the previous section.

Tables 5.22 and 5.23 present the obtained results under DC2 of models 3 and 4 of the original configuration. The Rothoblaas' changed models are presented in Tables 5.24 and 5.25.

Table 5.22 – Average displacements, maximum base shear and average stiffness by load case for model 3 - DC2.

Description	1 <sup>st</sup> floor		2 <sup>nd</sup> floor		Base Shear (kN)	K (kN/m)
	Avg. d (mm)	Rel. d (%)	Avg. d (mm)	Rel. d (%)		
NP EN 1998-1 (2010) Type 1	2.3	0.0927%	2.9	0.1208%	91	31376
NP EN 1998-1 (2010) Type 2	2.1	0.0875%	2.7	0.1125%	85	31541
UNI EN 1998-1 (2007)	2.4	0.0990%	3.1	0.1292%	98	31723

Table 5.23 – Average displacements, maximum base shear and average stiffness by load case for model 6 - DC2.

Description	1 <sup>st</sup> floor		2 <sup>nd</sup> floor		Base Shear (kN)	K (kN/m)
	Avg. d (mm)	Rel. d (%)	Avg. d (mm)	Rel. d (%)		
NP EN 1998-1 (2010) Type 1	2.3	0.0938%	2.8	0.1167%	78	27886
NP EN 1998-1 (2010) Type 2	2.8	0.1167%	3.5	0.1458%	97	28235
UNI EN 1998-1 (2007)	2.6	0.1083%	3.3	0.1354%	91	28003

Table 5.24 – Average displacements, maximum base shear and average stiffness by load case for Rothoblaas changed model 3 - DC2.

Description	1 <sup>st</sup> floor		2 <sup>nd</sup> floor		Base Shear (kN)	K (kN/m)
	Avg. d (mm)	Rel. d (%)	Avg. d (mm)	Rel. d (%)		
NP EN 1998-1 (2010) Type 1	2.2	0.0927%	2.9	0.1208%	91	31466
NP EN 1998-1 (2010) Type 2	2.1	0.0875%	2.7	0.1125%	85	31626
UNI EN 1998-1 (2007)	2.4	0.1010%	3.2	0.1313%	99	31314

Table 5.25 – Average displacements, maximum base shear and average stiffness by load case for Rothoblaas changed model 6 - DC2.

Description	1 <sup>st</sup> floor		2 <sup>nd</sup> floor		Base Shear (kN)	K (kN/m)
	Avg. d (mm)	Rel. d (%)	Avg. d (mm)	Rel. d (%)		
NP EN 1998-1 (2010) Type 1	2.3	0.0938%	2.8	0.1167%	78	27903
NP EN 1998-1 (2010) Type 2	2.8	0.1167%	3.5	0.1448%	91	25233
UNI EN 1998-1 (2007)	2.6	0.1083%	3.3	0.1354%	91	28049

Results show small differences between the original configuration and the one using the less stiff angle bracket. The explanation for this is that both angle brackets have similar behaviour under elastic range, *id est*, small loads and displacements. It was possible to notice the higher differences in determined load cases, such as the Type 2 Portuguese RSC. The range was from 26.70% to 54.67% in this scenario. Comparison between ductile classes is presented in Tables 5.26, 5.27, 5.28 and 5.29. The Average Relative Difference (Avg.Rel. Difference) is taken as the average of the ratio between the maximum displacements in DC1 and DC2.

In general, the results indicated that as the model becomes more flexible and its energy dissipation is carried out, the higher the impact of using the Ductile Class 2 during design. On average, model 6 resulted in a reduction of 32.52% while model 3 was only 25.14%. This difference of approximately 7.0% indicates that under the proposed conditions the enhancement of the structural design can have even greater benefits when observed the EC8 possibility of energy dissipation.

On average, model 3 reduced displacements by 16.05% considering both pavements. On the other hand, model 6 under DC2 had 24.52% reduction in displacements. When submitted to NP EN 1998-1 (2010) Type 2 excitation, the deformed configuration was almost 32% lower, differently from the near 9% of the other two analysed load cases.

Table 5.26 – Model 3 results comparison between DC1 and DC2.

Description	1 <sup>st</sup> floor		2 <sup>nd</sup> floor		Avg. Rel. Difference (%)
	DC1 (mm)	DC2 (mm)	DC1 (mm)	DC2 (mm)	
NP EN 1998-1 (2010) Type 1	2.5	2.3	3.3	2.9	10.06%
NP EN 1998-1 (2010) Type 2	3.1	2.1	4.0	2.7	32.38%
UNI EN 1998-1 (2007)	2.6	2.4	3.4	3.1	8.26%

Table 5.27 – Model 6 results comparison between DC1 and DC2.

Description	1 <sup>st</sup> floor		2 <sup>nd</sup> floor		Avg. Rel. Difference (%)
	DC1 (mm)	DC2 (mm)	DC1 (mm)	DC2 (mm)	
NP EN 1998-1 (2010) Type 1	3.1	2.3	3.8	2.8	26.06%
NP EN 1998-1 (2010) Type 2	3.8	2.8	4.8	3.5	26.70%
UNI EN 1998-1 (2007)	3.3	2.6	4.1	3.3	20.36%

Table 5.28 – Rothoblaas changed model 3 results comparison between DC1 and DC2.

Description	1 <sup>st</sup> floor		2 <sup>nd</sup> floor		Avg. Rel. Difference (%)
	DC1 (mm)	DC2 (mm)	DC1 (mm)	DC2 (mm)	
NP EN 1998-1 (2010) Type 1	3.7	2.3	4.8	2.9	38.71%
NP EN 1998-1 (2010) Type 2	4.6	2.1	6.0	2.7	54.67%
UNI EN 1998-1 (2007)	2.6	2.4	3.4	3.2	6.79%



Table 5.29 – Rothoblaas changed model 6 results comparison between DC1 and DC2.

Description	1 <sup>st</sup> floor		2 <sup>nd</sup> floor		Avg. Rel. Difference (%)
	DC1 (mm)	DC2 (mm)	DC1 (mm)	DC2 (mm)	
NP EN 1998-1 (2010) Type 1	4.5	2.3	5.7	2.8	49.88%
NP EN 1998-1 (2010) Type 2	5.7	2.8	7.1	3.5	50.79%
UNI EN 1998-1 (2007)	3.3	2.6	4.2	3.3	21.32%

## 5.4 PUSHOVER ANALYSIS - N2 METHOD

During this section, it will be presented the results obtained due to the pushover analysis carried out on the model. As previously stated, the method encompasses a static nonlinear calculation, using the capacity curve of the structure generated as a result of an incremental load. That being said, the N2 method was subdivided into 3 phases: the pushover analysis; the equivalent Single-Degree-of-Freedom system determination; and the capacity curve and performance displacement point calculation.

### 5.4.1 Pushover Load Pattern

The load pattern is related to the configuration of the load applied to the structure to be able to implement the pushover analysis. The European code states that the loads shall be located in the location of the masses of the model and, considering the proposed design, the analysis load must be applied to the slabs, where there are elevated concentrations of mass (De MATOS, 2020). Concerning the intensity of the load, it was implemented a triangular load, since it is similar to the first vibration mode shape. This load pattern is broadly used to reach acceptable results and reach low convergence issues. The proposed load can be shown in Figure 5.11.

### 5.4.2 Equivalent SDOF of the MDOF structure

In this subsection, it is presented the determination of the equivalent SDOF system of the MDOF structure that was previously presented. Initially, it is necessary to, by means of Eqs. 3.29 and 3.32, determine the modal mass and the transformation factor. The modal mass is a weighting of the concentration of masses due to its height. The building under analysis was considered with equal masses located in each slab, calculated from the mass of the structure and the additional permanent masses used in the experimental campaign. Hence, it is possible to reach:

$$m^* = \sum m_i \Phi_i = m_1 \Phi_1 + m_2 \Phi_2 = 20.3 t$$

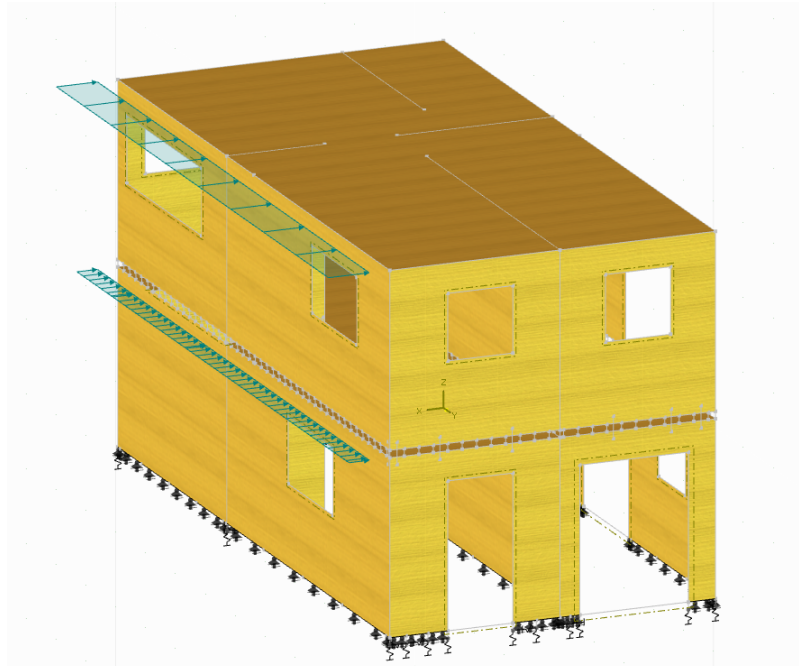


Figure 5.11 – Load pattern similar to first vibration mode - 1 kN/m and 0.5 kN/m at the top and middle, respectively.

$$\Gamma = \frac{m^*}{\sum m_i \Phi_i^2} = \frac{m_1 \Phi_1 + m_2 \Phi_2}{m_1 \Phi_1^2 + m_2 \Phi_2^2} = 1.2$$

The modal parameters were determined using the information presented in Figure 5.12.

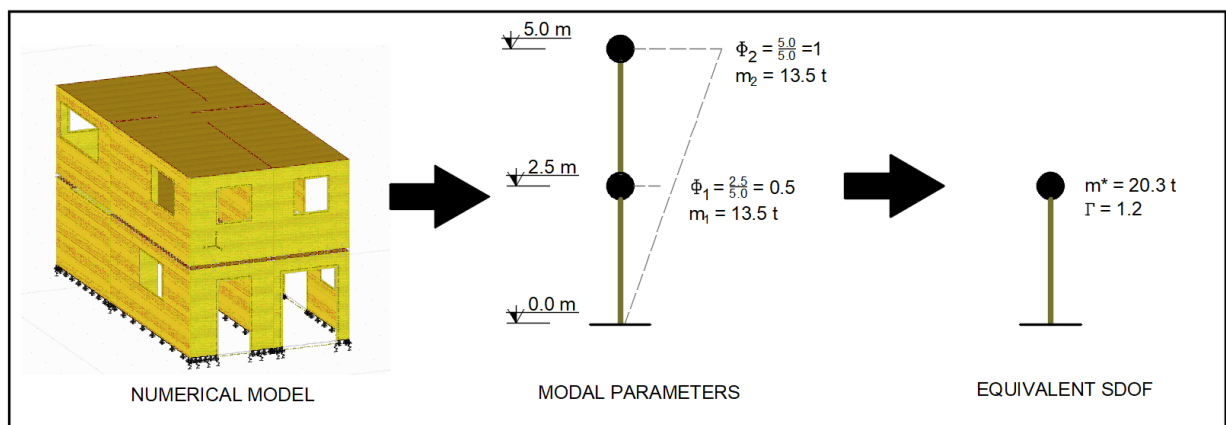


Figure 5.12 – Equivalent SDOF transformation.

### 5.4.3 Target Displacement

The load pattern is related to the configuration of the load applied to the structure to be able to implement the pushover analysis. The European code states that the loads shall be located in the masses of the model and, considering the proposed design, the analysis load must be applied to the slabs, where there are elevated concentrations of mass (De MATOS, 2020). Concerning

the intensity of the load, it was implemented a triangular load, since it is similar to the first vibration mode shape. This load pattern is broadly used to reach acceptable results and reach low convergence issues.

The target displacement shall be defined using the interpolation of both the capacity curve of the SDOF system and the RSC. However, it is not possible to compare them directly since both have different axes, which shall be the object of transformation before the comparison. Firstly, it is necessary to change the vertical axis from base shear to acceleration, which is carried out using Eq. 5.1. The second modification that is needed is the change of the horizontal axis from period to elastic displacement, carried out using Eq. 5.2.

$$S_e = \frac{F^*}{m^*} \quad (5.1)$$

$$d_e^* = S_e(T^*) \left[ \frac{T^*}{2\pi} \right] \quad (5.2)$$

As a result of the usage of Eq. 5.1, the obtained result of the capacity curve is shown in Figure 5.13.

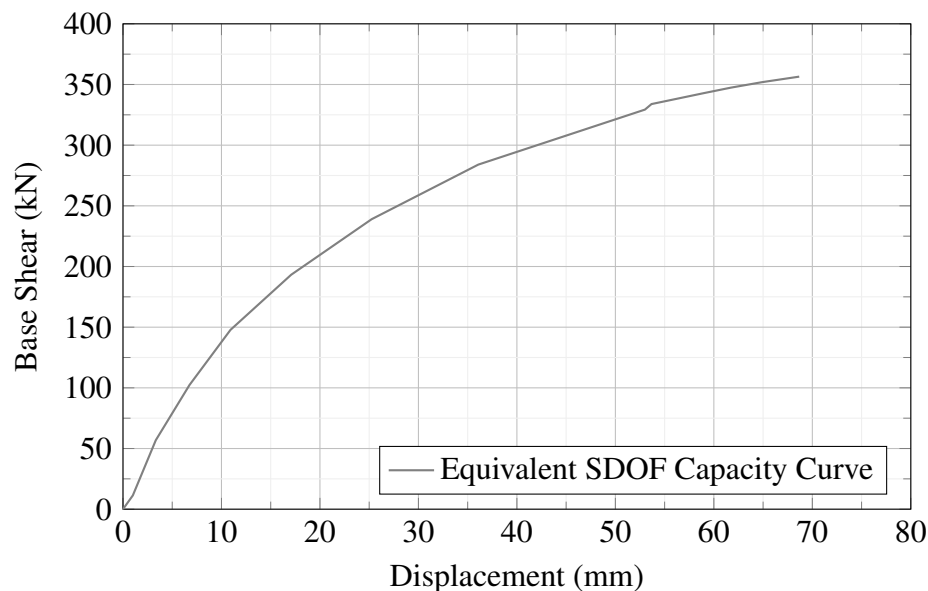


Figure 5.13 – Equivalent SDOF capacity curve.

The determination of  $d_y^*$  is done considering the previously presented relation, Eq. 3.31. This displacement represents the point into which both capacity and bilinear curves have the same area under the curve, representing the same amount of energy. The comparison between both curves is presented in Figure 5.14. Hence:

$$d_y^* = 2 \left( 68.67 - \frac{17,122}{356.47} \right) = 41.27 \text{ mm}$$

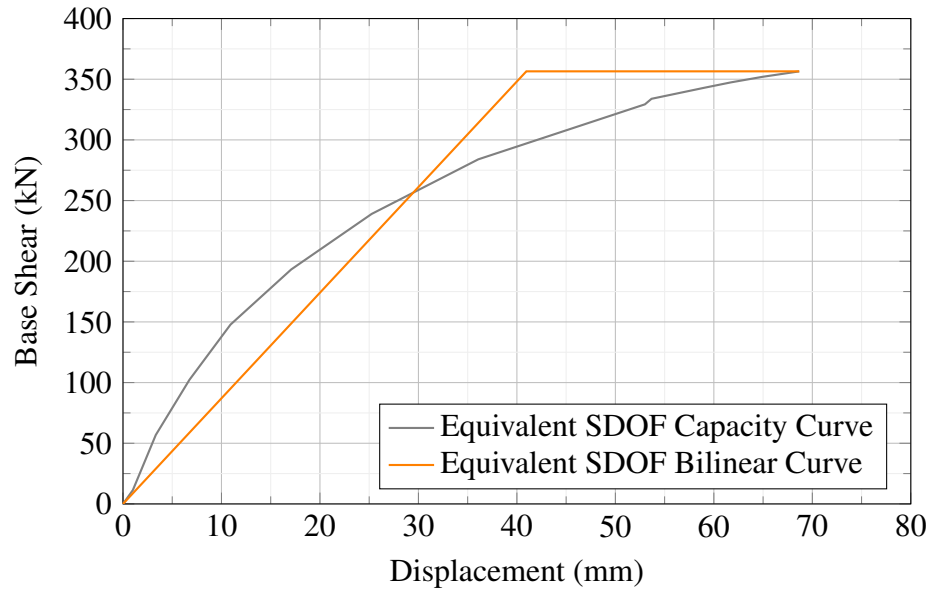


Figure 5.14 – Equivalent SDOF capacity and bilinear curves.

#### 5.4.4 MDOF Displacement Results

In order to finish the pushover analysis, it is necessary to establish a Response Spectrum Curve as a reference to evaluate frequency content and achieve a final displacement value. The European normative determines the employment of the elastic response spectrum in this assessment. Since the Brazilian code does not specify any approach concerning pushover analysis, the same procedure was done. That being said, Figure 5.15 presents all curves used in the current study, after unit conversion.

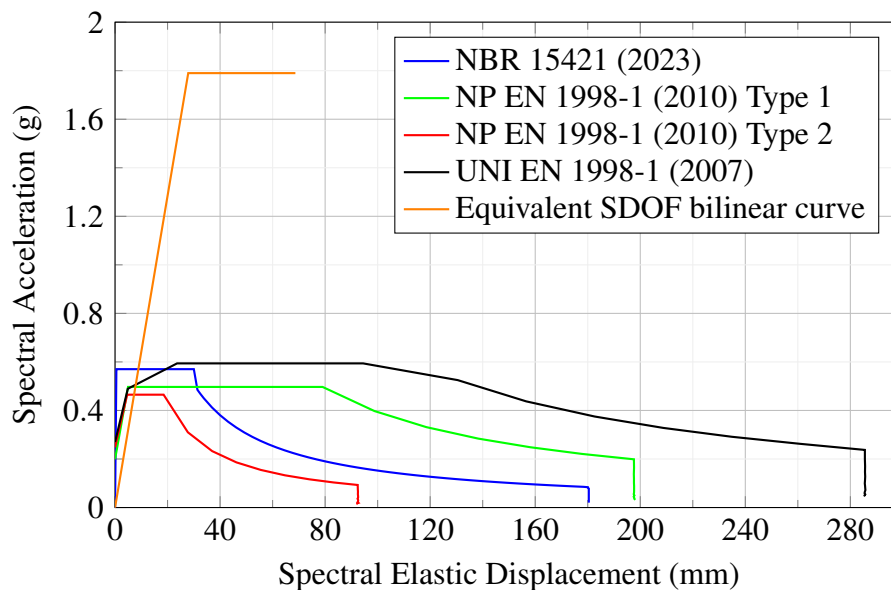


Figure 5.15 – Comparison between RSC and Bilinear Capacity curves.

As one can note, the capacity curve of the structure resulted in a much higher acceleration when compared to the curves obtained by the employment of the calculation methods of the codes. This is an indication that in all scenarios, the structure was loaded and its response was in the elastic range, resulting in no energy dissipation through plastic deformation. Therefore, it is possible to indicate that the proposed design of the structure is considered oversized considering the parameters previously proposed. Further in Section 5.6 it will be presented the ductility calculation to endorse this conclusion.

Concerning the obtained results of the pushover analysis, Table 5.30 shows the displacements considering the RSC construction of each code.

Table 5.30 – Significant Damage Limit State Displacements.

Description	2 <sup>nd</sup> floor		
	$d_{et}^*$ (mm)	$d_t$ (mm)	Rel. $d_t$ (%)
NBR 15421 (2023)	8.85	10.63	0.1832%
NP EN 1998-1 (2010) Type 1	6.17	7.41	0.1277%
NP EN 1998-1 (2010) Type 2	7.79	9.36	0.1613%
UNI EN 1998-1 (2007)	5.85	7.02	0.1211%

## 5.5 HYBRID CLT-CONCRETE COMPOSITE BUILDING

In Engineering, it is not enough to attend to safety limits when designing a building. Considering this need to encompass a variety of comfort measures, it is proposed the implementation of a CLT-concrete composite panel to substitute the CLT panel used as the slabs in the current model.

The usage of the hybrid CLT-concrete material is intended to modify the mass of the structure since concrete is approximately 6 times the weight of the timber and evaluate the modifications in the natural frequencies. Hence, it is possible to assess the seismic performance of the building as its mechanical properties are changed.

The CLT-concrete composite panel is represented in Figure 5.16. During the present study, due to simplicity, it was only configured in the RF-Laminate RFEM's add-on the mechanical properties of the concrete as well as the differences in layer thickness. No assessment was carried out concerning the slippery between layers nor the usage of special elements to represent the bond between different layers, being considered rigid with perfect load transfer through these elements. Concerning the slab configuration, it was proposed that the final thickness remained unaltered to reduce the influence on the bending stiffness, taking a 4-layer panel, 3 made out of 2 cm thickness CLT lamellae and 1 built with reinforced concrete of 6 cm. The characteristic compressive strength adopted was 30 MPa.

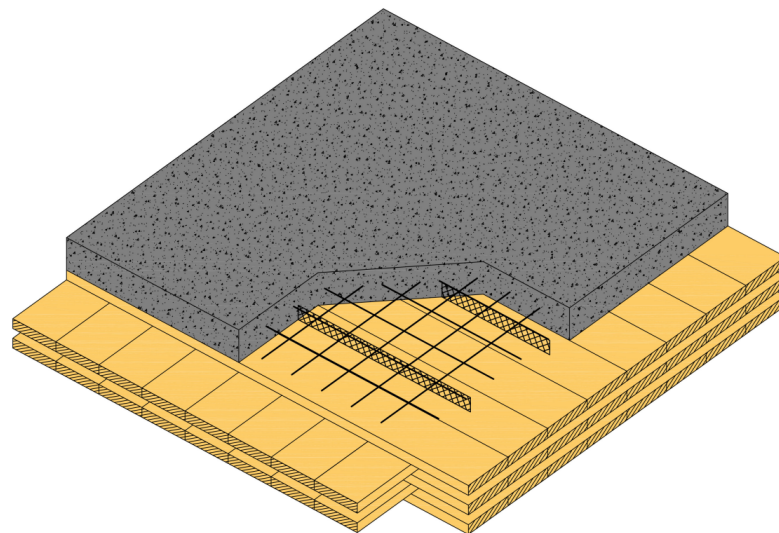


Figure 5.16 – CLT-concrete composite panel representation (SETRAGIAN; KUSUMA, 2018).

In order to implement the proposed hybrid CLT-concrete panel, it was necessary to study its influence on overall stiffness, not only the slab itself, to better comprehend the results. In this case, it was implemented that the same procedure was enforced to create the capacity curve of the model under study, presented in the pushover analysis - see Secs. 3.8 and 5.4 - concerning load pattern and load values. After the application of the load, the capacity curve was compared to the previously obtained and the stiffness of both models was observed by means of the area under each curve. Figure 5.17 shows the comparison between both curves. One can note that the differences are minimal, being confirmed when the calculation of both areas resulted in a difference of 0.28%. This can be explained considering the employment of this material only on

selected surfaces, as well as the moment of inertia had small changes considering there was no alteration in height, which would result in a significant rise in stiffness.

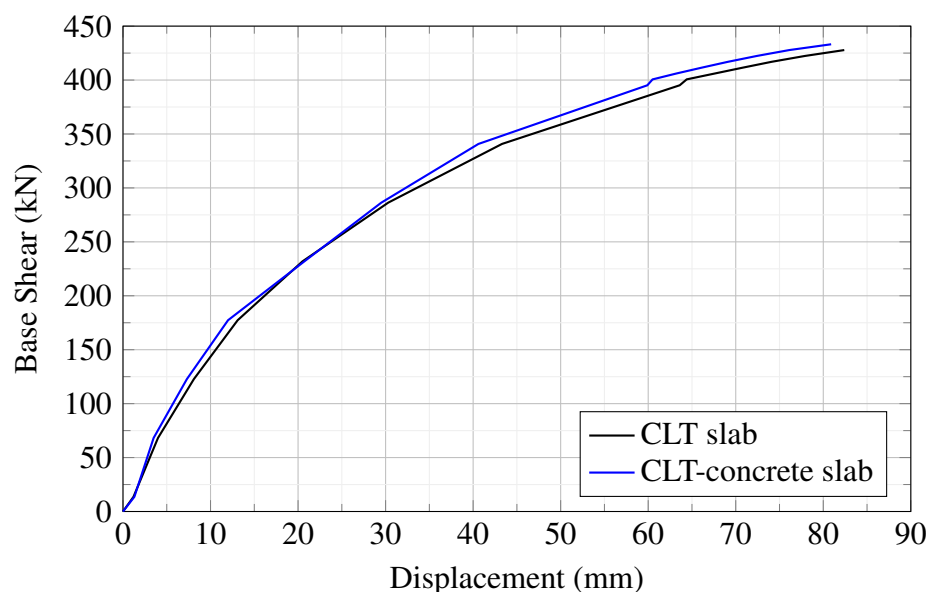


Figure 5.17 – Models capacity curve comparison.

Since there is no major alteration in global stiffness that leads to a misread of the analysis, it was carried out the simulation of the CLT-concrete changed model submitted to RSC excitation due to the different codes observed. The obtained results when submitted to the RSC loads are shown in Table 5.31. As one can note displacements are considerably higher in all scenarios, except when observed in the NP EN 1998-1 (2010) Type 1 RSC. Undoubtedly these differences are the product of the reduction of the natural frequency of the altered model, which decreased from 5.061 Hz to 4.173 Hz as the CLT-concrete material was implemented in the analysed building. On the other hand, the frequency content of the Type 1 RSC of the Portuguese National Annex resulted in similar loading despite this difference majorly observed in the mass of the structure. In disregard of the increase, one can note that the demanding load still resulted in displacements below the safety limits imposed by both codes and its annexes.

Table 5.31 – Average displacements (mm), maximum base shear (kN) and average stiffness (kN/m) by load case for hybrid CLT-concrete model.

Description	1 <sup>st</sup> floor		2 <sup>nd</sup> floor		Base Shear (kN)	K (kN/m)
	Avg. d (mm)	Rel. d (%)	Avg. d (mm)	Rel. d (%)		
NBR 15421 (2023)	6.8	0.2833%	8.6	0.3573%	302	35183
NP EN 1998-1 (2010) Type 1	3.9	0.1646%	4.9	0.2073%	175	35236
NP EN 1998-1 (2010) Type 2	5.0	0.2094%	6.2	0.2583%	219	35279
UNI EN 1998-1 (2007)	5.4	0.2250%	6.8	0.2813%	238	35265

## 5.6 RESULTS COMPARISON

As a summarisation of the presented results in all sections of this study, it is possible to infer that the structural behaviour of a CLT building is highly attached to the sizing of metallic connectors on the ground floor. As for the second pavement, it is an opportunity to enhance the geometry of the building using less steel in the construction, making it more efficient under sustainable aspects. Alongside that, it is necessary to consider the presence of a soft storey to prevent local failures as more pavements are used. This phenomenon was not observed during the numerical simulations carried out in the present study, most of this merit due to the low height of the building.

After the previously presented reflections, it is possible to establish a few conclusions, which are exhibited as follows;

1. The Cross-laminated Timber structure had good performance under all scenarios it was submitted to. After analysing the natural frequencies and response spectra, it can be concluded that this lightweight structure will likely reach a value close to the maximum of the corresponding response spectrum, considering the first vibration mode. Since the obtained results are far from the limitations imposed by both codes, it is possible to infer that despite the similarity of natural frequency and spectrum maximum energy, the model behaved well;
2. In the process of design, it is not uncommon for the designer to overlook certain aspects that may contribute to the overall comfort of the building. In studying the use of hybrid CLT-concrete slabs, it is observed that although they may experience higher displacements under similar conditions, they provide superior acoustic and thermal comfort without significant changes;
3. From previous Tables (see Tabs. 5.1 to 5.11 and 5.12 to 5.21) it is possible to infer that seismic design in Brazil has very conservative rules, especially considering its low seismicity. Since Portugal and Italy have locations with higher incidences of significant seismic shocks, it is not reasonable that under the same parametric conditions the Brazilian code results in higher seismic demands. This consideration, already previously commented on, is due to the lack of provision in the Brazilian normative of the usage of inelastic response spectrum considering the energy dissipation. Behaviour factors even in Ductile Class 1 help to provide an economical metallic connector design as it enables the engineer to take advantage of the ductility of the structural system as it partially dissipates the energy it is submitted to. Furthermore, Brazilian low seismicity also contributes to consequently low demands on the structures, making the majority of the projects carried out in the country not the determining excitation, when compared to wind load. Thus, the norm



concerning earthquakes in Brazil does not have the same broad usage as in Europe, even disregarding the verification in almost every structural design carried out in the region. Consequently, there is no joint effort to provide a more realistic methodology and to endeavour scientific production with experimental campaigns to evaluate energy dissipation and modification factors to the RSC;

4. When submitted to an artificial seism with a normalised PGA of 0.15g, specially constructed to induce resonance in the model, the structure had a good performance without achieving normative limits;
5. Ductile Class 2 provides displacement reductions from around 6% up to 54.67%, which represents significant gains in design enhancement. The consideration of energy dissipation throughout behaviour factors is a very important tool to enable economic structures within safety limits.

## 6 FINAL CONSIDERATIONS

This study aims to contribute to alternative solutions to traditional heavy construction systems. The Civil Industry is more and more concerned about the environmental impacts of its activity, establishing new methods, materials and technologies to minimise carbon footprint. So, CLT construction becomes an excellent option to develop from social housing up to a high-standard real state. However, there is still much to do regarding state-of-the-art literature, since its incipient applicability shall be understood as an opportunity to improve the construction method with better designing techniques and better literature development. Scepticism towards timber construction in countries without this culture can be outlined with the aid of solid codes and projects in this direction to help designers to better understand the importance of in-depth analysis to use advanced Engineering to reduce material consumption.

Seismic activity is an important excitation to take into consideration in the designing phase to prevent accidents. Regions with high seismicities, such as Italy, can use methods to increase buildings' ductility without safety losses and economic design when compared to structures designed to work under elastic behaviour. Despite the simplicity of the theory inherent to this, taking advantage of plastic deformation to dissipate energy is the next level of structural enhancement, since this discussion, and all complexity derived from this designing hypothesis aims to reduce time consumption during construction and optimise supplies usage.

A normative comparison was carried out in order to evaluate the 2021 proposal of reformulation of the current Eurocode 8, which assesses the seismic excitation in Europe, and the recently republished NBR 15421. The proposed analysis aimed to establish a basic ground of comparison, using the same conditions and ground acceleration in order to perform the metric of comparison. In its instance, the Brazilian code conserves an elastic design, reaching a higher quantity of connectors, resulting in an exaggerated amount of steel introduced to the model. Differently from EC8, NBR 15421 does not encompass energy dissipation in ductile members, such as metallic connections. Hence, the ductile analysis was conducted only facing Eurocode's parameters, not being able to evaluate NBR 15421 structural behaviour.

Regarding the numerical modelling, a seismic analysis was conducted in a 2-storey Cross-Laminated Timber building already studied in the literature by an experimental campaign. The seismic excitation was performed by means of response spectrum curves of the National Annexes of the Eurocode 8 and NBR 15421, as well as real events data in Portugal and Italy. No real seismic data was made available by the Brazilian seismic observational network. In order to

evaluate ductile behaviour and energy dissipation in the model, a linear dynamic analysis was carried out introducing more detailing in the model aiming to enable to use of Ductile Class 2 prescriptions of Eurocode 8 and, finally, it was conducted a non-linear static analysis, by means of a pushover analysis, to evaluate the ductile behaviour of the structure.

A parametric study was conducted in order to evaluate the usage of fasteners on both pavements. In total, 9 models were created, reducing by 25% the number of angle brackets in each pavement. It was possible to notice that the original configuration was overdesigned for the region it was installed and for all other hypothetical regions proposed, according to the standards of NP EN 1998, UNI EN 1998 and NBR 15421. It was possible to notice that, the reduction in connectors can lead to economical design when it is placed in higher pavements. Alongside that, it was performed a reduction in the stiffness of the connectors, using another manufacturer's product with lower resistance to shear and tension. It was possible to notice that similar results were reached, where reductions on the second pavement lead to similar lateral stiffness.

Regarding ductility class, the results of the models that were elected as more efficient during the parametric study showed that this is an important tool in seismic engineering to reach economic design. Better detailing the structure is the counterpart of the code to use less intense seismic activity, when it is performed, reduction showed that it can represent up to almost 55% in displacement considering Type 2 RSC of the Portuguese Annex.

However, concerning ductility itself, it was observed by means of the pushover analysis that the building had a high ductility behaviour. This result indicates that there's plenty of space to use plastic deformation in order to dissipate loading energy.

As a suggestion for a continuance of this work, it is presented few topics:

- Improvement of computational model used in the present study and in De Matos (2020), using different ways to connect CLT panels and to better describe mechanical behaviour;
- Study CLT behaviour under other dynamic loads, such as wind and human excitations;
- Usage of other timber species in the constituent material of CLT panels in order to enable the implementation of the material in other regions and assess its behaviour;
- Implement an algorithm of optimisation aiming to enhance CLT panels connections;
- Consider different types of connection between orthogonal panels (nailed or dowelled);
- Perform an analysis of an enhanced geometry to seismic excitation under acoustic and thermal performance.

## REFERENCES

APA - THE ENGINEERED WOOD ASSOCIATION. **Standard for performance-rated cross laminated timber**. Tacoma, United States of America, 2018. 20 p. One citation in page 30.

AQUINO, C. D. **Uncertainty quantification related to dowel-type timber joints**. Dissertation (MSc.) — Centro Tecnológico, Universidade Federal de Santa Catarina, Florianópolis, Brazil, 2020. One citation in page 25.

ARAUJO, V. de et al. Is cross-laminated timber (clt) a wood panel, a building, or a construction system? a systematic review on its functions, characteristics, performances, and applications. **Forests**, vol. 14, n. 264, 2023. One citation in page 28.

ASSOCIAÇÃO BRASILEIRA DE NORMAS TÉCNICAS. **NBR 15421**: Projeto de estruturas resistentes a sismos – procedimento. Rio de Janeiro, 2006. 9 p. Citation 2 times in pages 10 and 56.

\_\_\_\_\_. **NBR 15421**: Projeto de estruturas resistentes a sismos – procedimento. Rio de Janeiro, 2023. 35 p. Citation 18 times in pages 7, 8, 10, 52, 53, 55, 79, 80, 81, 82, 83, 84, 85, 88, 89, 90, 100, and 102.

ASSUMPCÃO, M.; DIAS NETO, C. M. **Decifrando a Terra**. São Paulo, Brazil: Oficina de Textos, 2000. One citation in page 35.

AWRUCH, A. M.; LINN, R. V.; MORSCH, I. B. **Teoria da Elasticidade Aplicada à Mecânica Estrutural - 2a ed.** Porto Alegre, Brazil: Editora da UFRGS, 2018. One citation in page 60.

AYANSOLA, G. S.; TANNERT, T.; VALLEE, T. Experimental investigations of glued-in rod connections in clt. **Construction and Building Materials**, vol. 324, n. 126680, 2022. One citation in page 63.

AZEVEDO, J. J. R. T. **Vibrações Aleatórias - Dinâmica estocástica**. Dissertation (MSc.) — Instituto Superior Técnico, Lisbon, Portugal, 2020. One citation in page 75.

BELIZÁRIO, A. C.; OLIVEIRA, F. L. de; ICIMOTO, F. H.; VAIRO, M. Performance comparison between preservative products concerning termites attack on pine timber. **Revista Árvore**, vol. 47, p. 8, 2023. One citation in page 28.

BELLINI, A.; BENEDETTI, L.; POZZA, L.; MAZZOTTI, C. Experimental characterization of monotonic and cyclic behavior of steel-to-clt nailed joints strengthened with composite plies. **Construction Building Materials**, vol. 256, n. 119460, 2020. One citation in page 63.

BHATT, A. D. Comparison of interstorey drift in general rc buildings in pounding and no pounding case. **A Peer Reviewed Technical Journal**, vol. 2, n. 1, p. 40–47, 2020. One citation in page 45.

BLASS, H. J.; FELLMOSE, P. Design of solid wood panels with cross layers. In: **8th World Conference on Timber Engineering, Lahti, Finland**. [S.l.: s.n.], 2004. vol. 2. One citation in page 31.

BRANCO, J. M.; MATOS, F. T.; LOURENÇO, P. B.; ROCHA, T. D. P. Lateral tests on a two-story CLT house. **Guimarães IABSE Symposium**, 2019. Citation 2 times in pages 19 and 24.

BRANDNER, R. Production and technology of cross laminated timber (CLT): A state-of-the-art report. In: **Proceeding of the Focus Solid Timber Solutions - European Conference on Cross Laminated Timber (CLT)**. Austria: [s.n.], 2013. Citation 3 times in pages 10, 24, and 28.

BROWN, J. R.; LI, M. Structural performance of dowelled cross-laminated timber hold-down connections with increased row spacing and end distance. **Construction Building Materials**, vol. 271, n. 121595, 2021. One citation in page 63.

BROWN, J. R.; LI, M.; TANNERT, T.; MORODER, D. Experimental study on orthogonal joints in cross-laminated timber with self-tapping screws installed with mixed angles. **Engineering Structures**, vol. 228, n. 111560, 2021. Citation 4 times in pages 8, 63, 64, and 65.

CHAPMAN, C. H. **Fundamentals of Seismic Wave Propagation**. United States of America: Cambridge University Press, 2004. One citation in page 36.

CHIESA, D. D.; MIGUEL, L. F. F. Geração de uma excitação sísmica através do espectro de kanai-tajimi. **Revista Brasileira de Computação Aplicada**, vol. 9, n. 1, p. 31–41, 2017. Citation 3 times in pages 72, 75, and 76.

COMITÉ EUROPÉEN DE NORMALISATION. **CEN EN 1995**: Design of timber structures. Brussels, 2004. 123 p. One citation in page 29.

\_\_\_\_\_. **CEN EN 12512**: Timber structures - test methods - cyclic testing of joints made with mechanical fasteners. Brussels, 2006. 14 p. Citation 3 times in pages 25, 61, and 86.

\_\_\_\_\_. **EN 1998**: Earthquake resistance design of structures - 2021 proposed revision. Brussels, 2021. 358 p. Citation 10 times in pages 7, 10, 43, 44, 45, 46, 47, 51, 52, and 58.

COSTA, A. A. P. da. **Construção de Edifícios com Cross Laminated Timber (CLT)**. Dissertation (MSc.) — University of Porto, Porto, Portugal, 2013. One citation in page 27.

CREPELL, P.; GAGNON, S. **Cross Laminated Timber: a Primer**. Pointe-Claire: FPIinnovations, 2010. Citation 2 times in pages 23 and 28.

DAGDELEN, T.; RUHANI, S. **Finite Element Analysis of the Dynamic Effect of Soil-Structure Interaction of Portal Frame Bridges**. 2018. Citation 2 times in pages 7 and 34.

De MATOS, F. T. **Seismic behavior assessment of CLT building applying current regulation approaches**. Thesis (PhD.) — School of Engineering, University of Minho, Guimarães, Portugal, 2020. Citation 19 times in pages 7, 8, 21, 23, 25, 26, 27, 60, 61, 63, 65, 66, 68, 69, 70, 72, 96, 97, and 106.

DI BELLA, A.; MITROVIC, M. Acoustic characteristics of cross-laminated timber systems. **Sustainability**, vol. 5612, n. 12, 2020. Citation 2 times in pages 7 and 26.

DIANA. **Chapter 13 - Beam Elements**. s.d. <<https://manuals.dianafea.com/d102/Theory/Theorych13.html>>. Accessed: 2023-10-15. Citation 2 times in pages 8 and 66.

DLUBAL SOFTWARE GMBH. **RFEM 5 - spatial models calculated according to finite element method**. Tiefenbach, Germany, 2020. Citation 2 times in pages 59 and 63.

DVORKIN, E. N.; PANTUSO, D.; REPETTO, E. A. A formulation of the mitc4 shell element for finite strain elasto-plastic analysis. **Computational Methods in Applied Mechanics and Engineering**, n. 125, p. 17–40, 1995. Citation 2 times in pages 8 and 67.

EINI, A.; ZHOU, L.; NI, C. Behavior of self-tapping screws used in hybrid light wood frame structures connected to a clt core. **Buildings**, vol. 12, n. 1018, 2022. One citation in page 63.

ELGHAZOULI, A. Y. **Seismic design of buildings to Eurocode 8**. Boca Raton, FL, USA: CRC Press, Taylor & Francis Group, 2017. Citation 2 times in pages 40 and 41.

ENTE NAZIONALE ITALIANO DI UNIFICAZIONE. **UNI-EN-1998-1: Progetto delle structure in zona sismica.**: Parte 1 - regole general, azione sismica e regole per gli edifici. Rome, Italy, 2007. 20 p. Citation 13 times in pages 80, 81, 83, 84, 85, 88, 89, 90, 94, 95, 96, 100, and 102.

ESPINOZA, O.; TRUJILLO, V. R.; MALLO, M. F. L.; BUEHLMANN, U. Cross-laminated timber: Status and research need in europe. **BioRes.**, vol. 11, n. 1, p. 281–295, 2016. One citation in page 27.

EUROPEAN COMMISSION. **Mandate for Amending Existing Eurocodes and Extending the Scope of Structural Eurocodes**. Brussels, Belgium, 2019. 8 p. One citation in page 21.

FAJFAR, P. A nonlinear analysis method for performance-based seismic design. **Earthquake Spectra**, vol. 16, n. 3, p. 573–592, 2000. One citation in page 51.

\_\_\_\_\_. **The Story of the N2 Method**. Tokyo-Japan: International Association for Earthquake Engineering (IAEE), 2021. One citation in page 56.

FAN, F.-G.; AHMADI, G. Nonstationary kanai-tajimi models for el centro 1940 and mexico city 1985 earthquakes. **Probabilistic Engineering Mechanics**, vol. 5, n. 4, p. 171–181, 1990. One citation in page 75.

FRAGIACOMO, M.; DUJIC, B.; SUSTERSIC, I. Elastic and ductile design of multi-storey crosslam massive woden buildings under seismic actions. **Engineering Structures**, vol. 33, p. 3043–3053, 2011. One citation in page 40.

GARCIA, H. V. S. et al. Desempenho de painéis de madeira laminada colada cruzada constituídos com eucalipto, seringueira e bambu. **Research, Society and Development**, vol. 10, n. 8, 2021. One citation in page 31.

GOMES, J. de O.; LACERDA, J. F. S. B. Uma visão mais sustentável dos sistemas construtivos no Brasil: Análise do estado da arte. **E-tech: Tecnologias para Competitividade Industrial**, vol. 7, n. 2, p. 167–186, 2014. One citation in page 28.

GRAVIC, I.; FRAGIACOMO, M.; CECCOTTI, A. Cyclic behavior of typical screwed connections for cross-laminated (clt) structures. **European Journal of Wood and Wood Products**, vol. 73, p. 179–191, 2015. One citation in page 63.

HANKS, T. C.; KANAMORI, H. A moment magnitude scale. **Journal of Geophysical Research**, vol. 84, n. B5, p. 1–3, 1979. One citation in page 38.

HE, M.; SUN, X.; LI, Z. Bending and compressive properties of cross-laminated timber (clt) panels made from canadian hemlock. **Construction and Building Materials**, vol. 185, p. 175–183, 2018. One citation in page 30.

HINDMAN, D.; BOULDIN, J. C. Mechanical properties of southern pine cross-laminated timber. **Journal of Material in Civil Engineering**, vol. 27, n. 9, 2014. One citation in page 31.

INSTITUTO PORTUGUÊS DE QUALIDADE. **Eurocódigo 8: Projecto de estruturas para resiliência aos sismos**: Parte 1: Regras gerais, acções sísmicas e regras pra edifícios. Caparica, Portugal, 2010. 230 p. Citation 15 times in pages 7, 48, 80, 81, 83, 84, 85, 88, 89, 90, 94, 95, 96, 100, and 102.

INTERNATIONAL ORGANISATION FOR STANDARDISATION. **ISO/FDIS 21581**: Timber structures - static and cyclic lateral load test methods for shear walls. Geneva, 2010. One citation in page 68.

IZZI, M.; CASAGRANDE, D.; BEZZI, S.; PASCA, D.; FOLLESA, M. Seismic behaviour of cross-laminated timber structures: A state-of-the-art review. **Engineering Structures**, vol. 170, p. 42–52, 2018. One citation in page 32.

JORISSEN, A.; FRAGIACOMO, M. General notes on ductility in timber structures. **Engineering Structures**, vol. 33, p. 2987–2997, 2011. Citation 2 times in pages 31 and 40.

KANAI, K. An empirical formula for the spectrum of strong earthquake motions. **Bulletin of the Earthquake Research Institute**, vol. 39, p. 88–95, 1961. One citation in page 75.

KIRKEGAARD, P. H.; SØRENSEN, J. D.; ČIZMAR, D.; RAJČIĆ, V. System reliability of timber structures with ductile behaviour. **Engineering Structures**, vol. 33, n. 11, p. 3093–3098, 2011. One citation in page 40.

LAGUARDA-MALLO, M.; ESPINOZA, O. Cross-Laminated Timber vs. Concrete/Steel: Cost comparison using a case study. In: **Proceeding of the World Conference on Timber Engineering**. Austria: Vienna University of Technology, 2016. One citation in page 23.

LANZANO, G. et al. Accessing european strong-motion data: An update on orfeus coordinated services. **Seismological Research Letters**, vol. 92, n. 3, p. 1642–1658, 2021. One citation in page 72.

LEE, P.-S.; BATHE, K.-J. Development of mitc isotropic triangular shell finite elements. **Computers and Structures**, vol. 82, p. 945–962, 2004. One citation in page 66.

LEE, Y.; LEE, P.-S.; BATHE, K.-J. The mitc3+ shell element and its performance. **Computers & Structures**, vol. 138, p. 12–23, 2014. Citation 2 times in pages 8 and 67.

LI, Z.; TSAVDARIDIS, K. D. Design for seismic resilient cross laminated timber (clt) structures: A review of research, novel connections, challenges and opportunities. **Buildings**, vol. 13, n. 505, 2023. Citation 2 times in pages 31 and 32.

LIU, G. R.; QUEK, S. S. Chapter 2 - briefing on mechanics for solids and structures. In: \_\_\_\_\_. **The Finite Element Method (Second Edition)**. Oxford: Butterworth-Heinemann, 2014. p. 13–41. One citation in page 60.

LLANES-TIZOC, M. D. et al. Local, story, and global ductility evaluation for complex 2d steel buildings: Pushover and dynamic analysis. **Applied Sciences**, vol. 9, n. 200, p. 1–21, 2019. One citation in page 41.

- LUKACS, I.; BJÖRNFOT, A.; TOMASI, R. Strength and stiffness of cross-laminated timber (CLT) shear walls: State-of-the-art of analytical approaches. **Engineering Structures**, n. 178, p. 136–147, 2019. One citation in page 24.
- LUZI, L. et al. The engineering strong-motion database: A platform to access pan-european accelerometric data. **Seismological Research Letters**, vol. 87, n. 4, p. 987–997, 2016. Citation 4 times in pages 8, 72, 73, and 74.
- MARTÍNEZ-MARTÍNEZ, J. E.; ALONSO-MARTÍNEZ, F. P. A. R. M.; DÍAZ, J. J. del C. Finite element analysis of composite laminated timber (clt). In: **The 2nd International Research Conference on Sustainable Energy, Engineering, Materials and Environment**. [S.l.: s.n.], 2018. One citation in page 31.
- MARTÍNEZ-MORENO, F. **Detection and characterization of karstic caves: integration of geological and geophysical techniques**. Thesis (PhD.), 03 2015. Citation 2 times in pages 7 and 37.
- MATEJČEKOVÁ-FARHAT, M.; ÁROCH, R. Some remarks on the choice of ductility class for earthquake-resistant steel structures. **Slovak Journal of Civil Engineering**, XXI, n. 3, p. 1–10, 2013. One citation in page 41.
- MECHANICAL ENGINEERING DEPARTMENT. **Mathematical Models of Control Systems**. [S.l.], 2018. [Accessed September 9th, 2022.]. Available from Internet: <<https://med.neduet.edu.pk/node/131>>. Citation 2 times in pages 7 and 39.
- MENDES, R. A. B. **Comportamento Estrutural de Painéis *Cross-Laminated Timber* sob cargas perpendiculares ao seu plano: abordagem experimental e numérica**. Dissertation (MSc.) — Universidade Federal do Rio Grande do Sul, Porto Alegre, nov. 2020. One citation in page 31.
- MEZEIRO, R. M. M. **Construir em Madeira: Aplicabilidade de Painéis CLT em Habitação de Média Densidade em Portugal**. Dissertation (MSc.) — University of Lisbon, Lisbon, Portugal, 2018. One citation in page 28.
- MIGUEL, L. F. F.; MIGUEL, L. F. F.; LOPEZ, R. H. Methodology for the simultaneous optimization of location and parameters of friction dampers in the frequency domain. **Engineering Optimization**, vol. 50, n. 12, p. 2108–2122, 2017. One citation in page 39.
- NAVARATNAM, S.; CHRISTOPHER, P. B.; NGO, T.; LE, T. V. Bending and shear performance of australian radiata pine cross-laminated timber. **Construction and Building Materials**, vol. 232, 2020. One citation in page 31.
- NEELA, S. K. **Mode truncation analysis in forced response**. Dissertation (MSc.) — University of Texas, Arlington, United States of America, 2011. One citation in page 34.
- OLIVEIRA, G. L. **Cross Laminated Timber (CLT) no Brasil: processo construtivo e desempenho**. Dissertation (MSc.) — Faculdade de Arquitetura e Urbanismo, Universidade de São Paulo, São Paulo, Brasil, 2018. One citation in page 19.
- PANG, W. C.; ROSOWSKY, D. V. Beam-spring model for timber diaphragm and shear walls. **Structures and Buildings**, vol. 163, n. SB4, p. 227–244, 2010. One citation in page 20.



PAOLUCCI, R. et al. Checking the site categorization criteria and amplification factors of the 2021 draft of eurocode 8 part 1-1. **Bulletin of Earthquake Engineering**, vol. 19, p. 4199–4234, 2021. Citation 2 times in pages 20 and 47.

\_\_\_\_\_. Record processing in itaca, the new italian strong-motion database. In: \_\_\_\_\_. **Earthquake Data in Engineering Seismology: Predictive Models, Data Management and Networks**. Dordrecht: Springer Netherlands, 2011. p. 99–113. ISBN 978-94-007-0152-6. One citation in page 72.

PARK, R. State-of-the art report ductility evaluation from laboratory and analytical testing. **Proceedings of Ninth World Conference on Earthquake Engineering - Tokyo/Kyoto, Japan, VIII**, p. 605–616, 1988. One citation in page 41.

PENÃ, L. A. P. **Análise dos Efeitos Provocados por Abalos Sísmicos em Estruturas Irregulares**. Dissertation (MSc.) — Faculdade de Tecnologia, Universidade de Brasília, Brasília, Brasil, 2012. One citation in page 35.

PINA, F.; GONZÁLEZ, P.; LEIVA, C. B.; SAAVEDRA, E. Seismic design of a mid-rise building in chile using radiata pine cross laminated timber. In: **11th Canadian Conference on Earthquake Engineering**. Victoria, Canada: [s.n.], 2015. One citation in page 29.

REBOUÇAS, A. S.; MEHDIPOUR, Z.; BRANCO, J. M.; LOURENÇO, P. B. Ductile moment-resisting timber connections: A review. **Buildings**, vol. 12, n. 240, 2022. Citation 3 times in pages 10, 41, and 42.

REDDY, J. N. **Mechanics of Laminated Composite Plates and Shells**. Boca Raton, FL, USA: CRC Press, Taylor & Francis Group, 2004. One citation in page 31.

RICHTER, C. F. An instrumental earthquake magnitude scale. **Bulletin of the Seismological Society of America**, vol. 25, n. 1, p. 1–32, 1935. One citation in page 37.

ROSSATO, L. V.; MIGUEL, L. F. F.; MIGUEL, L. F. F. Estimativa de razão de massas ideal de amortecedores de massa sintonizada para controle de vibrações em estruturas. **Revista Interdisciplinar de Pesquisa em Engenharia**, 2016. One citation in page 37.

ROTHOBLAAS. **Experimental campaign on Rothoblaas products**: Mechanical property investigation via monotonic and cyclic loading. Trento, Italy, s.d. 104 p. Citation 3 times in pages 9, 86, and 87.

SANDHAAS, C. **Mechanical Behaviour of Timber Joints With Slotted-in Plates**. Thesis (PhD.) — University of Karlsruhe, Bühl, Germany, 2012. One citation in page 41.

SANTOS, C. I. dos. Análise de tensões, normais e de cisalhamento, e deslocamentos verticais em painéis de madeira lamelada colada cruzada via teoria de placas, métodos numéricos e simplificados. **Ambiente Construído**, vol. 24, 2023. One citation in page 60.

SCOTTA, R.; MARCHI, L.; TRUTALLI, D.; POZZA, L. A dissipative connector for clt buildings: concept, design and testing. **Materials**, vol. 9, n. 139, p. 1–17, 2016. One citation in page 24.

SETRAGIAN, Z. B.; KUSUMA, C. C. **Moisture Safety Evaluation of CLT-Concrete Composite Slab**. Dissertation (MSc.) — Chalmers University of Technology, Gothenburg, Sweden, 2018. Citation 2 times in pages 9 and 101.

SEYA, H.; TALBOTT, M. E.; HWANG, H. H. M. Probabilistic seismic analysis of a steel frame structure. **Probabilistic Engineering Mechanics**, n. 8, p. 127–136, 1993. Citation 3 times in pages 10, 76, and 77.

SIKORA, K. S.; HARTE, A. M.; MCPOLIN, D. O. Durability of adhesive bonds in cross-laminated timber (CLT) panels manufactured using irish sitka spruce. In: **Proceeding of the 57th International Convention of Society of Wood Science and Technology**. Slovakia: Vienna University of Technology, 2014. One citation in page 23.

SIKORA, K. S.; MCPOLIN, D. O.; HARTE, A. M. Effects of the thickness of cross-laminated timber (clt) panels made from irish sitka spruce on mechanical performance in bending and shear. **Construction and Building Materials**, vol. 116, p. 141–150, 2016. One citation in page 31.

SILVA, F. F. **Análise Sísmica de uma Estrutura de Concreto no Domínio do Tempo e no Domínio da Frequência**. 2021. One citation in page 75.

STURZENBECHER, R.; HOFSTETTER, K.; EBERHARDSTEINER, J. Structural design of cross laminated timber (clt) by advanced plate theories. **Composite Science and Technology**, n. 70, p. 1368–1379, 2010. One citation in page 31.

TAJIMI, H. A statistical method of determining the maximum response of a building structure during an earthquake. In: **2nd World Conference in Earthquake Engineering (WCEE)**. Tokyo, Japan: [s.n.], 1960. vol. 1, p. 781–797. One citation in page 75.

TEIXEIRA, M. Z.; SANTOS, S. da S.; TEREZO, R. F.; CORRÊA, C. A. Estado da arte do comportamento estrutural de madeira lamelada colada cruzada via método dos elementos finitos. In: **ENSUS 2023 - XI Encontro de Sustentabilidade em Projeto**. [S.l.: s.n.], 2023. p. 5. One citation in page 30.

TIE, S. S. **Connectors and Fasteners for CLT Construction**. 2020. <<https://www.calameo.com/read/00076408217b8204254b8?authid=DZkP4S4b5Z0m>>. Accessed: 2023-10-07. Citation 2 times in pages 7 and 64.

TRAN, D. K.; JEONG, G. Y. Nonlinear and elasto-plastic behaviors of cross-laminated timber (clt) walls under lateral loads. **Construction and Building Materials**, vol. 295, 2021. One citation in page 31.

UNTERWIESER, H.; SCHICKHOFER, G. R. **Characteristic values and test configurations of CLT with focus on selected properties**. Austria: Focus Solid Timber Solution - European Conference Cross Laminated Timber (CLT), 2013. One citation in page 23.

VILELA, R.; MASCIA, N. T. Avaliação de propriedades mecânicas de madeira de *Pinus taeda* provenientes de placas de cross laminated timber. **Ambiente Construído**, vol. 21, n. 4, p. 89–110, 2021. One citation in page 31.

## APPENDIX A – MATLAB KANAI-TAJIMI GENERATION CODE

```

1 % Seismic Excitation Generator
3 % Input Parameters
N = 1000; % Number of frequency samples
5 f_min = 1; % Minimum frequency (Hz)
f_max = 10; % Maximum frequency (Hz)
7 df = 0.05; % Frequency step
freq = f_min:df:f_max; % Frequency vector
9 t_initial = 0; % Initial time (seconds)
t_final = 20; % Final time (seconds)
11 dt = 0.01; % Time step
time = t_initial:dt:t_final; % Time vector
13 signal = zeros(1, length(time)); % Initialize the generated signal
phi = rand(1, length(freq)) * 2 * pi;
15
17 % Define Spectral Parameters
Sw = zeros(1, length(freq));
19 angular_frequency = 2 * pi * freq;
angular_frequency_g = 40; % Angular frequency (rad/s)
21 damping_ratio_g = 0.4; % Damping ratio
S0 = (0.02*damping_ratio_g)/ % Spectral density
23 (pi*angular_frequency_g*(4*damping_ratio_g^2+1));
25 % Kanai-Tajimi Filter
for j = 1:length(freq)
27 Sw(j) = S0*[(angular_frequency_g^4+
(4*angular_frequency_g^2*damping_ratio_g^2*angular_frequency(j)^2))/
29 ((angular_frequency(j)^2-angular_frequency_g^2)^2+
(4*angular_frequency_g^2*damping_ratio_g^2*angular_frequency(j)^2))];
31 end
33 % Shinozuka-Jan Equation Solution
V = zeros(1, length(freq));
35 for i = 1:length(time)
for j = 1:length(freq)
37 V(j)=sqrt(2*Sw(j)*df)*cos(2*pi*freq(j)*time(i)+phi(j));
end
39 signal(i) = sum(V);
end
41

```

```
43 % Normalise the Generated Signal
coef = signal / max(abs(signal)); % Normalisation coefficient
45
47 % Specify PGA (Peak Ground Acceleration)
PGA = 0.5 * 9.80665; % Peak ground acceleration (m/s^2)
49
51 % Scale the Generated Acceleration Signal
normalised_signal = PGA * coef;
53
55 % Save the normalized signal to a text file
dlmwrite('Generated_Signal.txt', normalised_signal);
57
59 % Display a message indicating completion
fprintf('Seismic excitation generation and data saving complete.\n');
```

Listing A.1 – MATLAB Kanai-Tajimi Filtering Code